Lawrence Berkeley National Laboratory
LBL Dissertations

## Title

EFFECT OF MASS TRANSPORT BOUNDARY LAYERS ON THE ELLIPSOMETRY OF SURFACES

## Permalink

https://escholarship.org/uc/item/0w04g0v4

## Author

Smith, Craig Gordon.

## Publication Date

1975-12-01

Thesis/dissertation

eScholarship.org Powered by the California Digital Library
University of California

0 0 0 4 0 3 9 7 0

LBL-3903
c. 1

# EFFECT OF MASS TRANSPORT BOUNDARY LAYERS ON THE ELLIPSOMETRY OF SURFACES

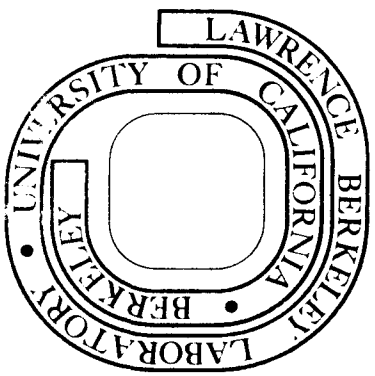
Craig Gordon Smith
(M. S. thesis)

December 1975

Prepared for the U. S. Energy Research and Development Administration under Contract W-7405-ENG-48

For Reference

Not to be taken from this room




LBL-3903
c. 1

## DISCLAIMER

This document was prepared as an account of work sponsored by the United States Government. While this document is believed to contain correct information, neither the United States Government nor any agency thereof, nor the Regents of the University of California, nor any of their employees, makes any warranty, express or implied, or assumes any legal responsibility for the accuracy, completeness, or usefulness of any information, apparatus, product, or process disclosed, or represents that its use would not infringe privately owned rights. Reference herein to any specific commercial product, process, or service by its trade name, trademark, manufacturer, or otherwise, does not necessarily constitute or imply its endorsement, recommendation, or favoring by the United States Government or any agency thereof, or the Regents of the University of California. The views and opinions of authors expressed herein do not necessarily state or reflect those of the United States Government or any agency thereof or the Regents of the University of California.

0 0 0 0 4 3 0 4 9 7 9



# EFFECT OF MASS TRANSPORT BOUNDARY LAYERS ON THE ELLIPSOMETRY OF SURFACES

Contents


Abstract . . . . . v

I. Introduction . . . . . 1

II. Mass Transport . . . . . 2

A. Transient Diffusion . . . . . 2

B. Forced Convection . . . . . 3

C. Natural Convection on Horizontal Electrodes . . . . . 4

III. The Optical Description . . . . . 6

A. The Inhomogeneous Film Model . . . . . 7

B. The Light-Deflection Model . . . . . 12

IV. Computations . . . . . 13

V. Experiments . . . . . 44

A. Apparatus . . . . . 44

B. Specimen Preparation . . . . . 47

C. Procedure . . . . . 54

1. Convection-Free Diffusion . . . . . 54

2. Forced Convection . . . . . 57

3. Natural Convection . . . . . 57

4. Growth of $Cu_2O$ Films . . . . . 57

D. Method of Analysis . . . . . 61

IV. Results and Discussion . . . . . 67

A. Convection-Free Diffusion . . . . . 67

B. Forced Convection . . . . . 67

C. Natural Convection . . . . . 71

D. Growth of $Cu_2O$ Film . . . . . 73

VII. Conclusions . . . . . 75

Acknowledgements . . . . . 76

Appendix A. Physical Properties of $CuSO_4$ . . . . . 77

Appendix B. Fresnel and Drude equations and the Ellipsometer Parameters $\psi$ and $\Delta$ . . . . . 83

Appendix C. Computer Programs . . . . . 107

INFILM . . . . . 107

DEFLCT . . . . . 120

References . . . . . 125

0 0 0 0 4 3 0 4 9 8 0



# EFFECT OF MASS TRANSPORT BOUNDARY LAYERS ON THE ELLIPSOMETRY OF SURFACES

Craig Gordon Smith

Materials and Molecular Research Division, Lawrence Berkeley Laboratory
and Department of Chemical Engineering, University of California
Berkeley, California 94720

## ABSTRACT

The effect of mass-transport boundary layers, that are often associated with surface reactions proceeding at high rates, on ellipsometer measurements of the underlying surface has been investigated for typical transport conditions in liquids. The effect can be of significant extent and depends primarily on concentration difference across the boundary layer, angle of incidence and optical constants of the surface. A simplified method for predicting boundary-layer effects based on light refraction is introduced. Computations are in good agreement with experiments.

0 0 0 0 4 3 0 4 9 8 1



# I. INTRODUCTION

Heterogeneous reactions on solid surfaces are generally accompanied by the formation of a mass-transport boundary layer, i.e., a region near the interface where the concentration of the reacting species in the fluid phase is different from that in the bulk fluid. In contrast to the conventional ellipsometry of static or slowly changing surfaces, it can be expected that the observation of fast-changing surfaces with automatic ellipsometers involves mass-transport (or diffusion) layers that have a significant optical effect. This work was undertaken to develop techniques to account for the effect of mass-transport boundary layers on the ellipsometric observation of surfaces, to establish this effect for typical electrochemical reactions and to explore the use of ellipsometry for the measurement of boundary layers, particularly those that are too thin for observation by interferometry.

## II. MASS TRANSPORT

The transport of material under the combined actions of convection and diffusion is described by the convective diffusion equation[1]

$$\frac{\partial c}{\partial t} + \underline{v}\cdot\nabla C = \nabla\cdot(D\nabla C) \quad . \tag{1}$$

The velocity field $\underline{v}$ satisfies the Navier-Stokes equation[2]

$$\rho \frac{\partial \underline{v}}{\partial t} + \rho\underline{v}\nabla\cdot\underline{v} = -\nabla p + \nu\nabla^2\underline{v} + \rho\underline{g} \quad . \tag{2}$$

### A. Transient Diffusion

When the fluid is stagnant, for one-directional diffusion, Eq. (1) reduces to

$$\frac{\partial c}{\partial t} = \frac{\partial}{\partial y}\left(D \frac{\partial c}{\partial y}\right) \quad . \tag{3}$$

Under galvanostatic conditions, the boundary conditions are

$$\frac{\partial c}{\partial y} = \frac{i(1 - t_+)}{zFD} \quad \text{at} \quad y = 0 \, , \; t > 0 \tag{4}$$

$$C = C_b \quad \text{at} \quad t = 0 \, , \text{ all } y \tag{5}$$

$$C = C_b \quad \text{as} \quad y \to \infty \tag{6}$$

For constant D and transference number $t_+$, the solution to Eqs. (3) through (6) is the Sand equation.[3] At the interface,

$$C_b - C_o(t) = \frac{2i}{zF}\sqrt{\frac{t}{DF}} = \frac{1.129i}{zF}\sqrt{\frac{t}{D}} \tag{7}$$

Under potentiostatic conditions, the boundary conditions are

0 0 3 0 4 3 0 4 9 8 2



$$C = C_i \text{ , a constant , at } y = 0 \text{ , } t > 0 \tag{8}$$

$$C = C_b \text{ at } t = 0 \text{ , all } y \tag{9}$$

$$C = C_b \text{ as } y \to \infty \tag{10}$$

Again for constant D and $t_+$, the solution to Eqs. (3), (8) through (10) is the Cottrell Equation. The current density at the interface is given by

$$i(t) = zF(C_b - C_o)\sqrt{\frac{D}{\pi t}} \tag{11}$$

B. Forced Convection

Under laminar flow, Eq. (2) may be solved for $\underline{v}$, which is used in Eq. (1) to obtain the steady-state solution for the rate of mass transfer to a surface[1]

$$Nu(x) = 1.2325 \left(ReSc \frac{d_h}{x}\right)^{1/3} \text{ , } Re < 3000 \tag{12}$$

where $Re = d_h v/\nu$, $Sc = \nu/D$, x is the distance along the planar electrode, and the Nusselt number

$$Nu = \frac{i(1 - t_+)\, d_h}{zFD(C_b - C_o)} = \frac{d_h}{\delta} \tag{13}$$

$\delta$ is the boundary layer thickness.

For turbulent flow, an analytic solution does not exist. Various semi-empirical correlations can be used.[4] By assuming $\underline{v}$ varies as $y^{1/7}$, use of the integral method[5] yields an expression for the friction factor

$$f = 0.079\ Re^{-1/4} \tag{14}$$

which, when used with the Chilton-Colburn analogy[6]

$$Nu = f/2\ ReSc^{1/3} \tag{15}$$

yields

$$Nu = 0.0395\ Re^{3/4}Sc^{1/3}\ ,\ Re > 5000 \tag{16}$$

Observations by Hickman,[7] using the limiting-current technique, have shown Nu to be proportional to $Re^{0.8}$.

C. Natural Convection on Horizontal Electrodes

A heterogeneous reaction at a solid-liquid interface can produce a gradient in the density of the solution. The action of gravity on this gradient leads to natural convection. For horizontal electrodes, the liquid remains stratified until a critical gradient is reached, at which point the fluid begins to circulate in cells. The cellular nature of flow complicates the mathematical description, and the use of empirical results[8] is necessary:

$$\begin{aligned} Nu &= 0.545\ Gr^{1/6}Sc^{1/6}\ ,\ Gr < 10^4 \\ &= 0.265\ Gr^{1/4}Sc^{1/4}\ ,\ 10^4 < Gr < 10^8 \\ &= 0.065\ Gr^{1/3}Sc^{1/3}\ ,\ Gr > 10^8 \end{aligned} \tag{17}$$

where the Grashof number

$$Gr \equiv \delta_c^3 g\beta\Delta c/\nu^2 \quad . \tag{18}$$

The coefficient $\beta$ is defined as

$$\beta = \left(\frac{\partial \rho}{\partial c}\right) \quad .$$

From the dependence on $\rho$ with c given in Appendix A, $\beta = 0.155$ gm/cm$^3$ $(MCuSO_4)^{-1}$ for $0 \leq C \leq 0.1$ M. The variable $\delta_c$ is a characteristic distance over which the change in density $\Delta\rho$ occurs.

## III. THE OPTICAL DESCRIPTION

Mass-transport boundary layers are optically inhomogeneous, with the refractive index varying continuously from the (homogeneous) bulk fluid to the interface. The concentration dependence on the distance y normal to the interface has been investigated by techniques such as interferometry.[9] Although more accurate descriptions of the concentration field are available, the inhomogeneity has been approximated by linear and parabolic functions, as well as various equivalent homogeneous films.

Experimentally, boundary layers have been generated by electrochemical (anodic) dissolution or (cathodic) deposition of copper under different convective conditions. The dependence of the refractive index of $CuSO_4$ upon concentration at 546.1 nm wavelength has been determined with a Bausch and Lomb refractometer. These results as well as published physical data for $CuSO_4$ are presented in Appendix A. A linear function fits the refractive-index data for the concentration $0 < C < 0.2$ M $CuSO_4$

$$n = 1.3345 + 0.029C \tag{19}$$

Although aqueous $CuSO_4$ solutions are colored, the optical computations are not perceptively affected by the very weak light absorption. The imaginary part of the refractive index ($k = 1.8\times10^{-6}$ Appendix A) has, therefore, been neglected. Using the linear refractive index relationship for concentration, the linear and parabolic functions approximating mass-transport boundary layers, with interfacial index $n_i$ and bulk fluid $n_b$, are

0 0 0 0 4 3 0 4 9 8 4



$$n = n_i + \frac{n_b - n_i}{\delta}\, y \tag{20}$$

$$n = n_i + (n_b - n_i)[1 - (1 - y/\delta)^2] \tag{21}$$

The profiles are plotted in Fig. 1 for $\delta n_i = n_b - n_i$ corresponding to a concentration difference $c_b - c_i = 0.1$ M $CuSO_4$ and $\delta = 10\mu$.

Two linear profiles are shown. One uses $\delta$ as in Eq. (20). The second is the Nernst profile with $\delta_n = 1/2\ \delta$, which is associated with interfacial mass transfer rates equivalent to the parabola. Calculations involving the linear profile used $\delta$ rather than $\delta_n$.

Besides the homogeneous film with $n = n_i$ and thickness equal to $\delta_n$ illustrated in Fig. 1, homogeneous films with $n = n_i + a(n_b - n_i)$, $a = 1/3$, $1/2$, or $2/3$, were also investigated. Various scaled values of $\delta$ were used in addition to the Nernst thickness.

### A. The Inhomogeneous Film Model

The multiple-film method[10] was used to treat the inhomogeneity described by Eq. (20) and Eq. (21). Figure 2 shows a schematic diagram of the method. Equally spaced planes parallel to the substrate separate the layer into a pile of homogeneous films. An average refractive index for each film is obtained by an integrated average of the profile between the values of y which limit the film. The number of films is increased until the calculated ellipsometer parameters $\Delta$ and $\psi$ converge (with respect to the number of films) to the desired accuracy.

The method begins by calculating the Fresnel reflection coefficients describing the light reflection at the substrate / lowest-film interface, as illustrated in Fig. 3:

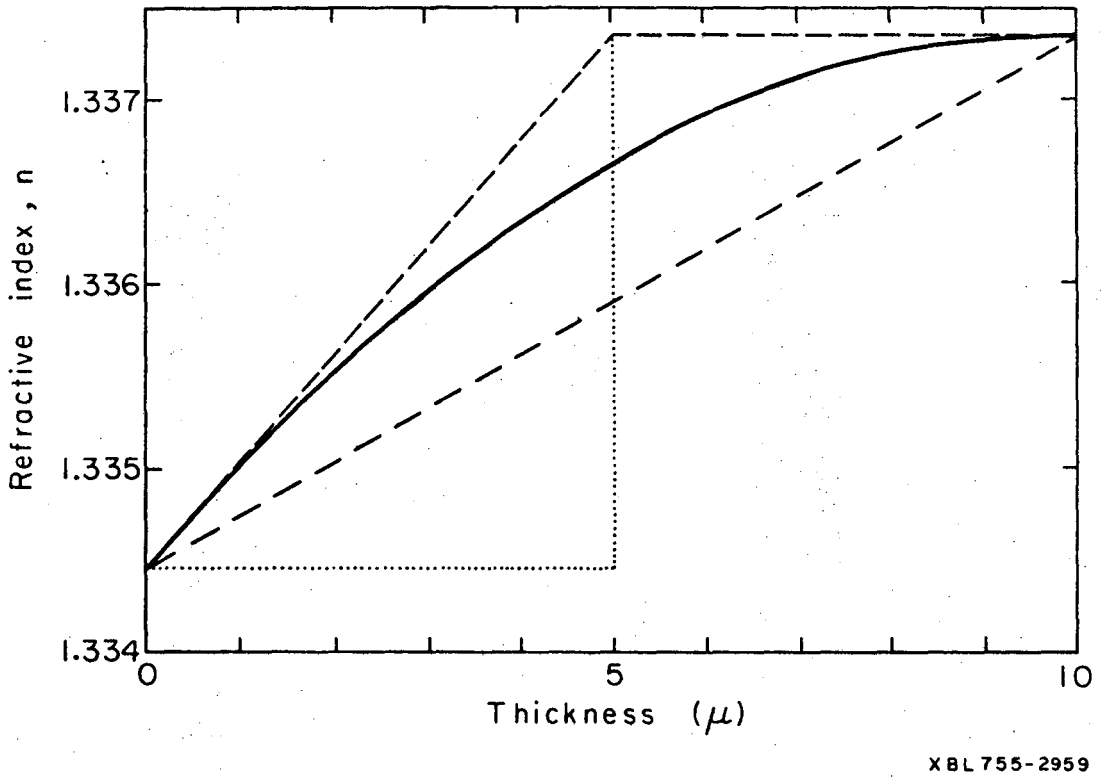
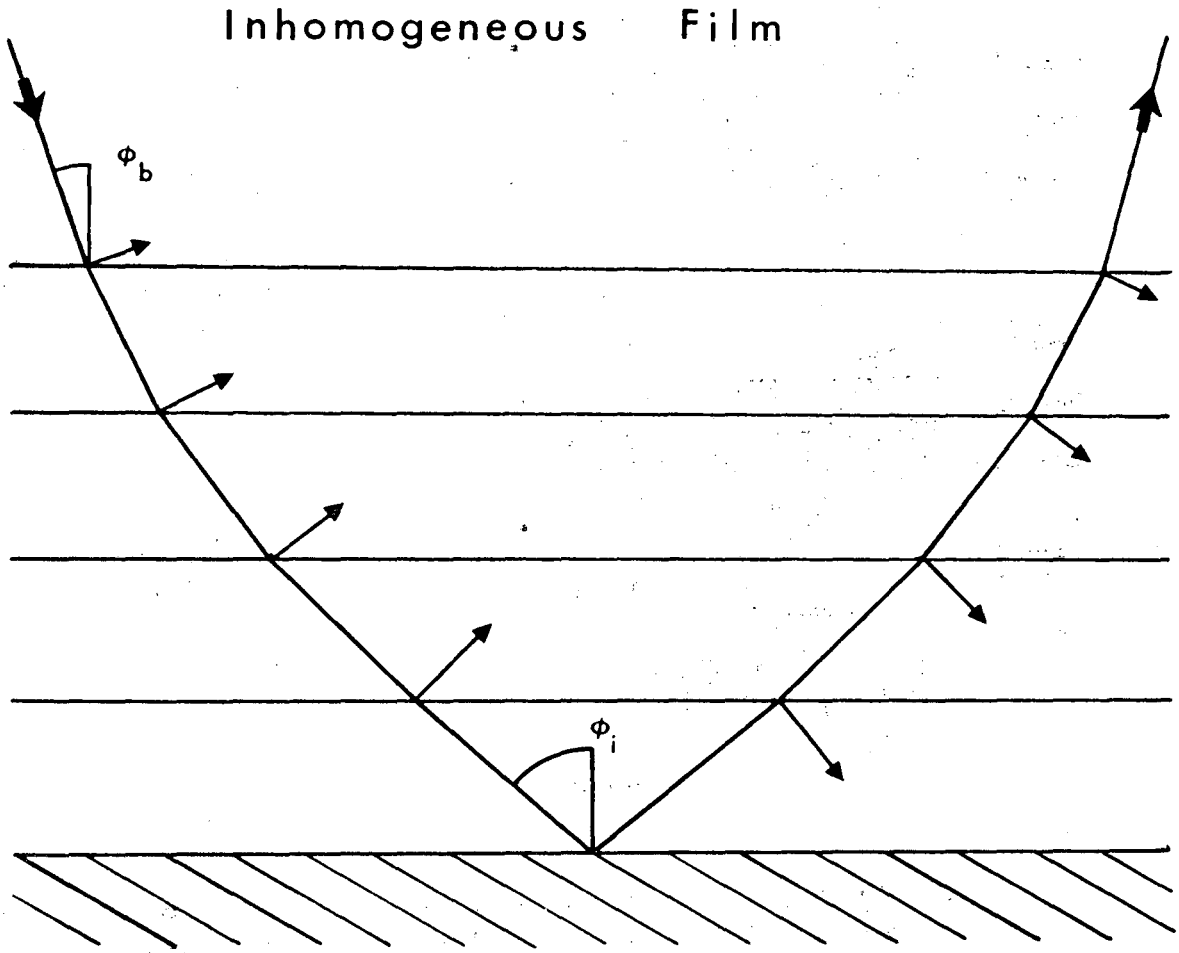



Fig. 1. Refractive index profiles approximating a 10μ thick mass-transport boundary layer. Change in refractive index corresponds to $\Delta C = 0.1$ M $CuSO_4$. ——— parabolic, - - - Nernst linear, · · · homogeneous film.

0 0 0 0 4 3 0 4 9 8 5






XBL 759-7342

Fig. 2. Multiple-film model representing the inhomogeneous boundary layer. Planes are drawn parallel to the solid phase (hatched) and form interfaces for reflection and light-deflection. $\phi_b$ is the angle of incidence upon the boundary layer. $\phi_i$ is the angle of incidence upon the substrate (solid phase).

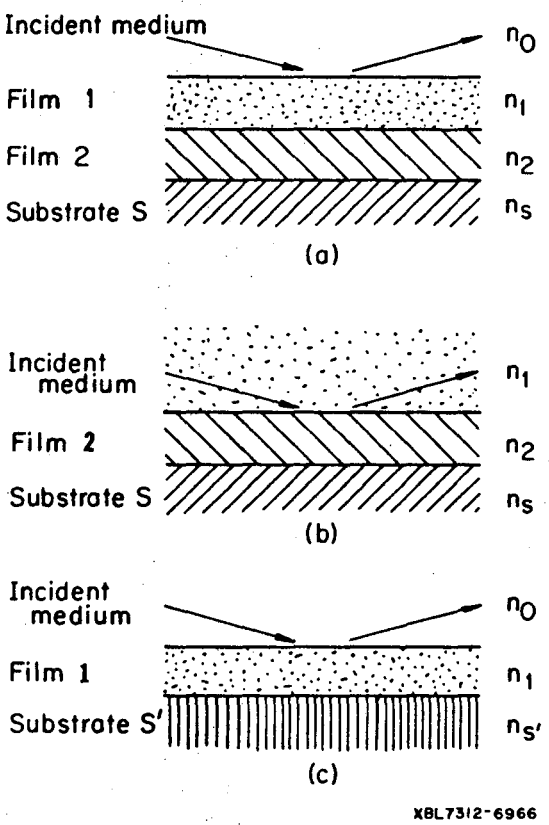



Fig. 3. Iterative procedure for multiple-film calculations. (a) Optical system consists of 2 homogeneous films above the substrate S. (b) Film 1 replaces the incident medium to calculate the optical effect of film 2 and substrate. (c) An effective substrate S' having the same optical effect as the combination of film 2 - S replaces the substrate for the incident medium--film 1 - S' interaction. Figure taken from Ref. 34.

0 0 0 0 4 3 0 4 9 8 6



$$r_{2s} = - \frac{\sin(\phi_{cf} - \phi_{cs})}{\sin(\phi_{cf} + \phi_{cs})} \tag{22}$$

$$r_{2p} = \frac{\tan(\phi_{cf} - \phi_{cs})}{\tan(\phi_{cf} + \phi_{cs})} \tag{23}$$

The squares of the coefficients, $r_{is} r_{is}^*$ and $r_{ip} r_{ip}^*$, represent the ratios of reflected to incident electric-field energy fluxes for orthogonal states of polarization perpendicular and parallel to the plane of incidence. The coefficients $r_{1s}$ and $r_{1p}$ for the reflection at the boundary between the bottom two films are also determined. The Drude equations[11] are then used to calculate the amplitude ratios $r_s$ and $r_p$ for the two reflections bounding the bottom film of thickness L:

$$r_\nu = \frac{r_{1\nu} + r_{2\nu} e^{-i2\tau}}{1 + r_{1\nu} r_{2\nu} e^{-i2\tau}} \tag{24}$$

where

$$\tau = \frac{2\pi}{\lambda_o} L n_{cf} \cos\phi_{cf} \quad ,$$

and $\nu$ is either s or p. The definition of symbols is presented with the derivation of the Drude equations in Appendix B.

The upper interface then becomes an effective substrate, $r_s \rightarrow r_{2s}$ and $r_p \rightarrow r_{2p}$. The procedure is repeated for each successively upper film, until the overall coefficients $r_s$ and $r_p$ for the inhomogeneous boundary layer have been obtained. The ellipsometer parameters $\Delta$ and $\psi$ are defined (Appendix B) by

$$\frac{r_p}{r_s} = \rho = \tan\psi e^{i\Delta} \tag{25}$$

Tan $\psi$ and $\Delta$ represent the relative attenuation and a relative shift in phase between the s and p components of the ellipse describing the electric field propagation.

B. The Light-Deflection Model

Successive application of Snell's law to each reflecting interface in the pile of films allows the determination of the angle of incidence for light upon the substrate

$$n_b \sin\phi_b = n_{f1} \sin\phi_{f1} = \ldots = n_{f(n-1)} \sin\phi_{f(n-1)} = n_{fn} \sin\phi_{fn}$$

or

$$n_b \sin\phi_b = n_{fn} \sin\phi_{fn} \tag{26}$$

where the subscript fi refers to the $i^{th}$ film from the top of the pile. Equation (26) indicates that the angle of light incident upon the substrate is known, given $n_b$, $n_i = n_{fn}$, and $\phi_b = \phi$, the angle of incidence upon the boundary layer.

Computations for the linear and parabolic profiles, which are presented in the following section, indicate that the reflections occurring at the boundaries of the pile of films become negligible for the limit of a thick inhomogeneous film. The angle of incidence upon the substrate, as visualized in Fig. 2, does remain changed by the light-deflection. A second method which utilizes this information calculates $\Delta$ and $\psi$ by using the reflection coefficients $r_p$ and $r_s$ for the single substrate/interfacial-solution surface. The correct angle of incidence as given by Eq. (26) is used.

0 0 0 0 4 3 0 4 9 8 7



## IV. COMPUTATIONS

Figure 4 shows the dependence of the relative phase $\Delta$ on the film thickness $\delta$, for cathodic deposition with the interfacial concentration $c_i$ held constant (potentiostatic mode). The figure illustrates two surprising results: (1) for transport regions greater than about 10$\mu$, $\Delta$ is independent of thickness but depends only on the concentration difference between bulk and interface; (2) $\Delta$ is not greatly affected by the nature of the concentration profile. The figure also illustrates that mass-transport boundary layers can change the ellipsometer parameter $\Delta$ by several degrees, an amount often not negligible in ellipsometer measurements. The change in $\psi$ is usually found to be smaller than that in $\Delta$, but it follows a similar thickness dependence. Figure 5 treats the anodic-dissolution mass transfer boundary layer and indicates that changes in $\Delta$ and $\psi$ are of the opposite sign but the same magnitude as those for the cathodic deposition.

The independence of ellipsometric parameters upon film thickness in the thick-film limit is most unusual, since the values of $\Delta$ and $\psi$ for a homogeneous transparent film show an unabated periodic behavior with increasing film thickness due to the sinusoidal dependence indicated by the complex exponential term in Eq. (24). Computed reflection coefficients from the interior of the inhomogeneous film show that the principal reason for this behavior is light deflection (refraction) in the film: At large boundary layer thicknesses, the refractive-index gradient is small enough to allow light to be deflected without attenuation by reflection, while at small thicknesses (large gradients), reflection occurs simultaneously with refraction.

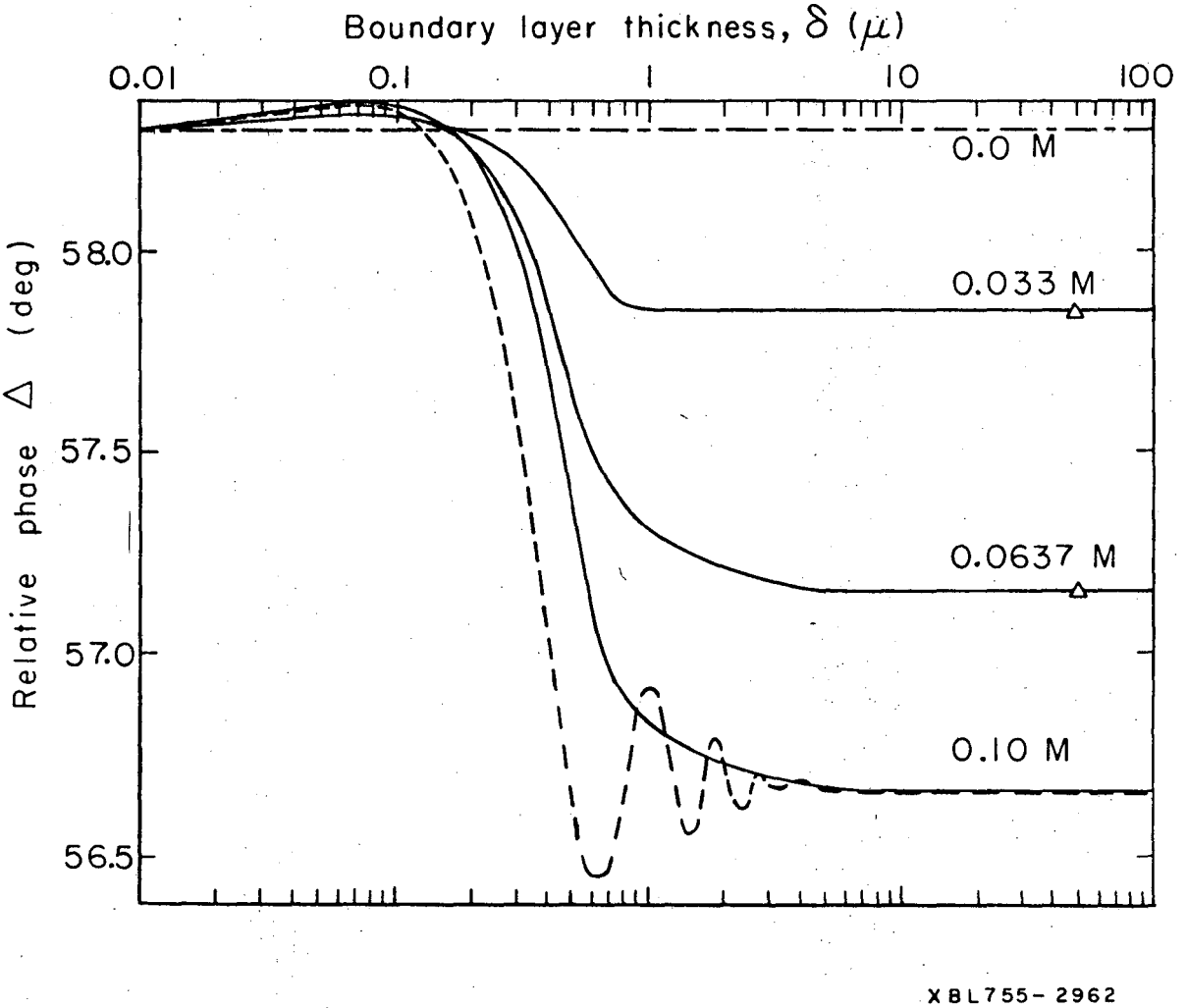



Fig. 4. Effect of mass-transport boundary layers of thickness $\delta$, resulting from the deposition of Cu from 0.1 M $CuSO_4$, on the ellipsometer parameter $\Delta$. Concentration difference between bulk and interface indicated along curves. ——— parabolic concentration profile, - - - $\Delta$ linear concentration profile. Refractive index of substrate 0.94-2.33i.

0 0 0 0 4 3 0 4 9 8 8



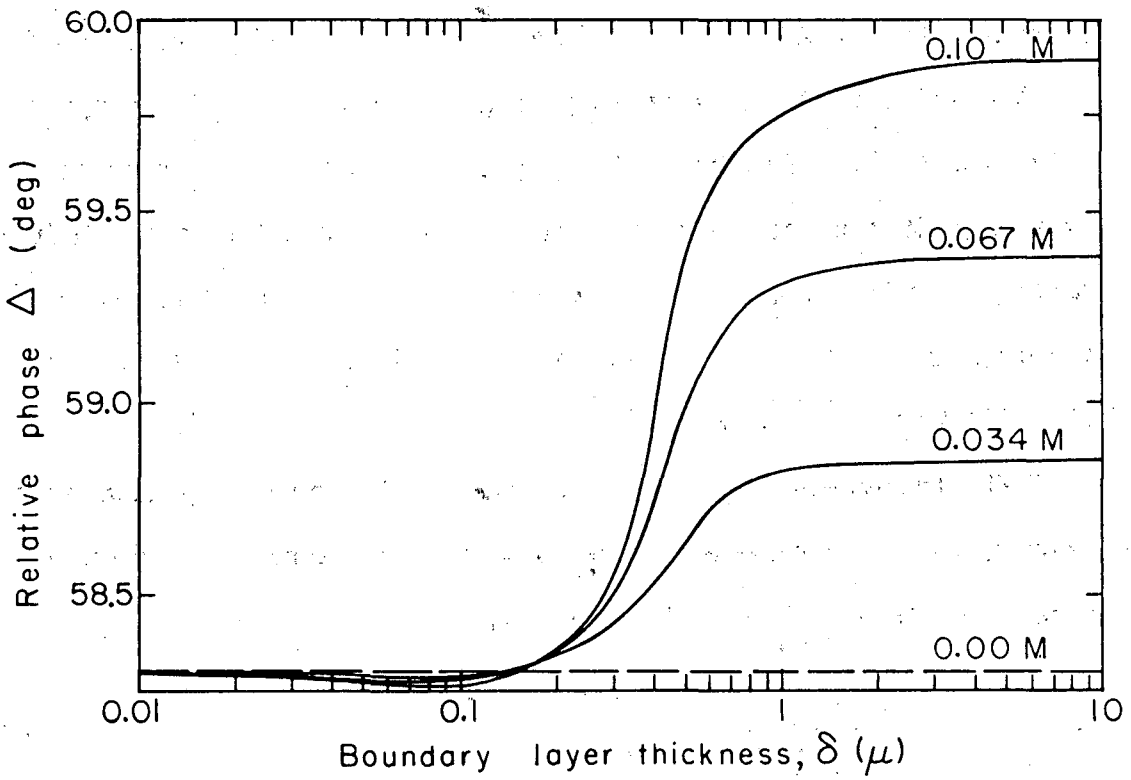



Fig. 5. Effect of mass-transport boundary layers of thickness $\delta$, resulting from the dissolusion of Cu from 0.1 M $CuSO_4$, on the ellipsometer parameter $\Delta$. Concentration difference between bulk and interface indicated along curves. Parabolic profile, refractive index of substrate 0.94-2.33i.

In the thick-film limit, the light-deflection model is expected to apply.

The validity of this approach to computing the optical effect of boundary layers is illustrated in Table I. Up to 400 layers in the multiple-film model are necessary to give convergence with respect to the number of layers for the largest concentration difference between bulk and interface. For a 5μ thick layer, the light-deflection model approximates the much more involved inhomogeneous-film computation quite well; agreement to the third decimal place is found for a 500μ thick layer.

The region where it is necessary to use the inhomogeneous film computation may be characterized in terms of the refractive index gradient at the surface. From Eq. (21),

$$\left.\frac{dn}{dy}\right|_{y=0} = \frac{2(n_b - n_i)}{\delta} \tag{27}$$

For the curve $\Delta C$ = 0.1 M $CuSO_4$ in Fig. 4, the gradient for a 10μ-thick boundary layer is dn/dy = 580 $cm^{-1}$. An alternate approach is to specify the electrode-current density from

$$i = \frac{mFD}{(1 - t_+)} \left.\frac{dc}{dy}\right|_{y=0} = \frac{2mFD}{(1 - t_+)} \frac{\Delta C}{\delta} \quad . \tag{28}$$

Using the average transport properties $D = 5\times10^{-6}$ $cm^2/s$ and $t_+ = 0.385$, Eq. (28) gives $i = 0.31$ amps/$cm^2$. A third characterization is to specify the flow conditions necessary to give $\delta$ = 10μ. For $\nu = 1.065\times10^{-2}$ $cm^2/s$ and $d_h$ = 1.36 cm, Eqs. (13) and (16) give a Reynolds number Re = 35,000.

Table I. Validity of light-deflection model for computing the effect of cathodic mass-transport boundary layers with parabolic concentration profiles. Bulk fluid 0.1 M $CuSO_4$, n = 1.3374; substrate Cu, n = 0.94-2.33i.

| Interfacial Concentration M $CuSO_4$ | Boundary Layer Thickness μ | Angle of Incidence | | Computation Based On | | | |
|---|---|---|---|---|---|---|---|
| | | Macroscopic | At Interface | Inhomogeneous Film | | Light Deflection | |
| | | deg | deg | ψ | Δ | ψ | Δ |
| 0.4 | 0 | 60 | 60.00 | 36.253 | 107.484 | 36.253 | 107.484 |
| 0.2 | 5 | 60 | 60.43 | 36.205 | 106.496 | 36.209 | 106.478 |
| 0.0 | 5 | 60 | 60.87 | 36.158 | 105.472 | 36.166 | 105.434 |
| 0.0 | 500 | 60 | 60.87 | 36.166 | 105.431 | 36.166 | 105.434 |
| 0.4 | 0 | 75 | 75.00 | 37.492 | 58.058 | 37.492 | 58.058 |
| 0.2 | 5 | 75 | 75.96 | 37.747 | 54.727 | 37.769 | 54.671 |
| 0.0 | 5 | 75 | 76.99 | 38.053 | 51.067 | 38.104 | 50.941 |
| 0.0 | 500 | 75 | 76.99 | 38.101 | 50.937 | 38.104 | 50.941 |



0 0 4 3 6 9 8

It would be desirable to represent the inhomogeneous boundary layer by an optically equivalent homogeneous film. This is possible only over the small range of thicknesses in Fig. 4 for which the parameter $\Delta$ changes rapidly. Figure 6 shows the variation of $\Delta$ with thickness $\delta$ for the homogeneous film with $n = n_i$, as well as the linear and parabolic profiles. The homogeneous film approximates the linear profile for about 1/4 of a cycle of oscillation. Equation (24) indicates one cycle corresponds to $\tau = \pi$. For 1/4 cycles, this gives

$$\frac{\pi}{4} = \frac{2\pi}{\lambda_o} \, Ln_i \cos\phi_i$$

which, with the use of Eq. (26) and $\cos^2\phi = 1 - \sin^2\phi$, results in

$$\delta = \frac{\lambda_o}{2\left(n_i^2 - n_b^2 \sin^2\phi\right)^{1/2}} \quad . \tag{29}$$

When the refractive index decreases toward the interface, total reflection in the boundary layer is possible. The ellipsometer measurements are then independent of the substrate. Some limiting concentration differences necessary for total reflection under different angles of incidence are listed in Table II.

The changes $\delta\Delta$ and $\delta\psi$ in ellipsometer parameters $\Delta$ and $\psi$, defined positive for an increase due to mass-transport boundary layers, depends on the angle of incidence, $\phi$. Computations for the thick-film limit, with different substrate optical constants $n_{cs}$, are shown in Fig. 7. The data relate to the slope of the dependence of $\Delta$ and $\psi$ on the angle of incidence as indicated in Fig. 8. Discrete changes $\delta\Delta$ and $\delta\psi$ result from discrete changes in the angle of incidence on the substrate. As

0 0 0 0 4 3 0 4 9 9 0



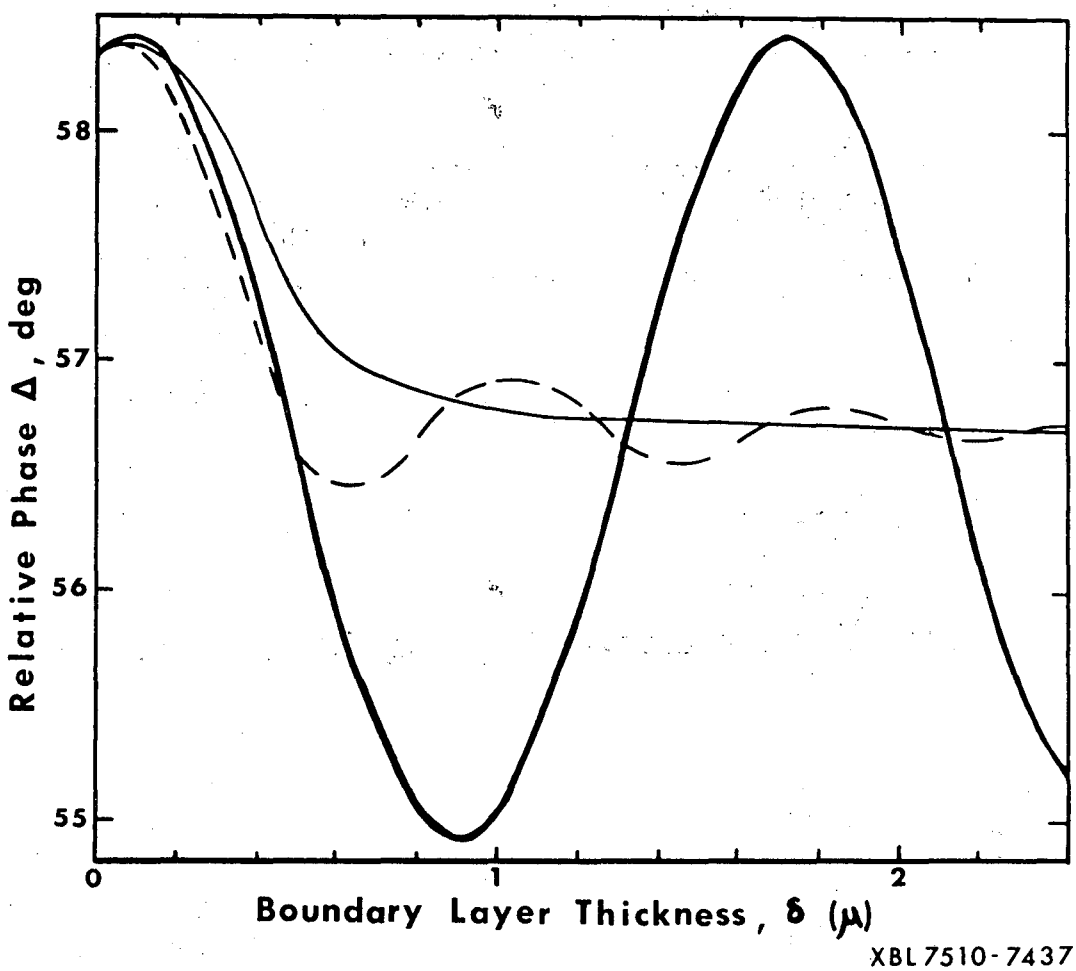



Fig. 6. Homogeneous film approximation to cathodic deposition mass-boundary layer. Dotted profile in Fig. 1. For $n = n_i$ corresponding to 0.0 M $CuSO_4$, $\Delta$ oscillates with increasing thickness $\delta$, in comparison with the linear profile - - -, and parabolic profile ———. Substrate refractive index $n_{cs} = 0.94\text{-}2.33i$, $\phi = 75°$.

Table II. Total reflection in cathodic boundary layers with parabolic concentration profile. Bulk fluid 1.0 M $CuSO_4$, n = 1.3635.

| Angle of Incidence (Macroscopic) deg | Boundary Layer: Minimum Interfacial Conc. M $CuSO_4$ |
|---|---|
| 75 | 0 |
| 79 | 0.14 |
| 81 | 0.42 |
| 83 | 0.65 |
| 85 | 0.82 |

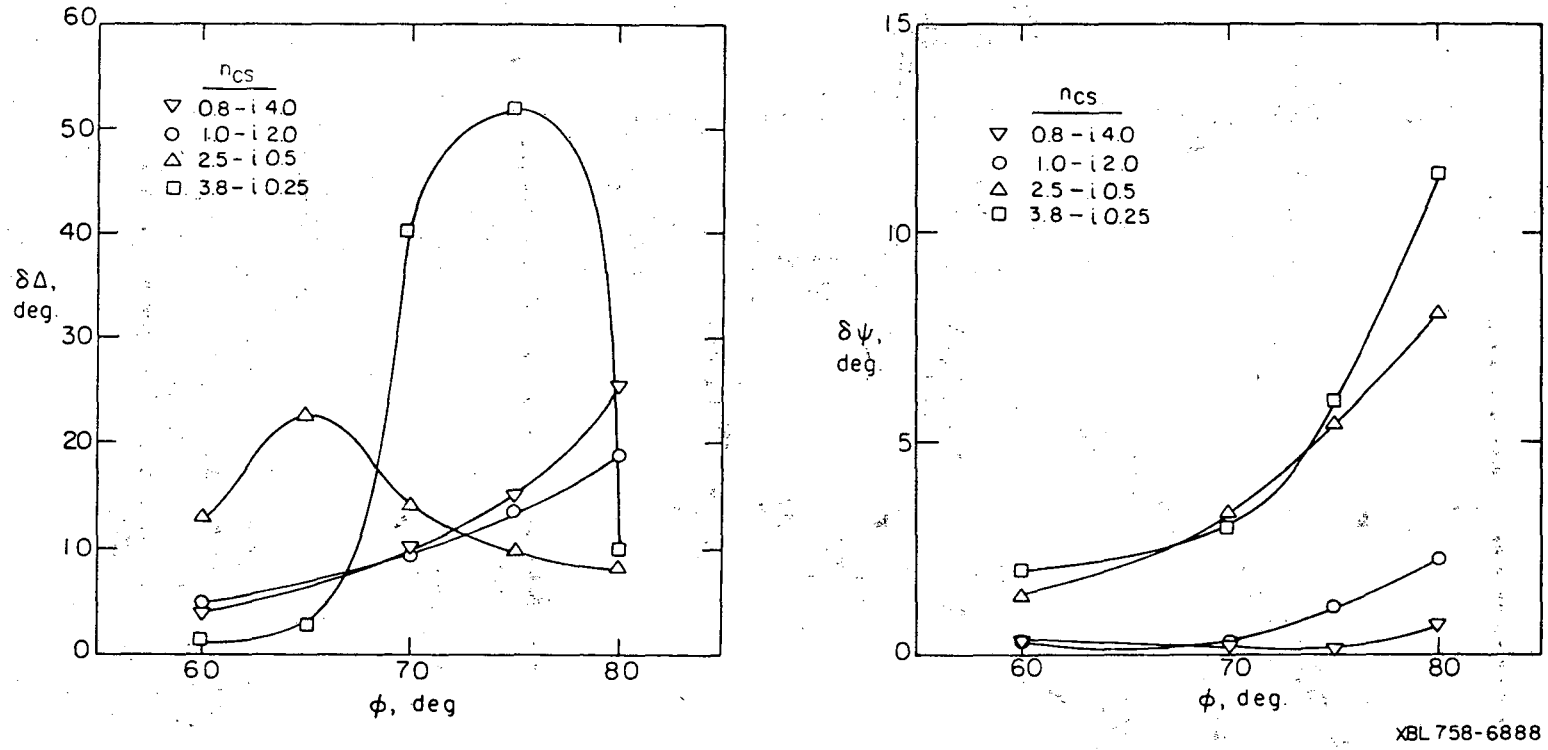
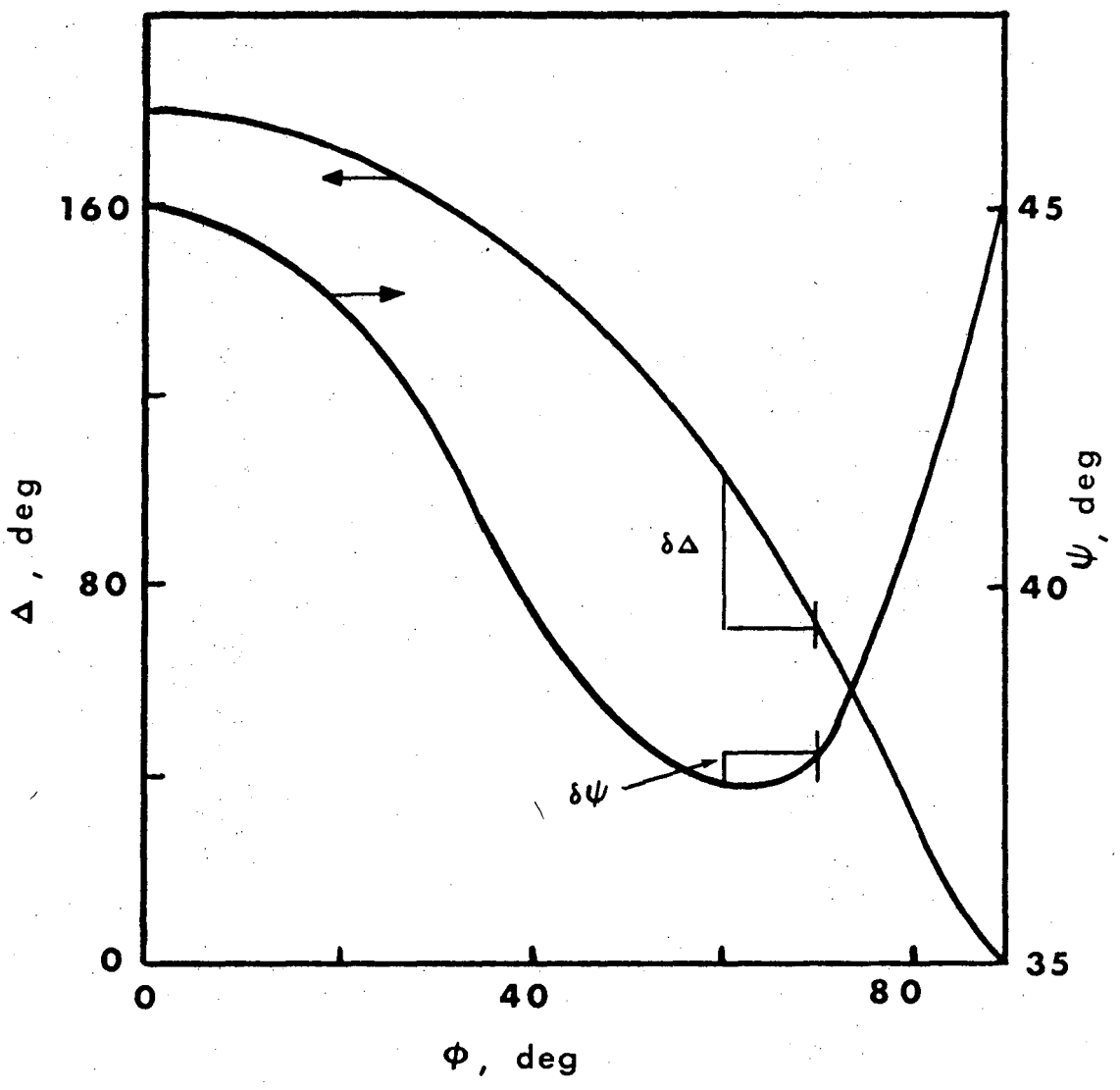



Fig. 7. Dependence of the change in $\Delta$ and $\psi$ due to anodic boundary layer on the angle of incidence $\phi$ for different substrate optical constants $n_{cs}$. Thick-film limit, bulk fluid refractive index $n_b$ = 1.3345, refractive index difference $\delta n_i$ = 0.03, corresponding to 1.1 M $CuSO_4$.



0 0 0 4 3 0 4 9 9 1




XBL 759-7340

Fig. 8. Dependence of $\Delta$ and $\psi$ on the angle of incidence $\phi$. $\delta\Delta$ and $\delta\psi$ correspond to discrete changes in $\phi$ due to light deflection in the boundary layer. Substrate refractive index $n_{cs}$ = 0.8-2.3i. Incident medium refractive index $n^{cs} \cong$ 1.3374.

0 0 0 0 4 3 0 4 9 9 2



illustrated in Fig. 9, the effect of boundary layers, under most conditions, is proportional to the concentration difference $\delta n_i = n_b - n_i$ across the layer.

Figures 10 through 25 allow an experimenter to estimate errors in ellipsometer measurements caused by mass-transport boundary layers with substrates of arbitrary optical constants. The errors are largest for substrates with large real parts and rather small imaginary parts of the refractive index.

Neglecting the effects of mass-transport boundary layers can lead to errors in the quantities derived from ellipsometer measurements, such as film thicknesses or optical constants of films or substrates. The magnitude of such errors has to be determined for each individual case. An example on the formation of cuprous oxide during the anodic dissolution of copper is illustrated in Fig. 26: $\Delta$ and $\psi$ values computed for oxide layers up to 200Å thickness are parallel-displaced by the presence of a boundary layer. For a 0.4 M concentration difference and no oxide present, erroneous substrate optical constants of 1.03-2.60i (compared to the real 0.94-2.24i) would be derived from the measurement. The shift in $\Delta$ is of similar magnitude as that due to a change in oxide thickness by 100Å. Table III gives the apparent substrate values for other concentration differences. An apparent value of the oxide refractive index was determined by using the correct thickness and the erroneous substrate values. From Table III, with the boundary layer corresponding to $\Delta C$ = 0.4 M, a 100Å thick oxide layer appears to possess a refractive index of

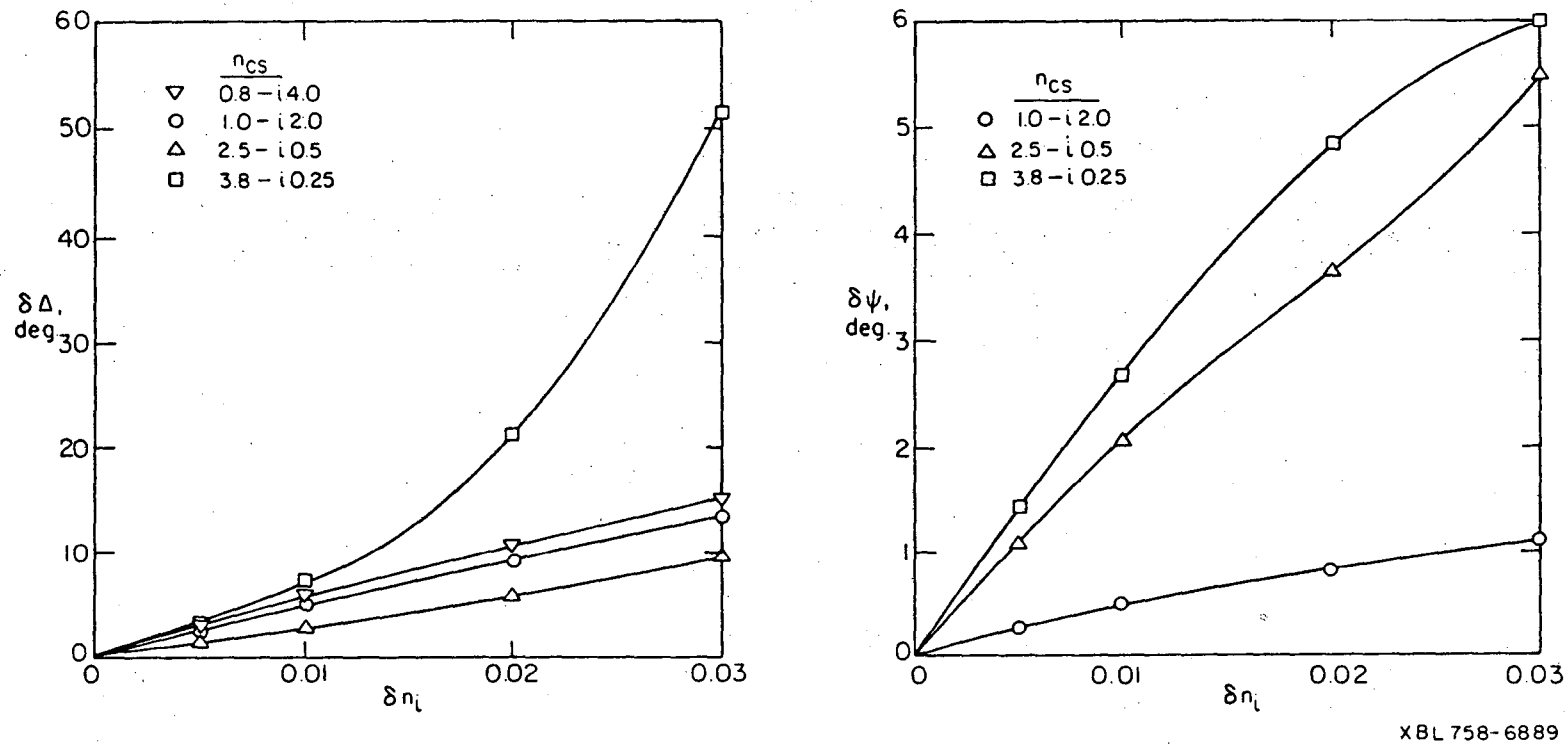
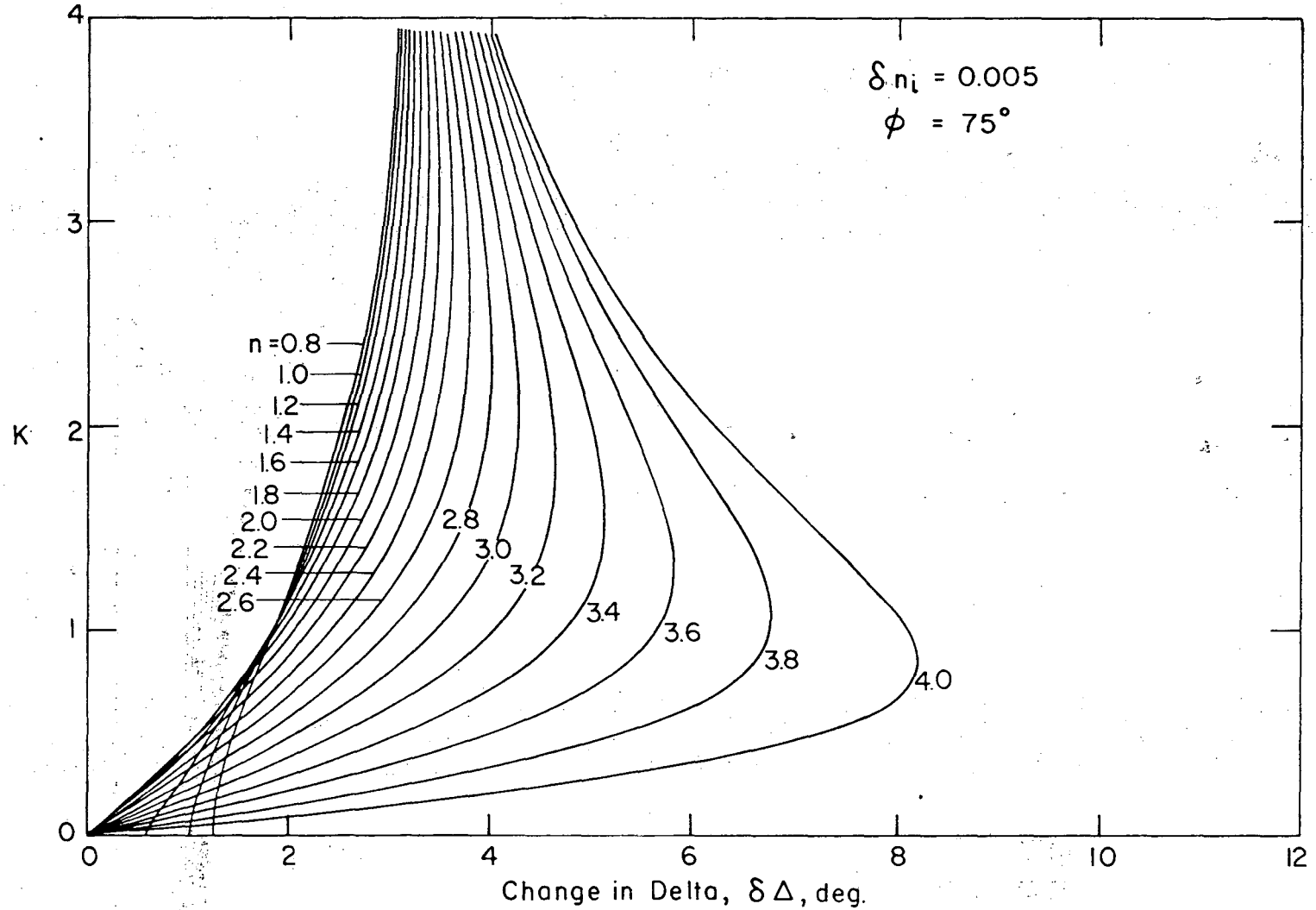



Fig. 9. Dependence of the change in $\Delta$ and $\psi$ due to anodic boundary layer on the refractive-index difference between bulk and interface $\delta n_i$ for different substrate optical constants $n_{cs}$. Thick-film limit, bulk fluid refractive index $n_b$ = 1.3345, angle of incidence $\phi$ = 70°.

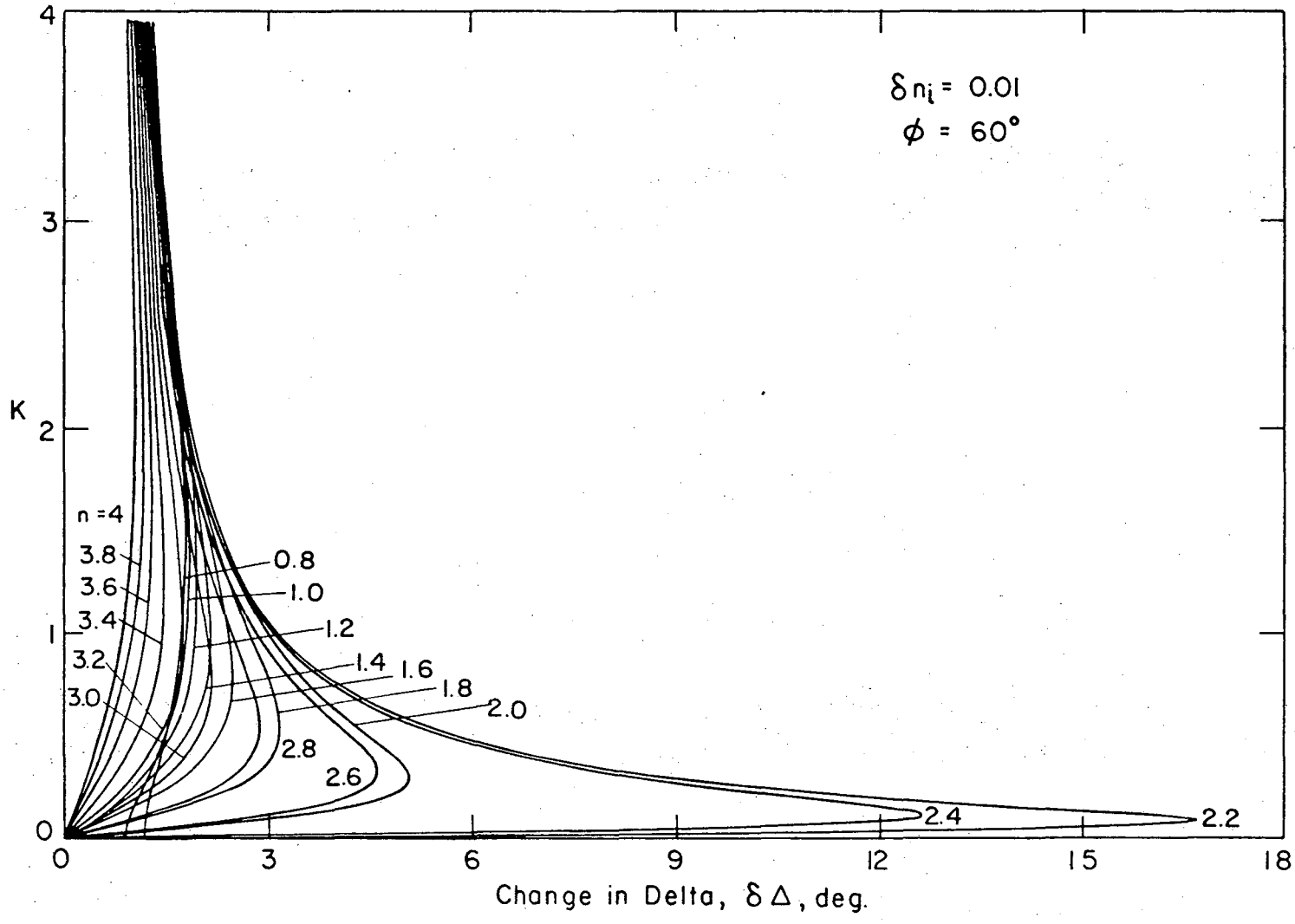



XBL 758-6894

Fig. 10. Dependence of the change in Δ due to anodic boundary on the substrate refractive index n - ik. Thick-film limit, bulk fluid refractive index $n_b$ = 1.3345. The angle of incidence φ = 75°, the refractive index difference $\delta n_i$ = 0.005.



0 0 0 4 3 0 4 6 9 3




XBL 758-6896

Fig. 11. As in Fig. 10, $\phi = 60°$, $\delta n_i = 0.01$.

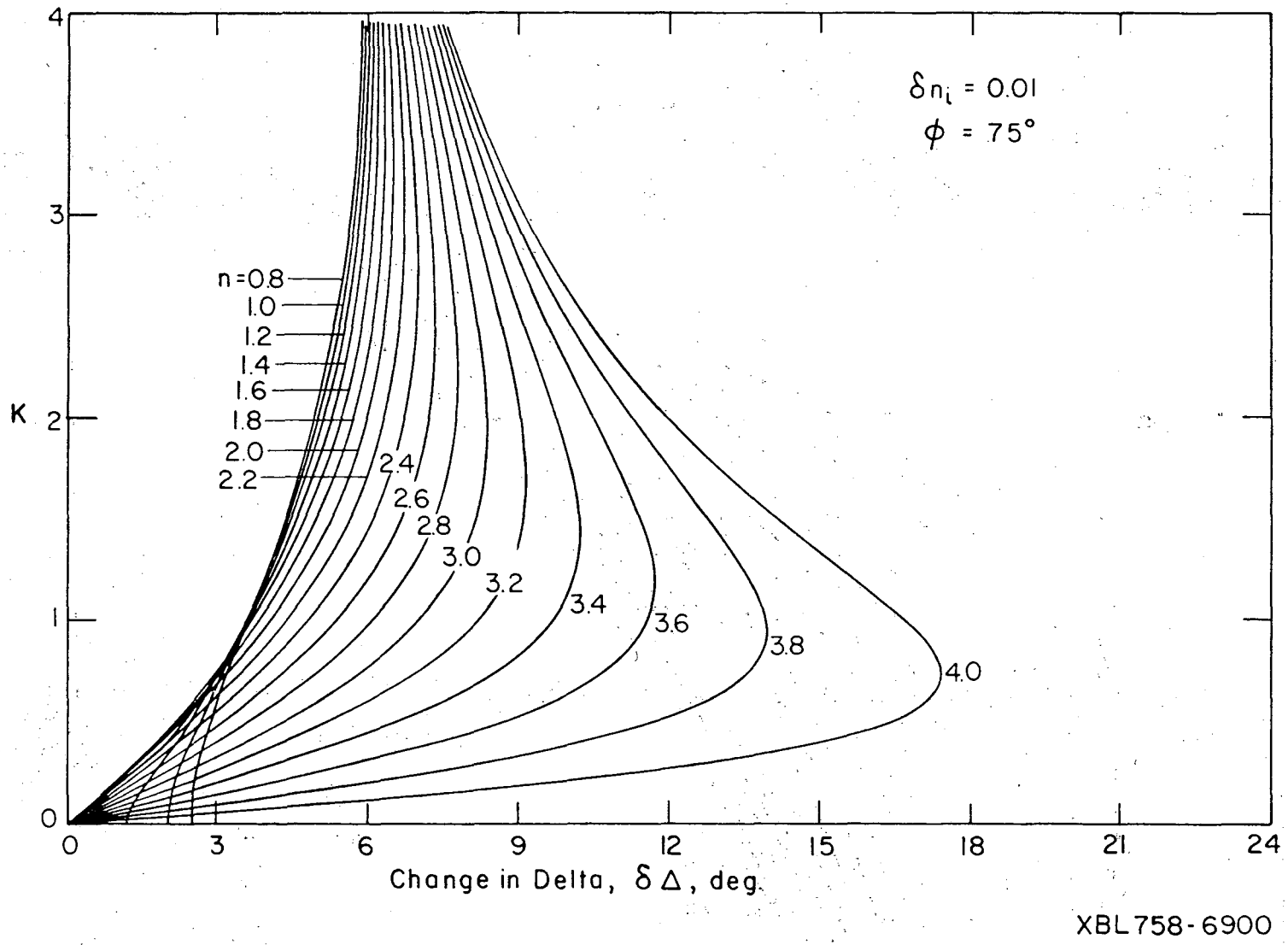



Fig. 12. As in Fig. 10, $\phi = 75°$, $\delta n_i = 0.01$.

LBL-6900

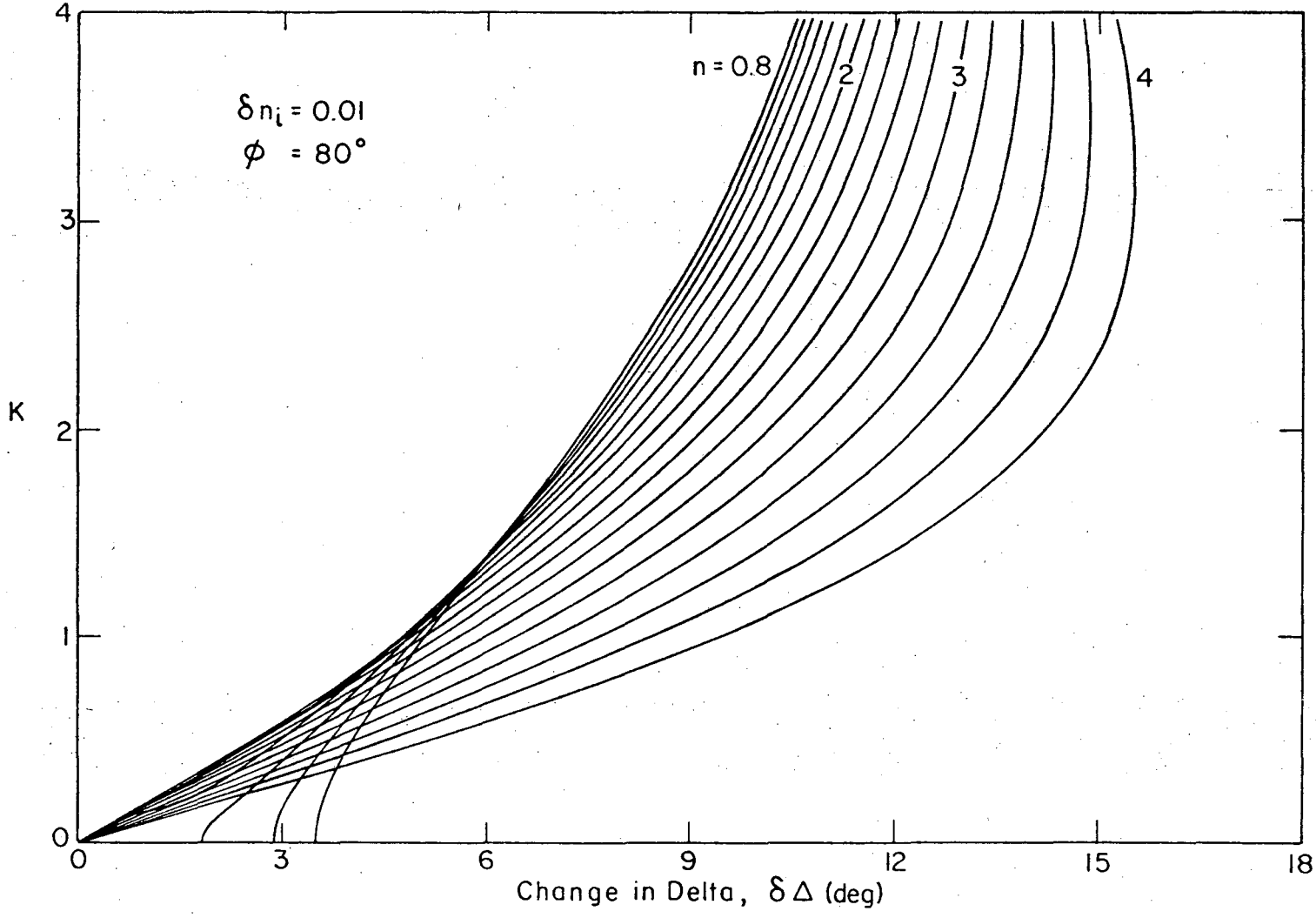
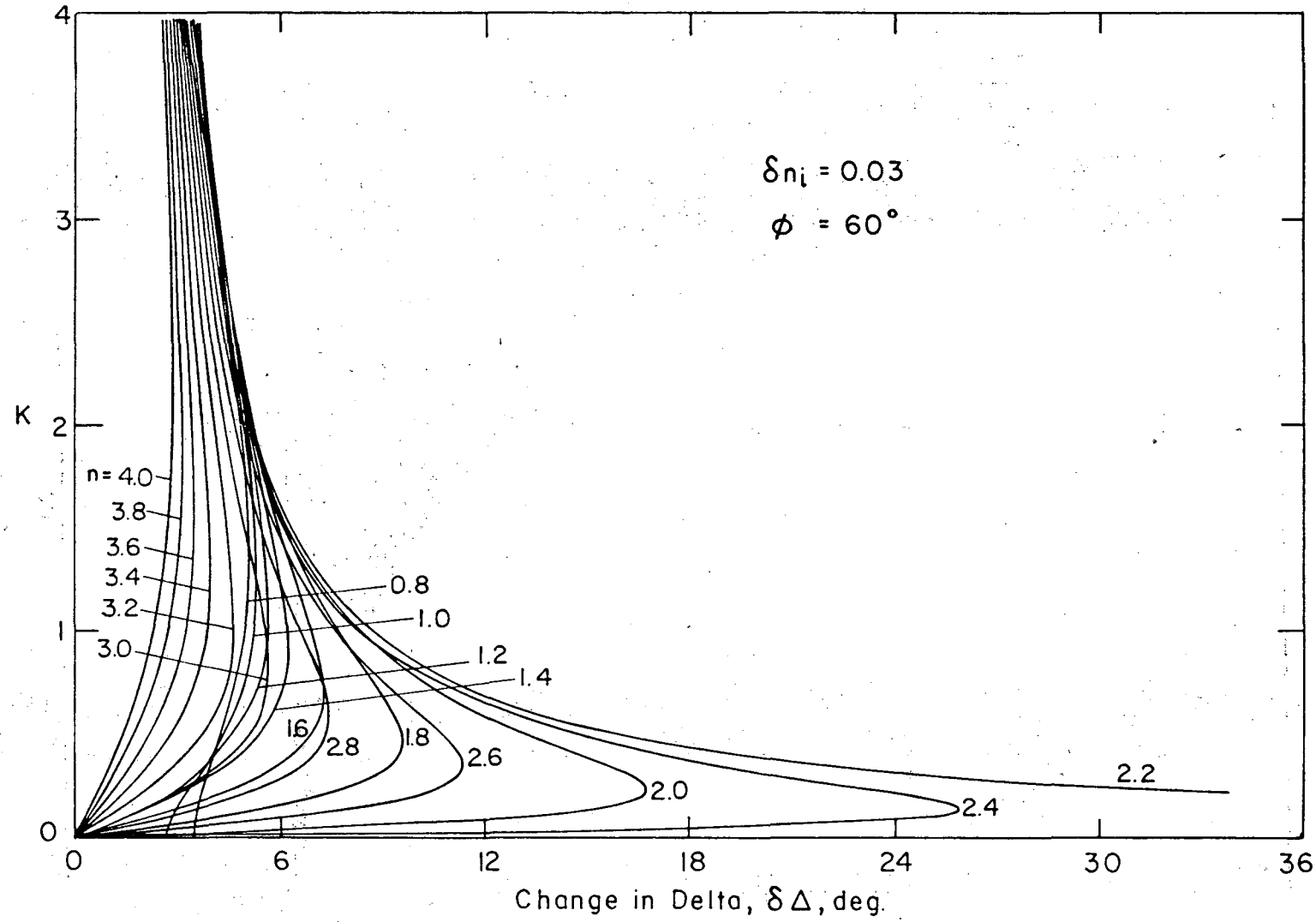


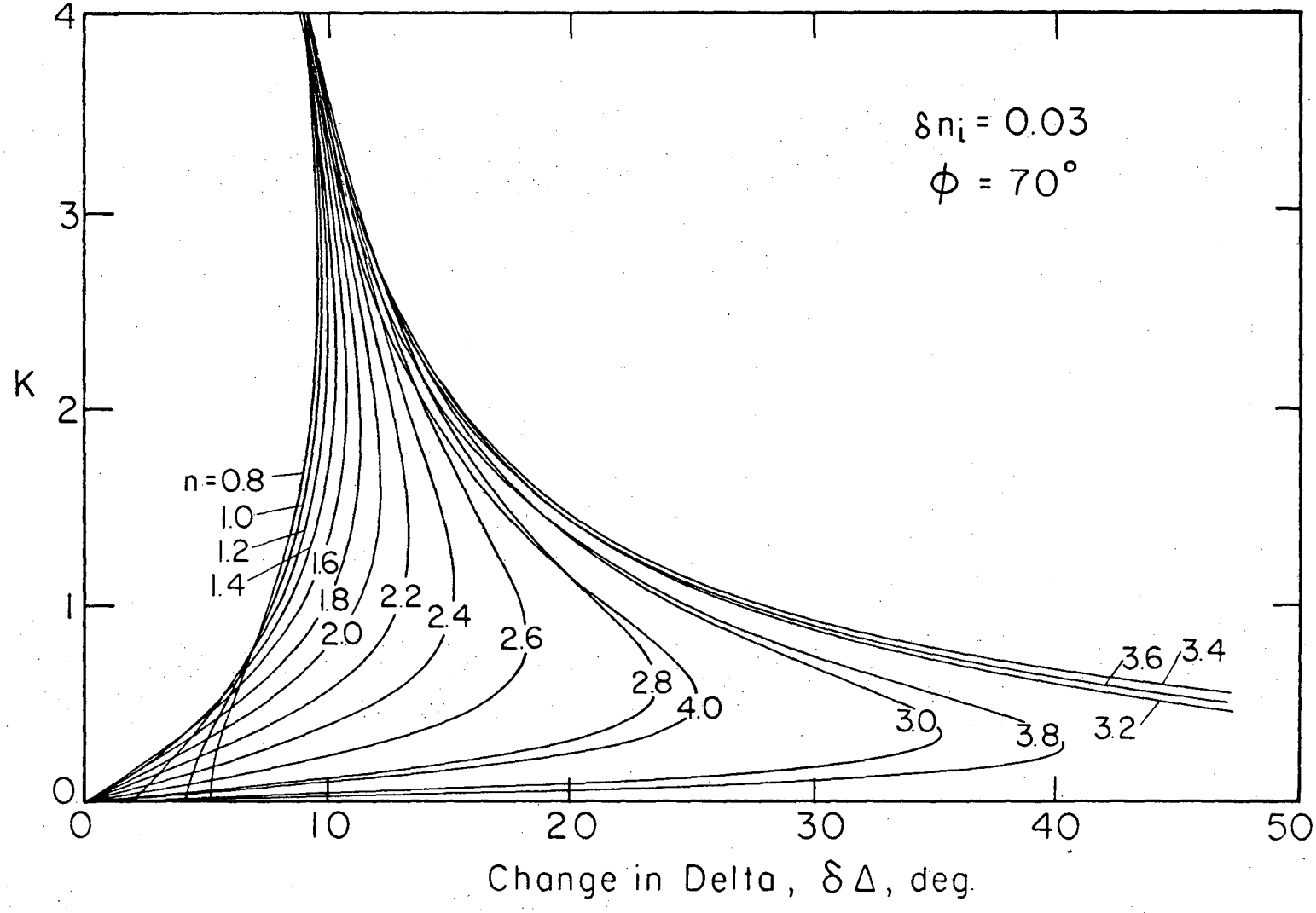

Fig. 13. As in Fig. 10, $\phi = 80°$, $\delta n_i = 0.01$.

0 0 0 4 5 0 4 6 9 5



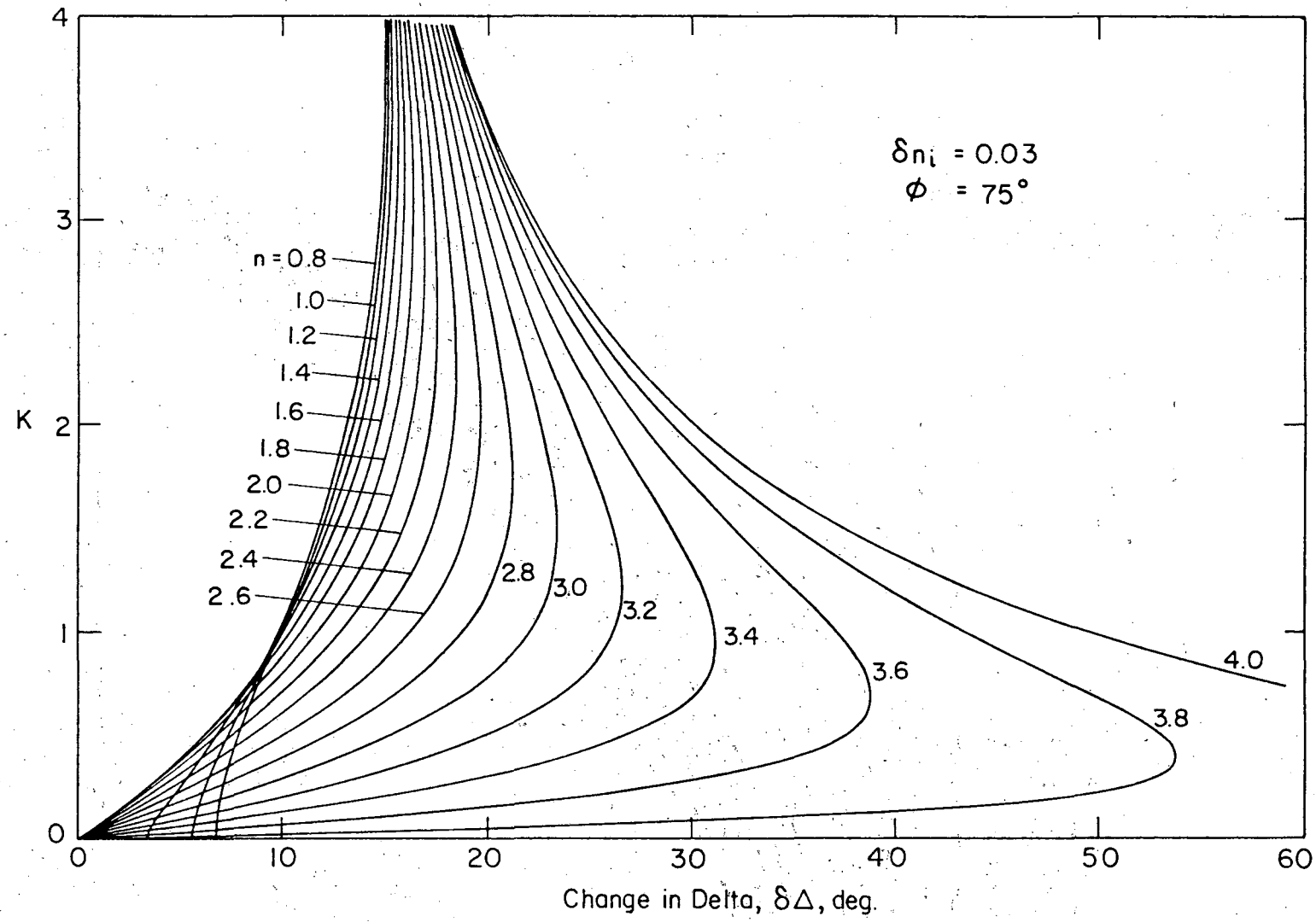

XBL 758-6904

Fig. 14. As in Fig. 10, $\phi = 60°$, $\delta n_i = 0.03$.




XBL 758-6883

Fig. 15. As in Fig. 10, $\phi = 70°$, $\delta n_i = 0.03$.

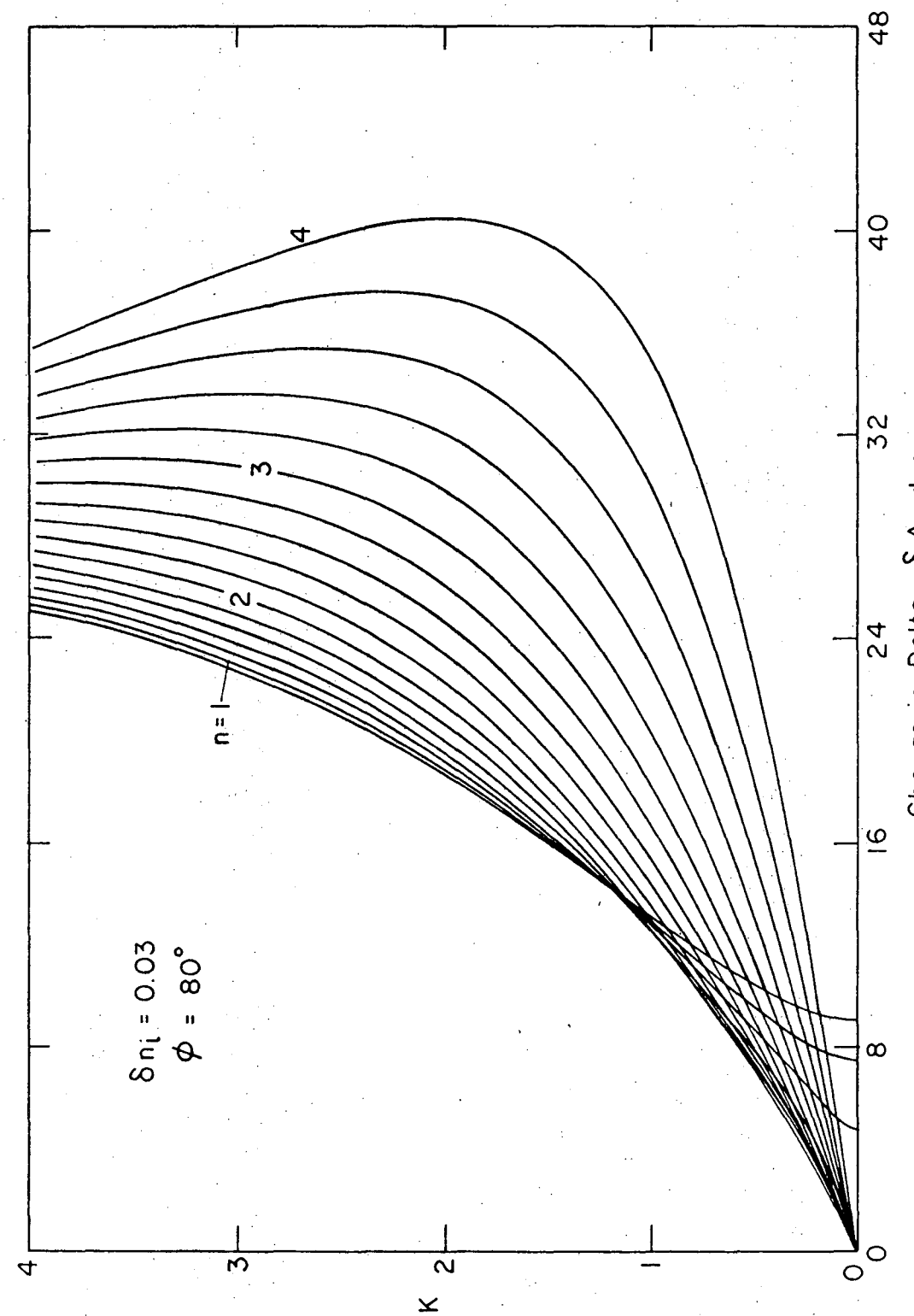



XBL758-6906

Fig. 16. As in Fig. 10, $\phi = 75°$, $\delta n_i = 0.03$.

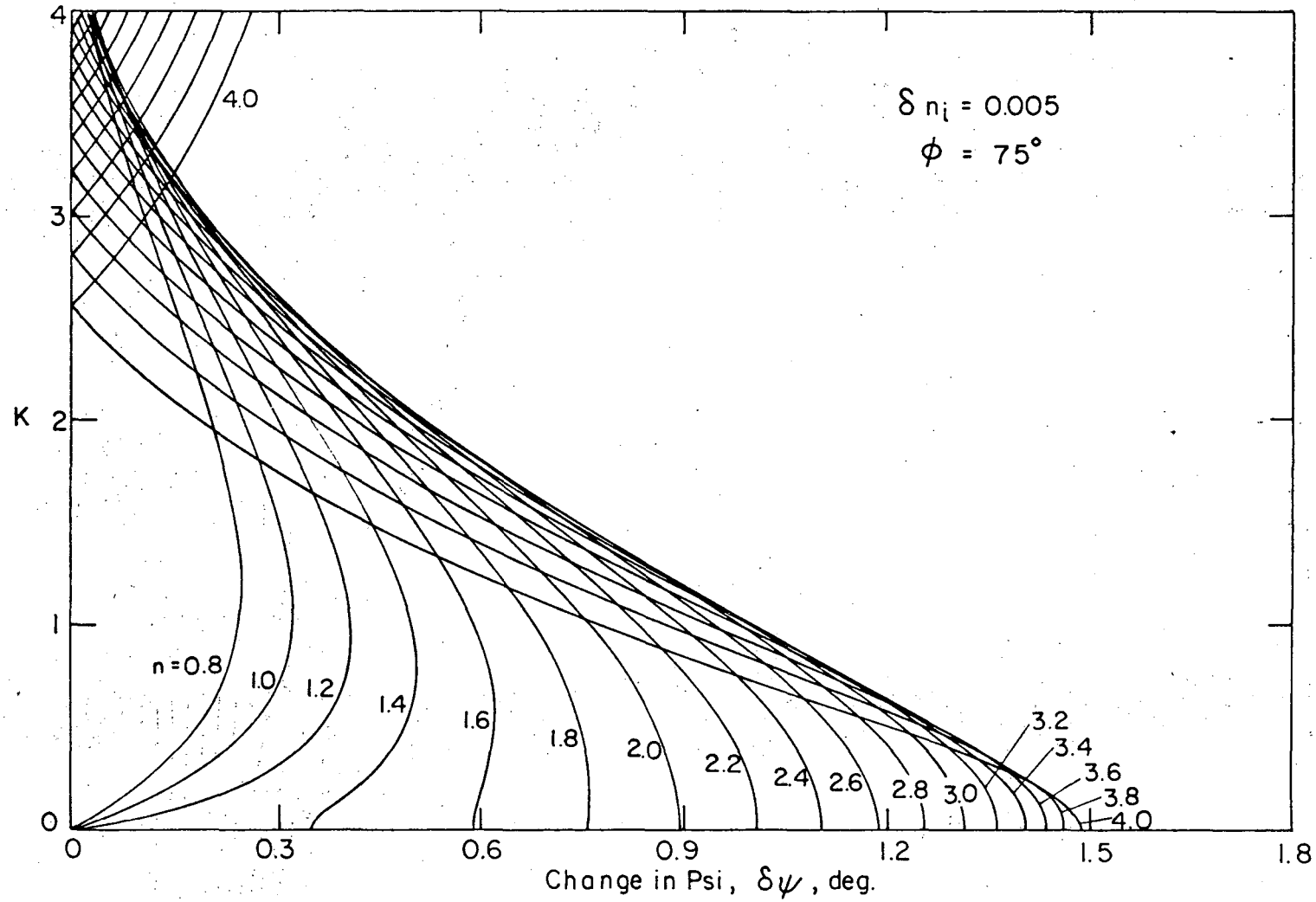


0 0 0 4 3 0 4 9 9 6




XBL 758-6908

Fig. 17. As in Fig. 10, $\phi = 80°$, $\delta n_i = 0.03$.




XBL 758-6893

Fig. 18. Dependence of the change in $\psi$ due to anodic boundary layer on the substract refractive index n - ik. Thick film limit, bulk fluid refractive index $n_b$ = 1.3345. The angle of incidence $\phi$ = 75°, the refractive index difference $\delta n_i$ = 0.005.



0 0 0 4 3 0 4 9 6 7

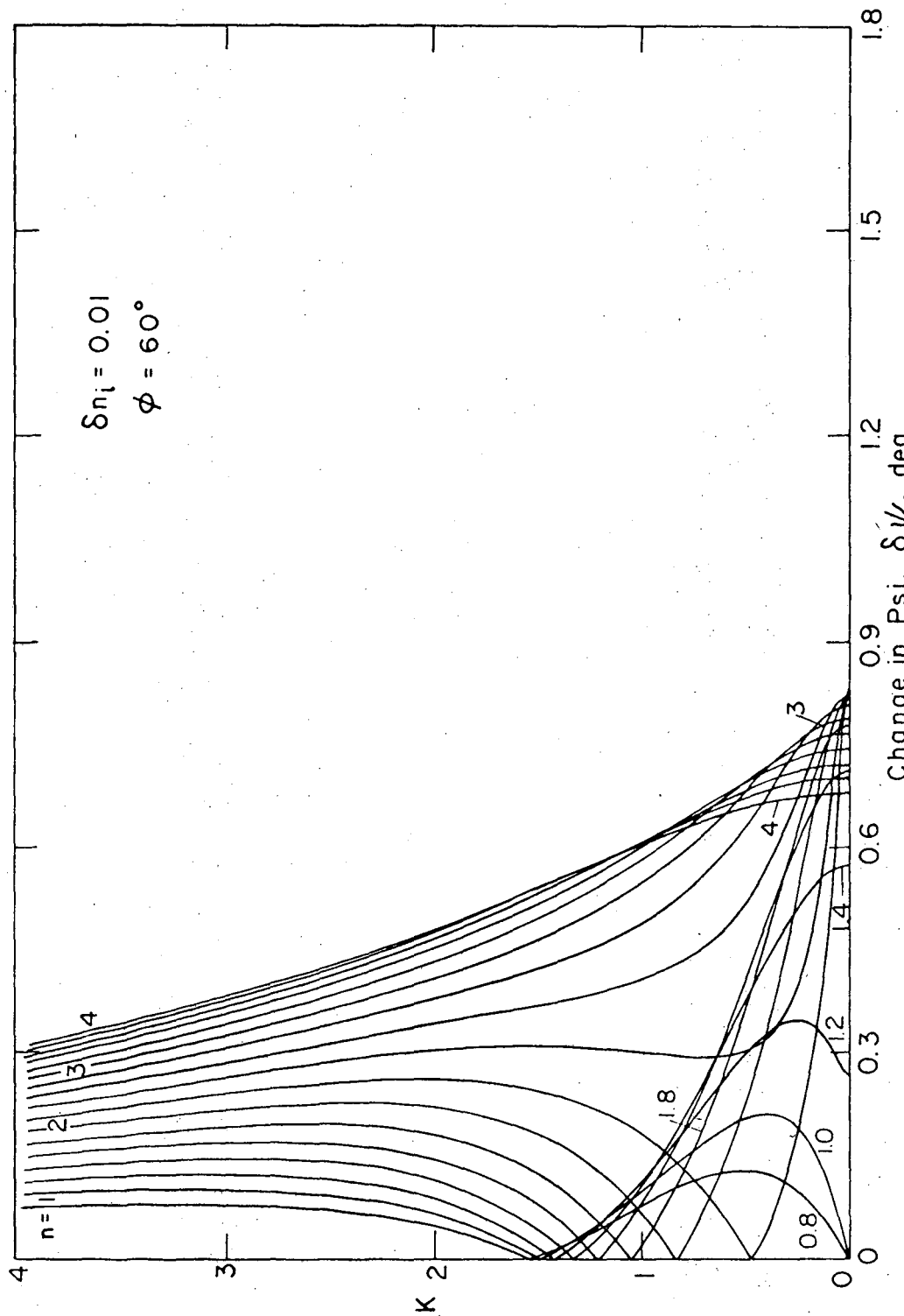



Fig. 19. As in Fig. 18, $\phi = 60°$, $\delta n_i = 0.01$.

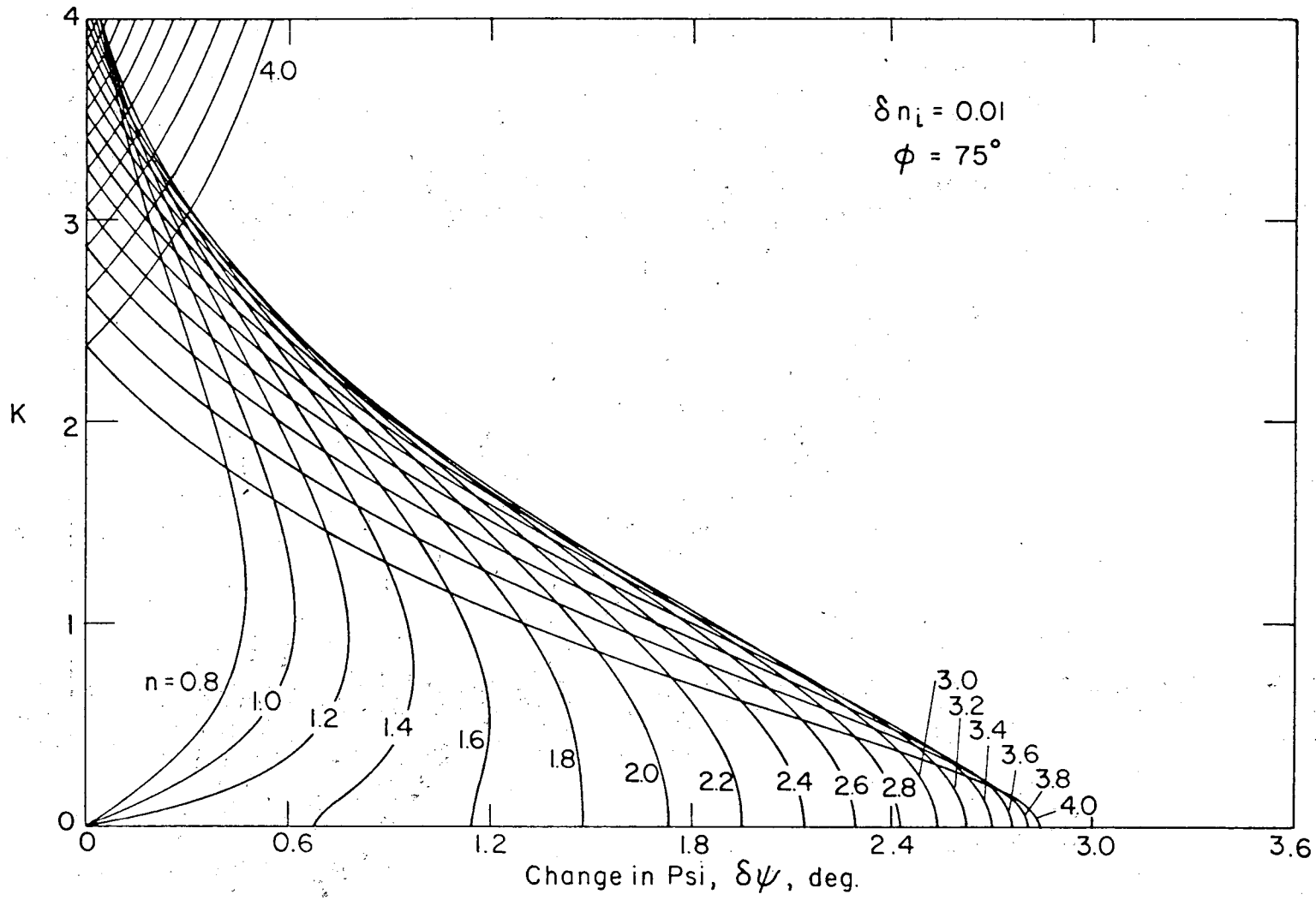
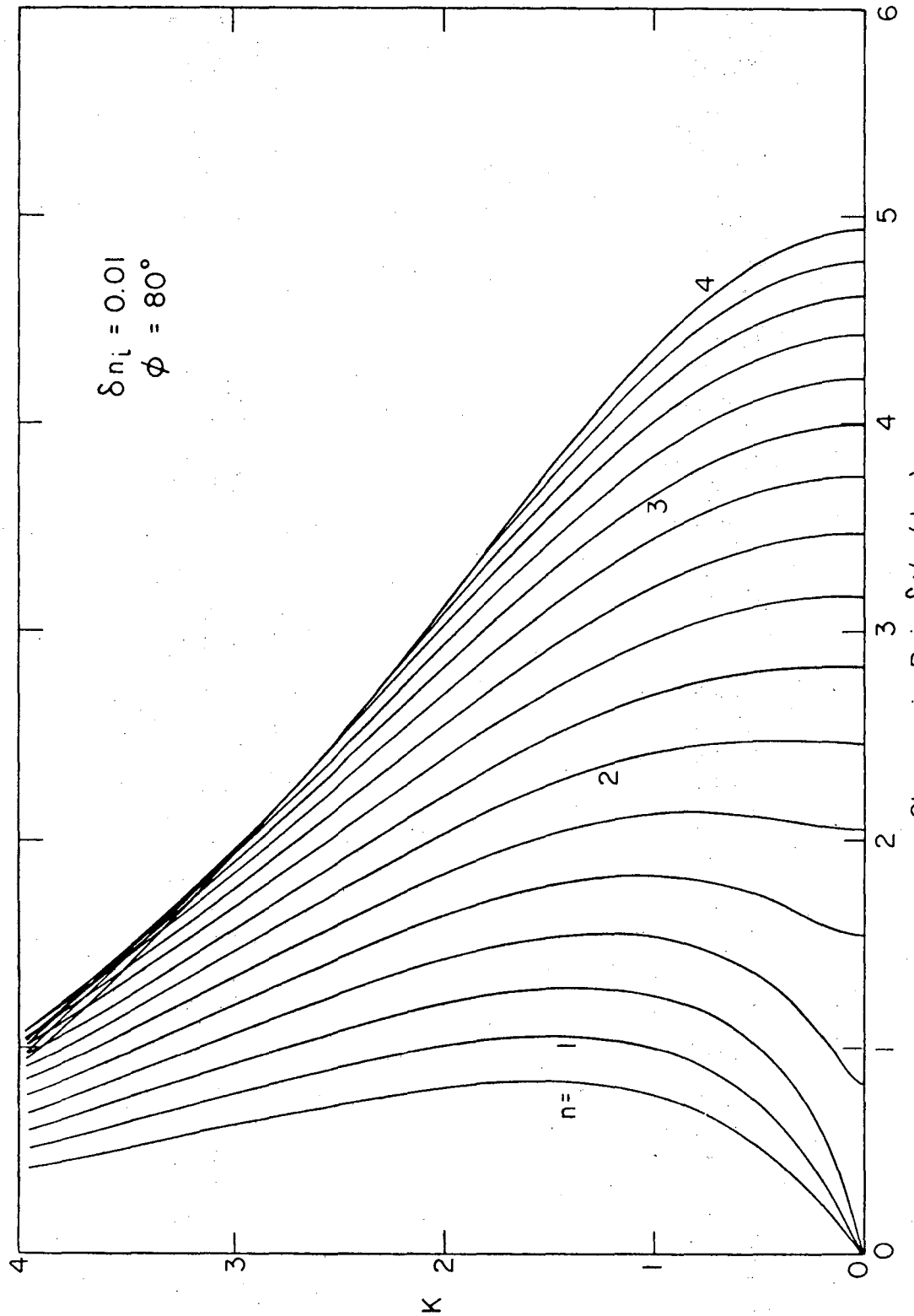



Fig. 20. As in Fig. 18, $\phi = 75°$, $\delta n_i = 0.01$.

XBL 758-6899



0 0 0 4 3 0 4 9 9 8




XBL 758-6901

Fig. 21. As in Fig. 18, $\phi = 80°$, $\delta n_i = 0.01$.

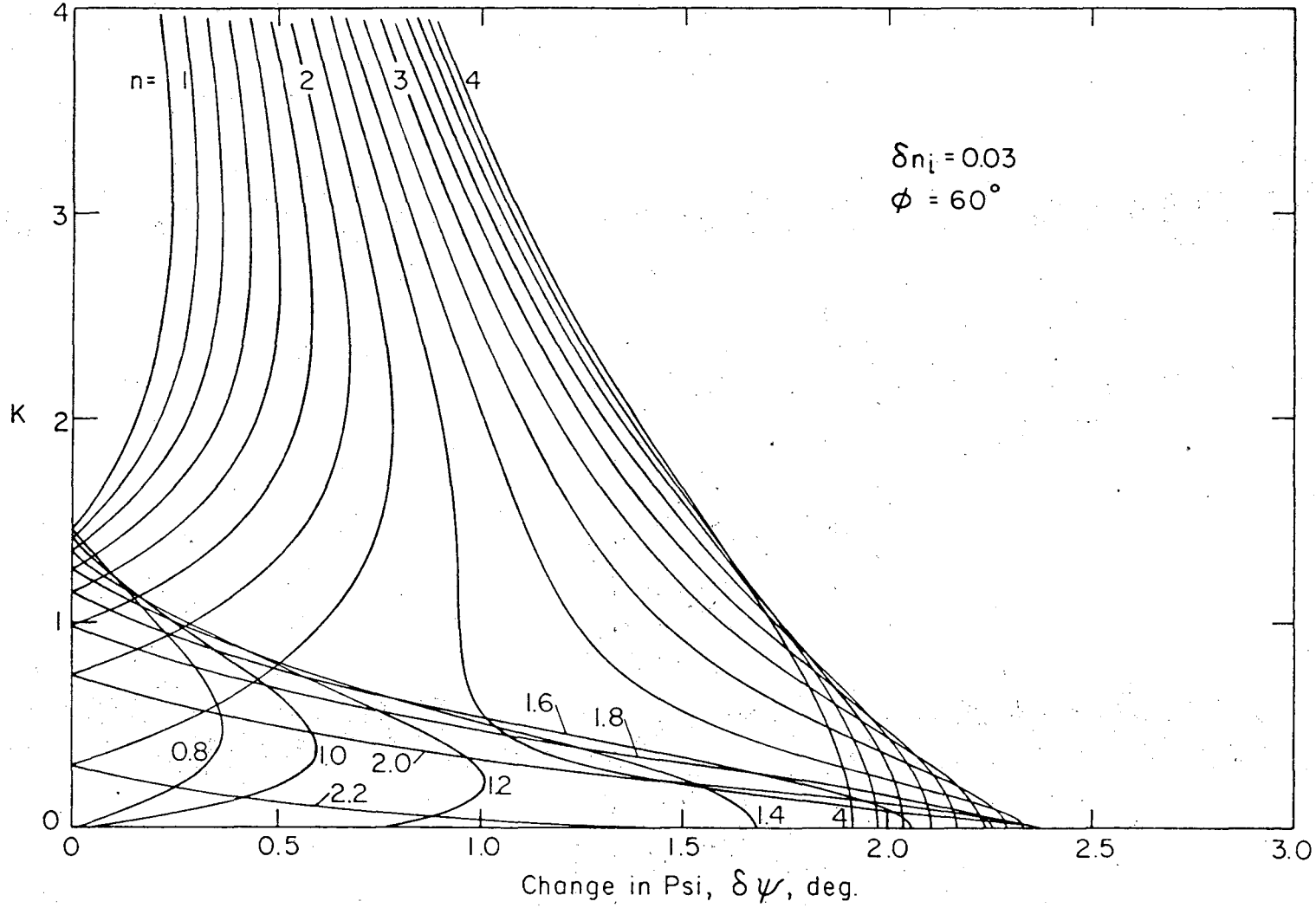



Fig. 22. As in Fig. 18, $\phi = 60°$, $\delta n_i = 0.03$.

XBL 758-6903



0 0 0 4 3 0 4 9 9

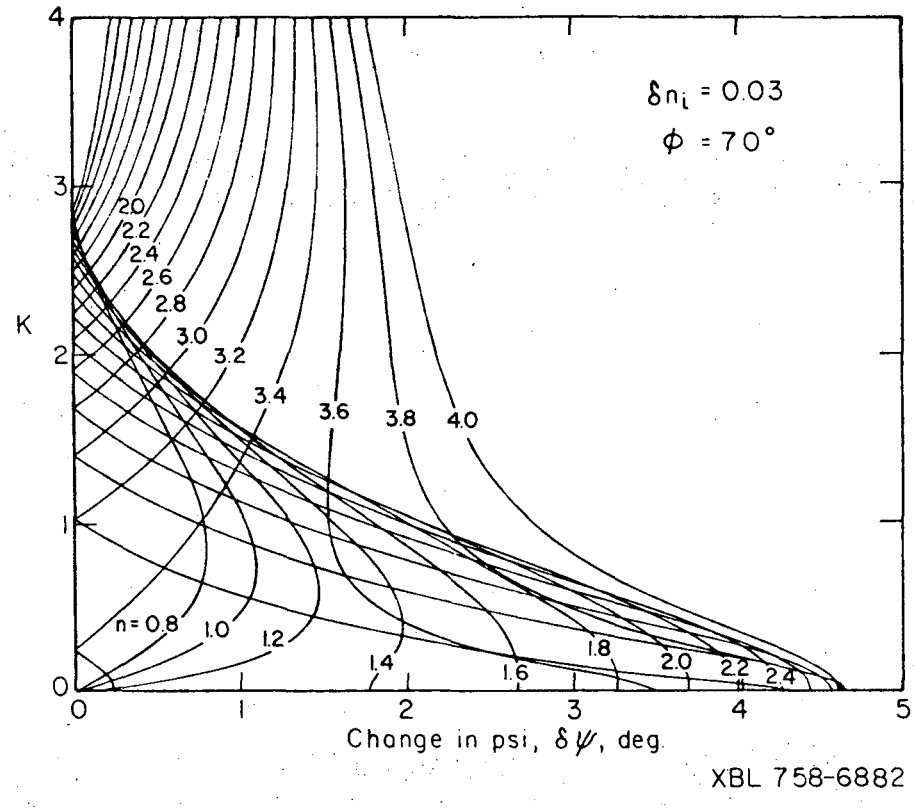



Fig. 23. As in Fig. 18, $\Phi = 70°$, $\delta n_i = 0.03$.

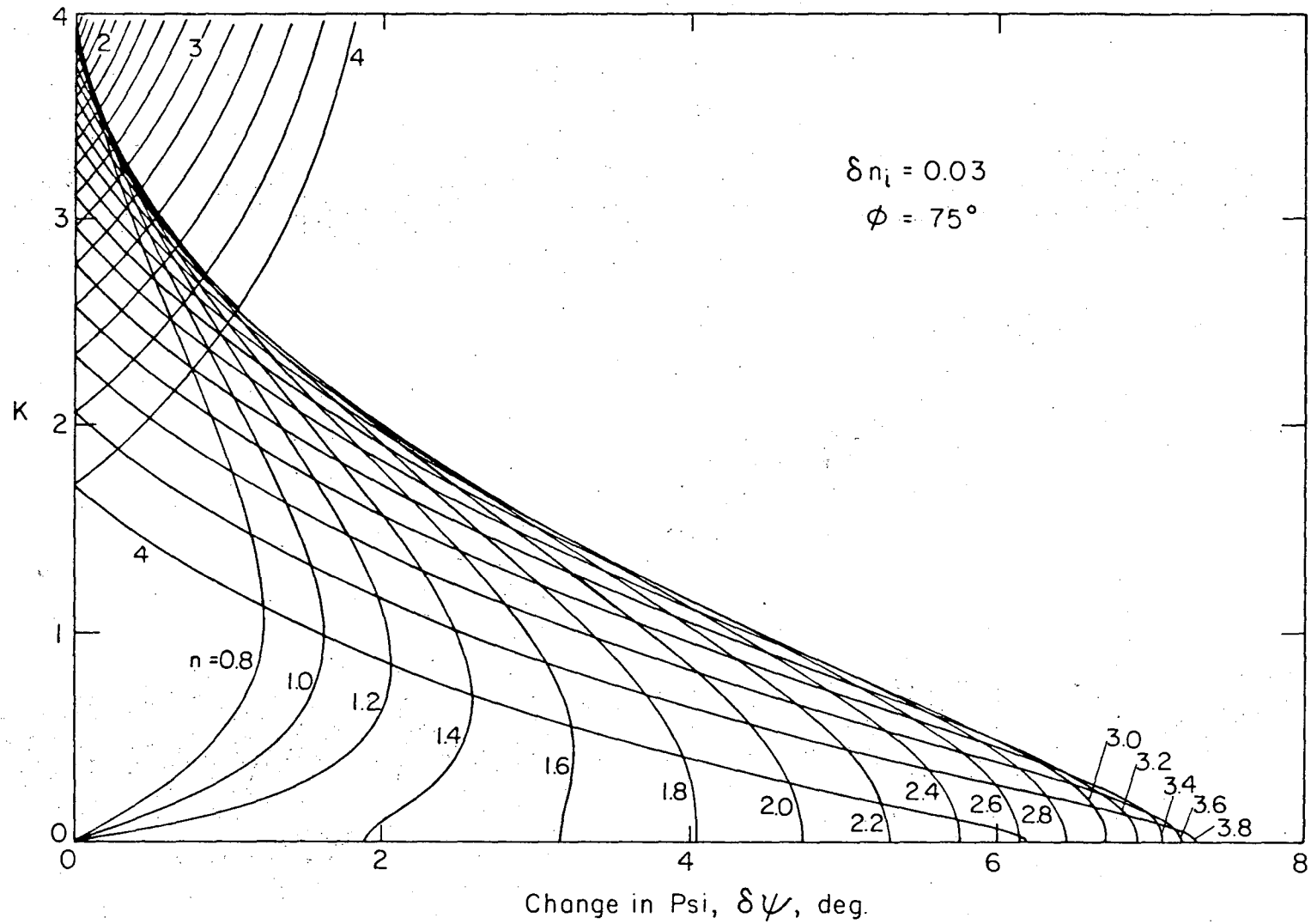
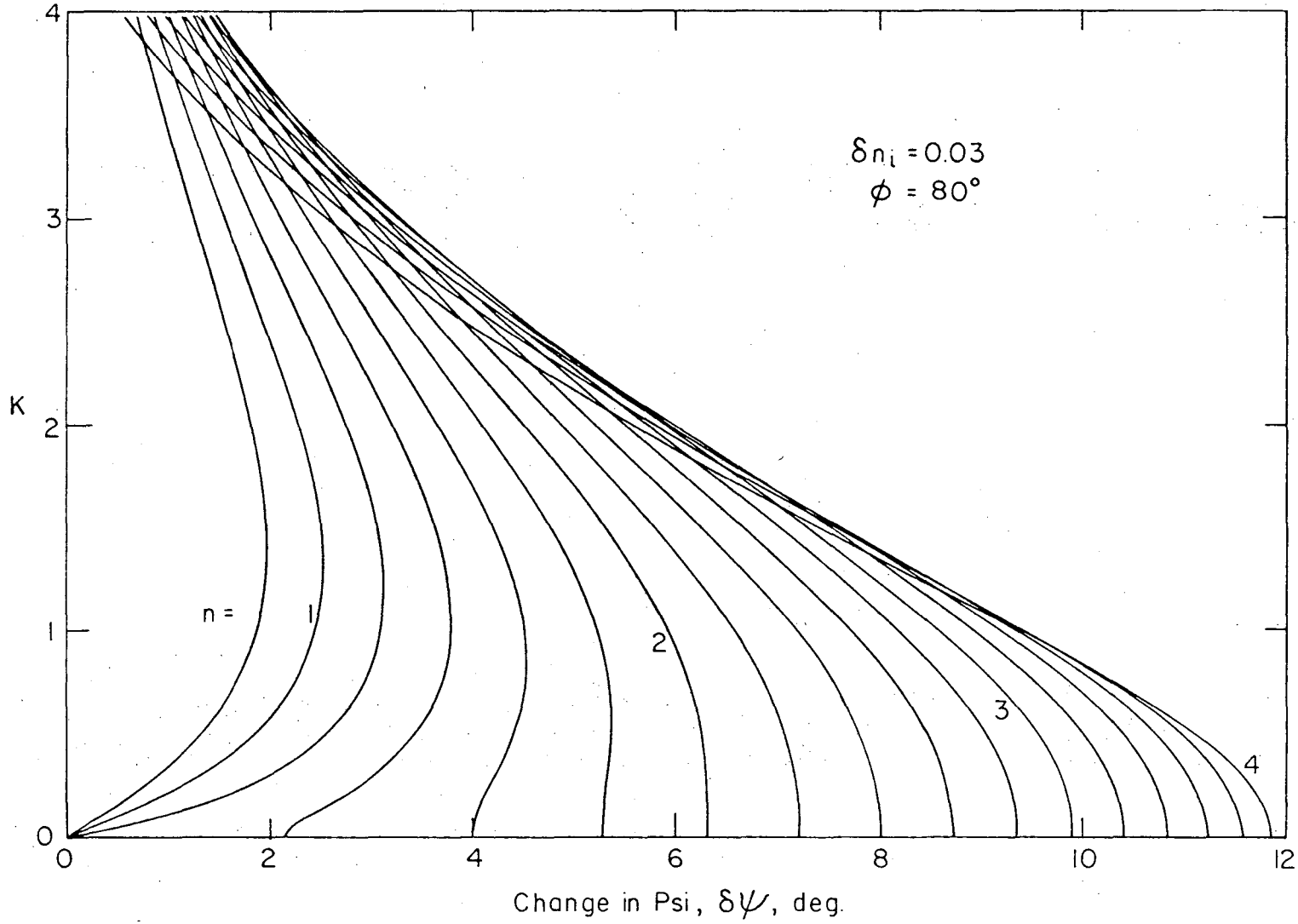



Fig. 24. As in Fig. 18, $\phi$ = 75°, $\delta n_i$ = 0.03. XBL758-6905

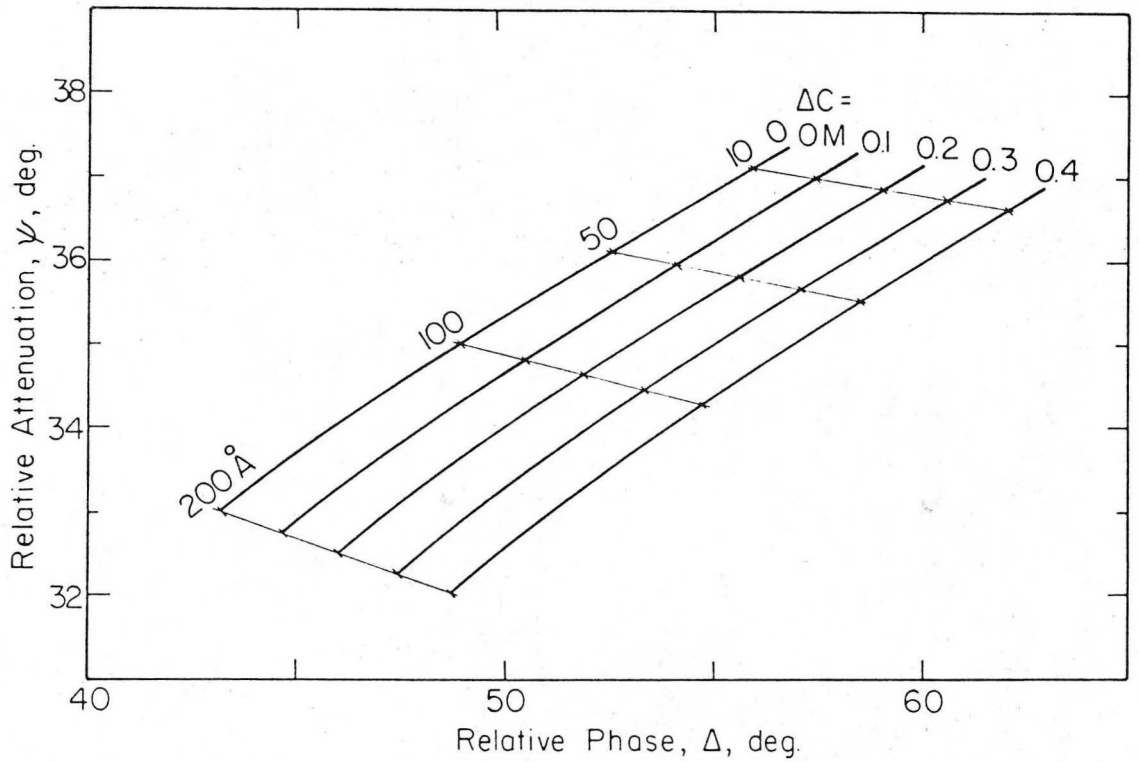


0 0 0 4 3 0 3 0 0 0




XBL 758-6907

Fig. 25. As in Fig. 18, $\phi = 80°$, $\delta n_i = 0.03$.




XBL 758-6884

Fig. 26. Effect of mass-transport boundary layer on observation of growing oxide film. Thick film limit, $\Delta C$ is change in $CuSO_4$ from bulk fluid value of 0.1 M. Porous $Cu_2O$ film of indicated thickness (n = 2.06-1.55i), on Cu(n = 0.94-2.24i).



0004300501

Table III. Errors in the optical constants of Cu substrate and $Cu_2O$ film caused by neglecting the mass-transport boundary layer. (Thick-film limit, $\phi$ = 75°).

| | Film Refractive Index, $n_{cs}$ | | | | |
|---|---|---|---|---|---|
| Thickness, Angstroms | $\delta c$ = 0 M | 0.1 M | 0.2 M | 0.3 M | 0.4 M |
| 0 | 0.94-i2.24 | 0.96-i2.33 | 0.99-i2.43 | 1.01-i2.52 | 1.03-i2.60 |
| 5 | 2.06- 1.55 | 2.05- 1.85 | 2.05- 1.40 | 2.15- 1.52 | 2.00- 1.85 |
| 10 | | 2.05- 1.75 | 2.05- 1.55 | 2.15- 1.70 | 2.00- 1.84 |
| 20 | | 2.05- 1.65 | 2.05- 1.60 | 2.10- 1.70 | 2.00- 1.82 |
| 50 | | 2.05- 1.58 | 2.05- 1.62 | 2.05- 1.70 | 2.00- 1.77 |
| 100 | | 2.05- 1.54 | 2.05- 1.62 | 2.05- 1.70 | 2.10- 1.77 |
| 200 | | 2.05- 1.54 | 2.06- 1.60 | 2.10- 1.67 | 2.10- 1.73 |

0 0 0 0 4 3 0 5 0 0 2



2.10-1.77i compared to the true value of 2.06-1.55i. With the true optical constants for film and substrate, a film thickness could not be derived from the measurement.

# V. EXPERIMENTS

Experimental observations of the effect of boundary layers on ellipsometer measurements have been made for comparison to theoretical predictions. Boundary layers have been generated by the electrochemical deposition and dissolution of copper from aqueous copper sulfate. Measurements have been conducted for pure diffusion, convective diffusion, and natural convection.

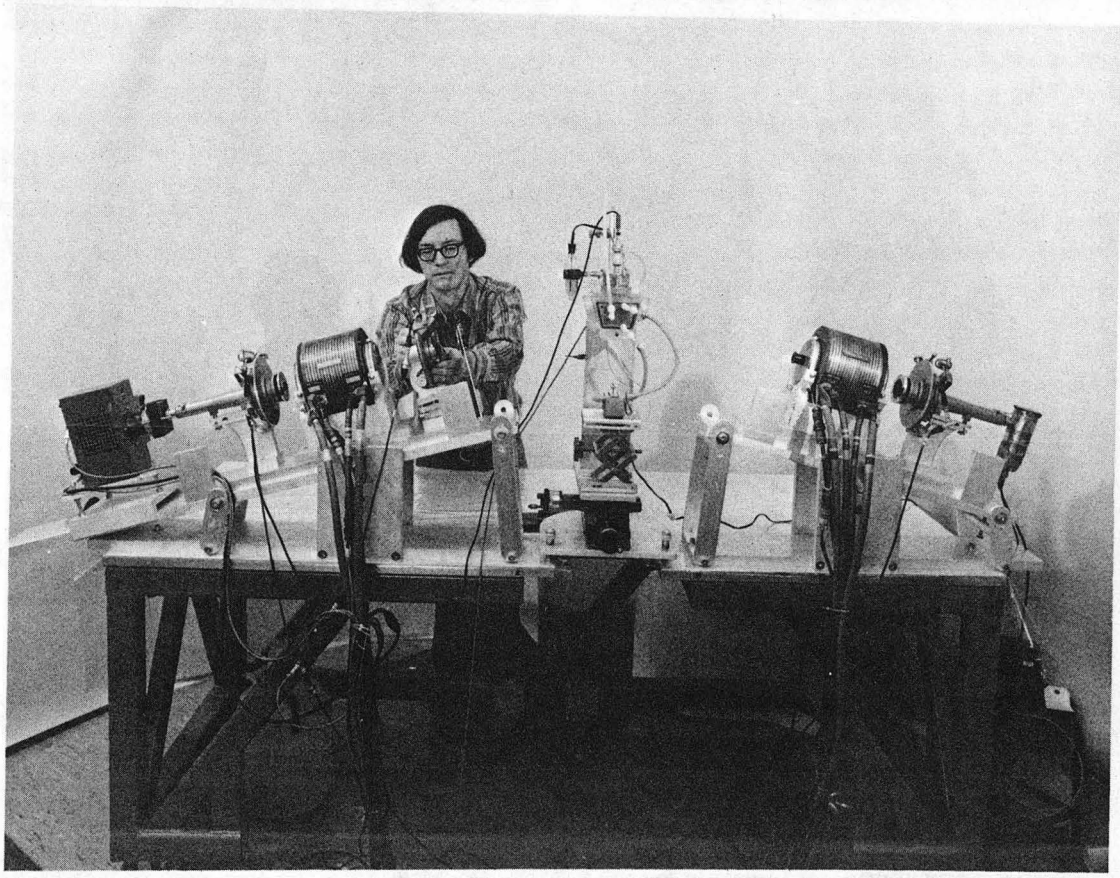
## A. Apparatus

An automatic ellipsometer[12] was used to conduct the measurements. The instrument is of the self-compensating type, and employs Faraday cells to rotate the plane of polarization of light at 546.1 nm wavelength. From the degree of rotation, the change in relative phase and amplitude are derived. Figure 27 shows the arrangement of the ellipsometer to allow observation of convection-free Cu deposition. The same arrangement was used for observation with natural convection during Cu dissolution. Alignment to a 75° angle of incidence was achieved through auto-collimation of a beam directed through the optical axis and reflected from an accurately cut prism mounted at the specimen location. The mechanical design of the support for the optical train allows the compounds to remain securely locked in position to maintain alignment.

Figure 28 shows a close-up of the optical cell housing the electrode being observed. The light enters and leaves the cell windows at normal incidence. The working electrode is directed face-down. For alignment purposes, the cell is mounted on a coordinate table giving x-y translations. The coordinate table is mounted on an adjustable

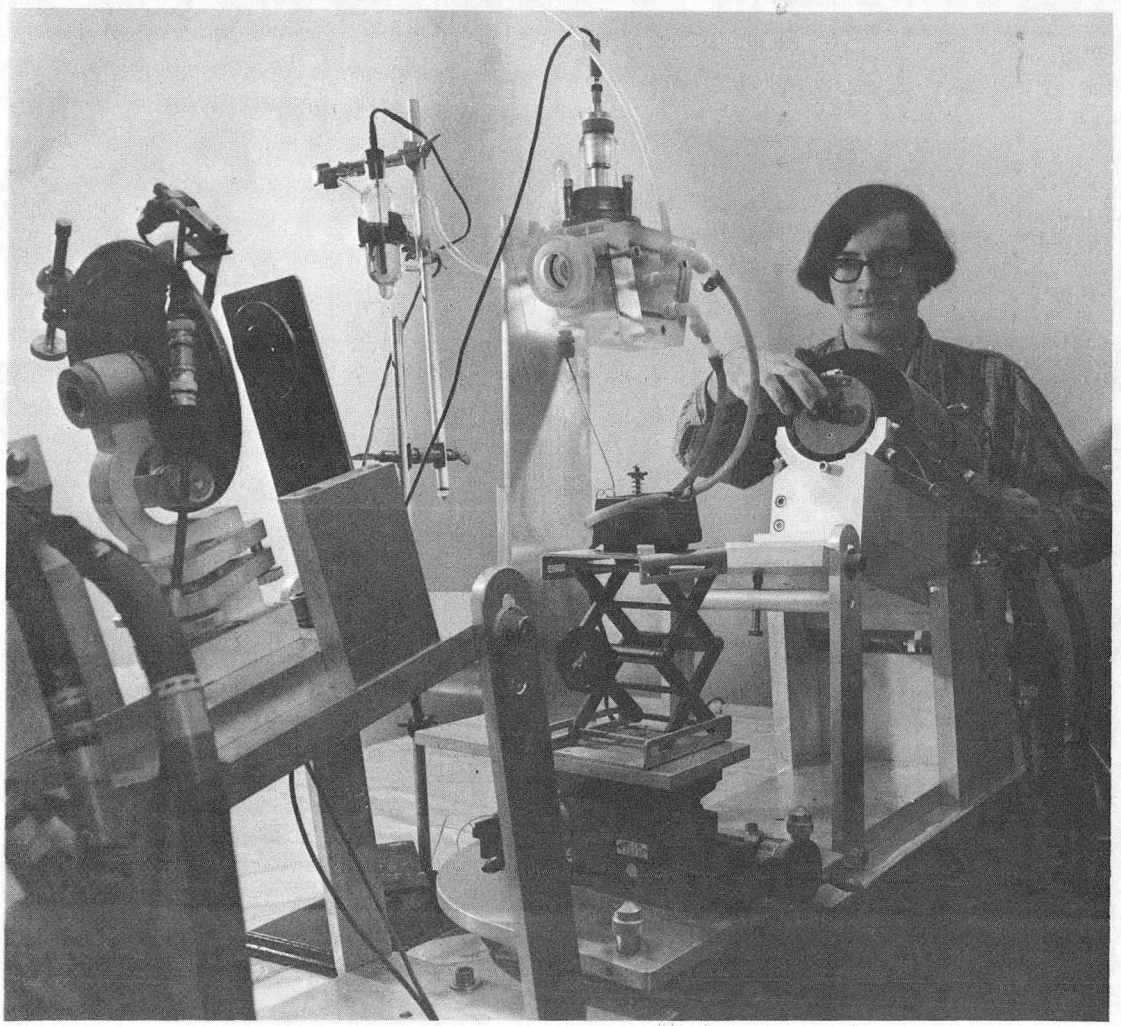
0 0 0 0 4 3 0 5 0 0 3





CBB 7510-7285

Fig. 27. Arrangement of ellipsometer components for the observation of convection-free Cu deposition from $CuSO_4$.



CBB 7510-7287

Fig. 28. Close-up of cell for convection-free diffusion experiments, showing reference electrode and liquid-circulating pump.

0 0 0 0 4 3 0 5 0 0 4



tripod base to give 3-dimensional rotations. The cell has four additional openings, as depicted in Fig. 29: (1) a capillary tube for the reference electrode; (2) a mount for filter medium used to bubble nitrogen gas for the removal of dissolved $O_2$ from the solution; and (3), (4) inlet and outlet for a "vibrostatic" pulsation pump used to remove the boundary layer formed in convection-free deposition by stirring the solution.

Forced convection experiments were conducted at 75° angle of incidence with the ellipsometer components mounted horizontally. The electrode was held vertically in a cell (Fig. 30) constructed to allow suitable entrance length to obtain fully-developed flow, as shown in Fig. 31. Alignment used the same autocollimation technique. Gravity feed supplied the electrolyte flow, which was measured with a rotameter.

## B. Specimen Preparation

The electrodes are Cu specimens with approximately 1×3 cm active surface. Polycrystalline samples fit in a cylindrical acrylic holder which mounts in the optical cell. The electrodes are detachable to allow study by scanning electron microscopy. "Kynar" has been used to electrically insulate the sides of the electrodes.

Single-crystal electrodes were also used for study. The electrodes were cut by electrochemical machining from two sources of copper single crystals: (1) crystals were grown by the author in a carbon mold from high-purity copper using the Bridgeman technique; (2) a crystal (notebook number 5935-34220) grown by T. Kosel using the same technique. The crystals were cast in epoxy due to their irregular

Fig. 29. Cross-section of stagnant solution cell.

A cell body

B observed electrode approximately 1×3 $cm^2$ area

C body for electrode (acrylic, exchangeable)

D electrical connection to electrode (chrome-plated brass)

E O-ring seal

F adjustable body for controlling electrode depth (chrome-plated brass)

G sealing nut for electrode body (aluminum)

H washer (Teflon)

I O-ring for electrode body (silicone rubber)

J holder for electrode body (polypropylene)

K screws for attaching holder to cell body

L O-ring seal for holder

M frame for window (acrylic, glued to cell body)

N sealing nut for window (acrylic)

O support for counter electrode (acrylic); also position for diaphram

P counter electrode, copper

Q O-ring for cell window

R cell window

S pressure sleeve for cell window

T screws for attaching fourth side

U O-ring seal for fourth side

0 0 0 0 4 3 0 5 0 0 5



Fig. 29. Cont.

| | |
|---|---|
| 1 | capillary outlet for reference electrode |
| 2 | outlet for sparging $N_2$ |
| 3 | pump outlet |
| 4 | pump inlet |
| 1-4 | in fourth side above cross section |

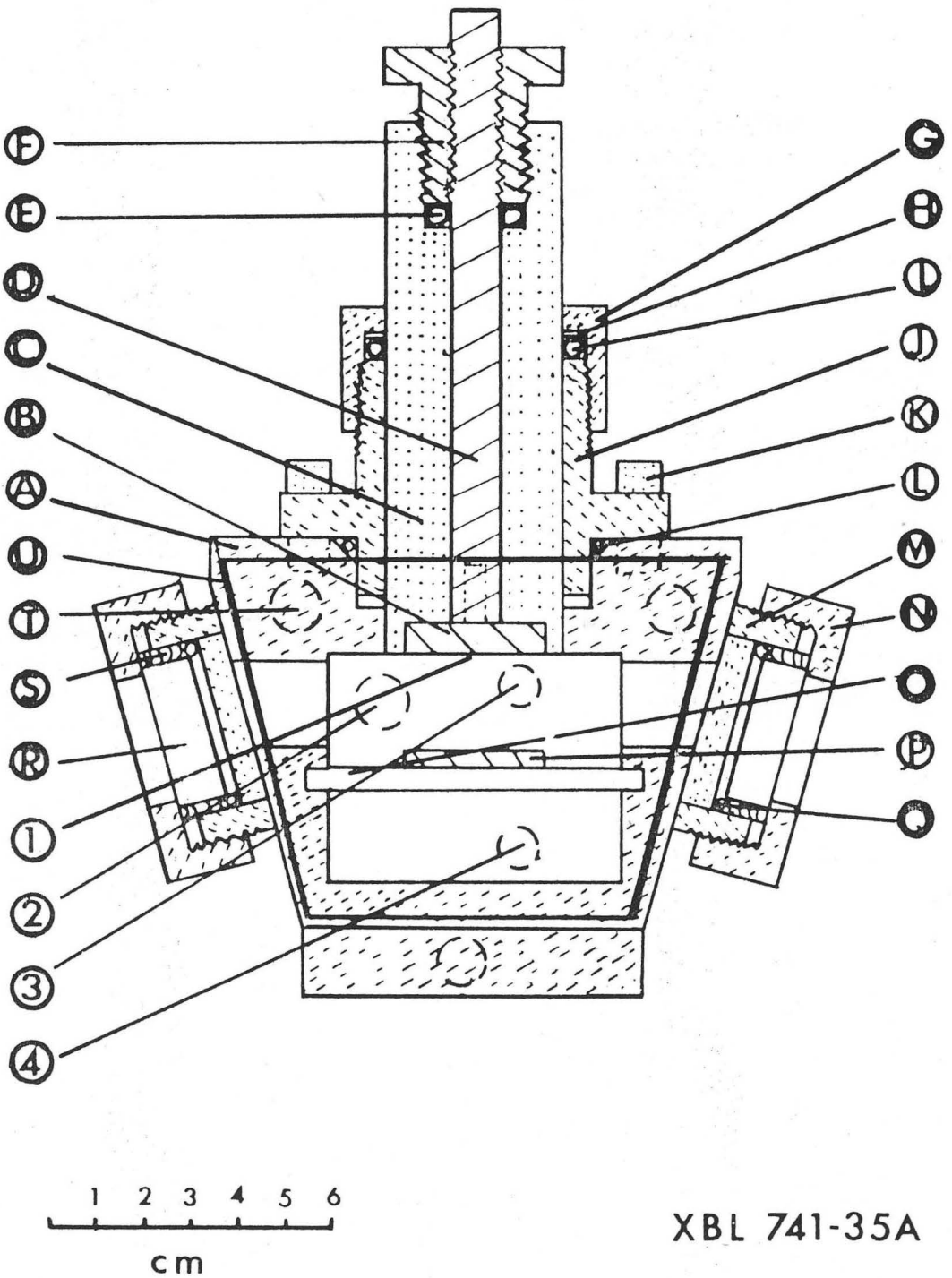



Fig. 29

0 0 0 0 4 3 0 5 0 0 6



Fig. 30. Cell for forced convection experiments. Taken from Ref. 35.

A body of flow channel (acrylic resin)

B observed electrode (anode), 1.2×3 cm area

C body for observed electrode (cast epoxy, exchangeable)

D electrical connection for observed electrode (brass, silver-soldered to electrode)

E sealing nut for electrode body (polypropylene)

F washer (Teflon)

G O-ring for electrode body (silicone rubber)

H holder for electrode body (polypropylene)

I screws to attach observed electrode with holder to flow channel

J O-ring seal for electrode holder

K counter electrode (cathode), 0.9×2.5 cm area (314 stainless)

L sealing material for rectangular counter electrode in round cavity (epoxy resin)

M stem for counter-electrode (stainless, silver-soldered)

N O-ring seal for counter electrode

O acorn nut with electrical connection for counter electrode (stainless)

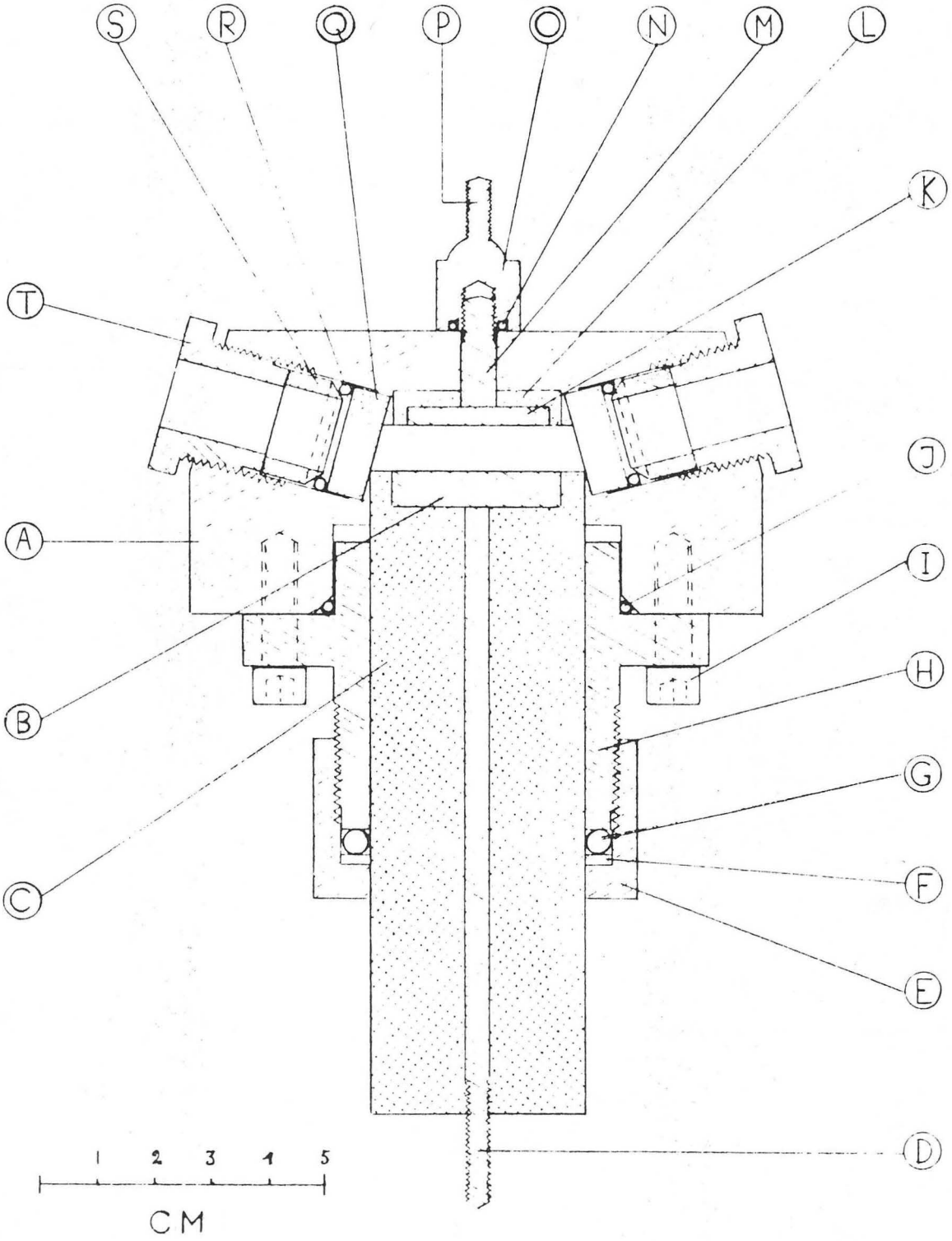
P electrical connection for counter-electrode

Q cell window (plate glass, 0.25 in. thick, 0.7 in. diam.)

R O-ring for cell window

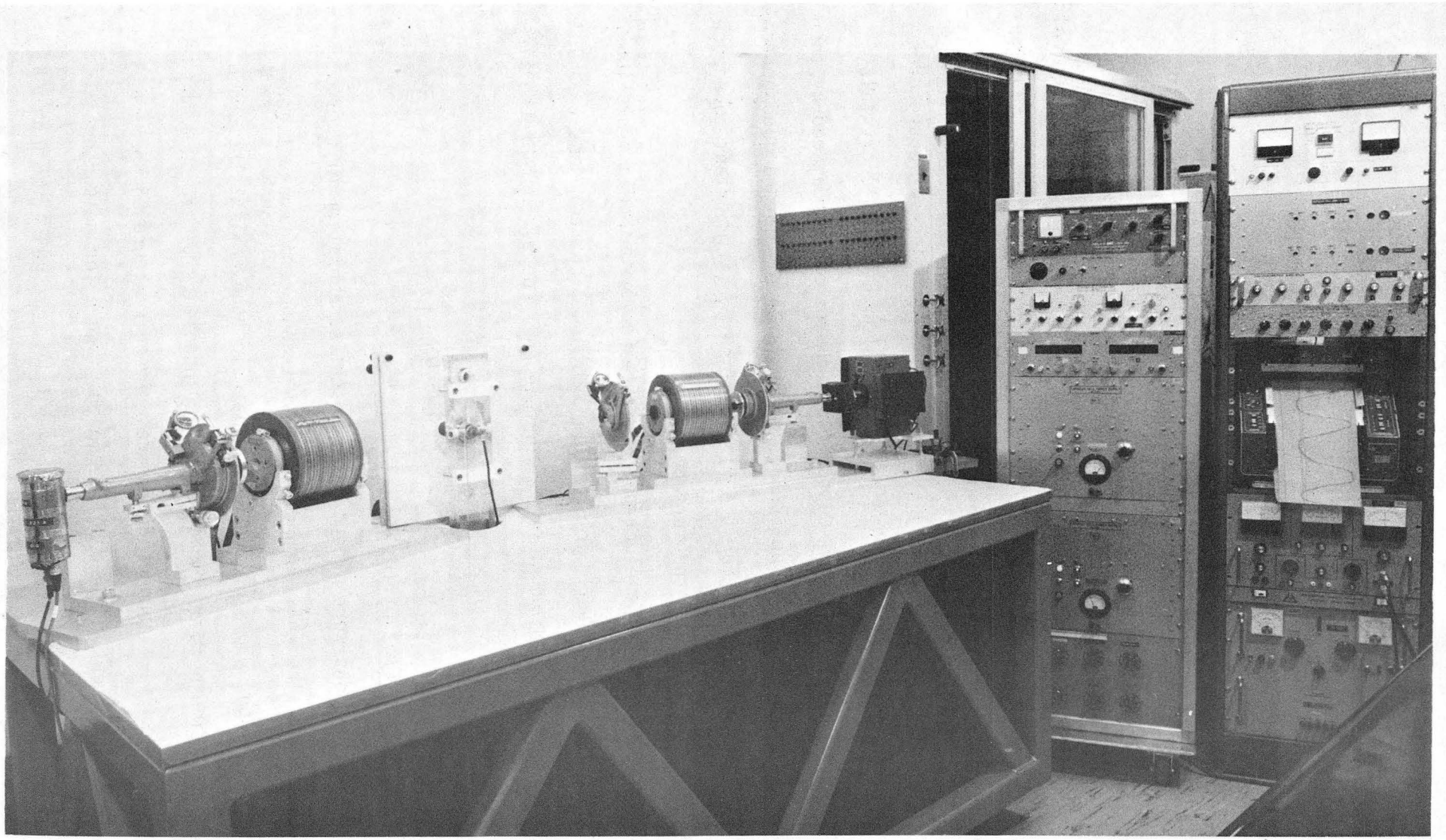
S pressure sleeve for cell window (PVC)

T sealing nut for cell window (brass)




XBL 741-34

Fig. 30



XBB 737-4396

Fig. 31. Horizontal orientation of ellipsometer components for forced-convection experiments.

0 0 0 0 4 3 0 5 0 5 3 9 7

shapes resulting from cutting. X-ray diffraction was used to determine the orientation of crystals for cutting, as well as for developing a mechanical polishing technique to minimize surface damage in the crystal. Figure 32 shows the acrylic electrode holder, a polycrystalline electrode, a single crystal (mounted in epoxy), and an electrochemical machining tool used to cut crystals. The tool descends vertically to expose a planar surface of the desired orientation.

The electrodes were polished mechanically using various grades of abrasive, down to a 1μ diamond paste. For the single crystals, controlled electrochemical dissolution removes layers damaged by the roughest abrasives. Re-polishing at the 1μ level gives a good optical finish. A clean wheel for the final polishing is important to reduce lattice distortion of the surface layers.

Prior to use, the electrodes are cleaned by cathodic evolution of hydrogen in 1 M NaOH for 3 min at 300 $mA/cm^2$ current density. This removes organics adsorbed on the surface and reduces much of the air-formed oxide.

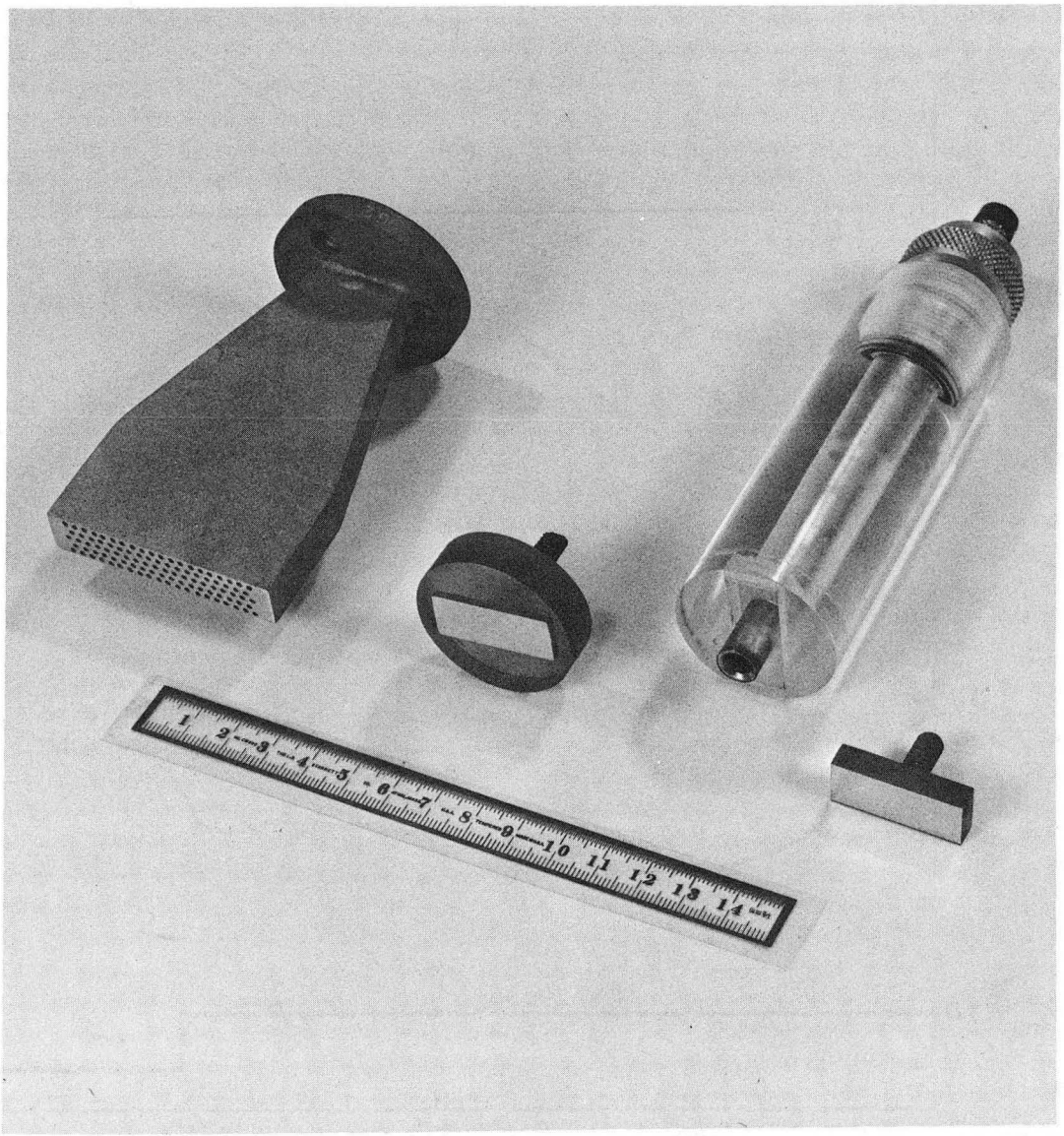
## C. Procedure

### 1. Convection-Free Diffusion

Observations were made of galvanostatic deposition of Cu from 0.2 M $CuSO_4$. The influence of the mass-transport boundary layer was determined by mixing the solution inside the cell at the end of the deposition period. This method was necessary to overcome the effects of surface changes during deposition. Figure 33 shows a typical experiment. The baseline in the figure for measuring $\delta\Delta$ was verified by observing $\Delta$ and $\psi$ remaining constant after current

0 0 0 0 4 3 0 5 0 0 8





XBB 7510-7340

Fig. 32. From left-to-right, electrochemical machining tool for cutting single crystals, Cu single crystal electrode cast in epoxy, acrylic electrode holder, and polycrystalline Cu electrode.

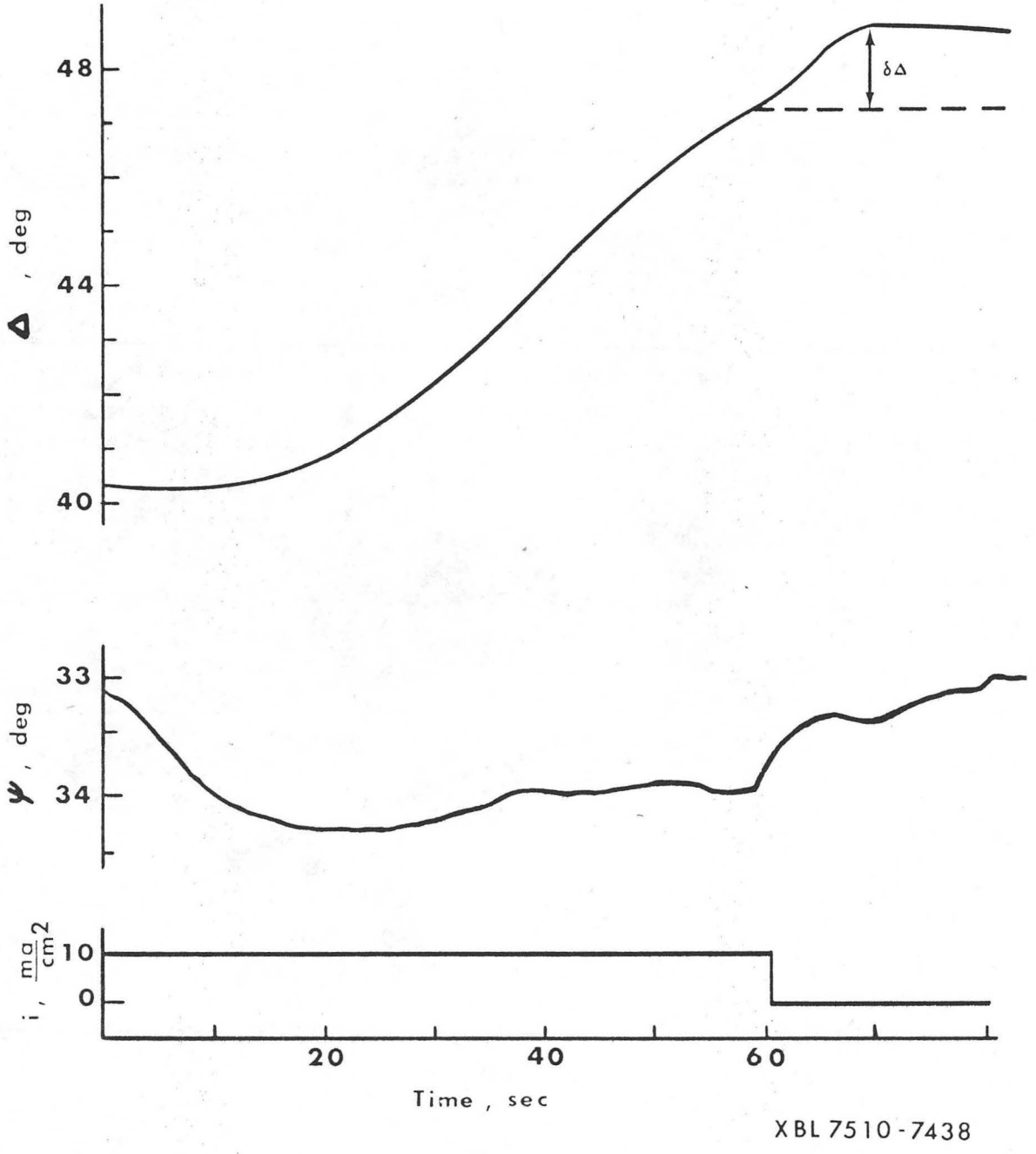



Fig. 33. Experimental observation of cathodic convection-free Cu deposition from 0.2 M $CuSO_4$. Single crystal electrode of dimensions 2.7×1.2 cm.

0 0 0 0 4 3 0 5 0 0 9



interruption when the solution was not mixed.

2. Forced Convection

Convective-diffusion mass-transport boundary layers were generated by potentiostatic deposition and dissolution of Cu from 0.1 M $CuSO_4$. Surface changes due primarily to roughening and oxide formation are again present. These were overcome using a current-interuption technique. Single crystals were used to control surface roughness. They are most effective for dissolution experiments, when their cubic-close packed structure can be retained. However, in the early stages of deposition when the deposit is thin, the single crystals were found to reduce the noise in the ellipsometer measurements. Figure 34 shows the measurement of $\delta\Delta$ and $\delta\psi$ for an electrolyte flow corresponding to Re = 600.

3. Natural Convection

Natural convection experiments were conducted by potentiostatic dissolution of Cu in 0.2 M $CuSO_4$. Single crystals were used, and sufficient time was allowed for steady state to be reached. Figure 35 shows the measurement of $\delta\Delta$. The pump was not necessary to remove the boundary layer. One observation is that the magnitude of the oscillations in $\Delta$ during dissolution agrees with the value of $\delta\Delta$ measured after current interruption.

4. Growth of $Cu_2O$ Films

Observations were made on the anodic dissolution of Cu in 0.1 M $CuSO_4$, accompanied by growth of cuprous oxide films. The convective diffusion case was observed. As shown in Fig. 36, copper was deposited onto the electrode prior to dissolution to reach an oxide-free surface.

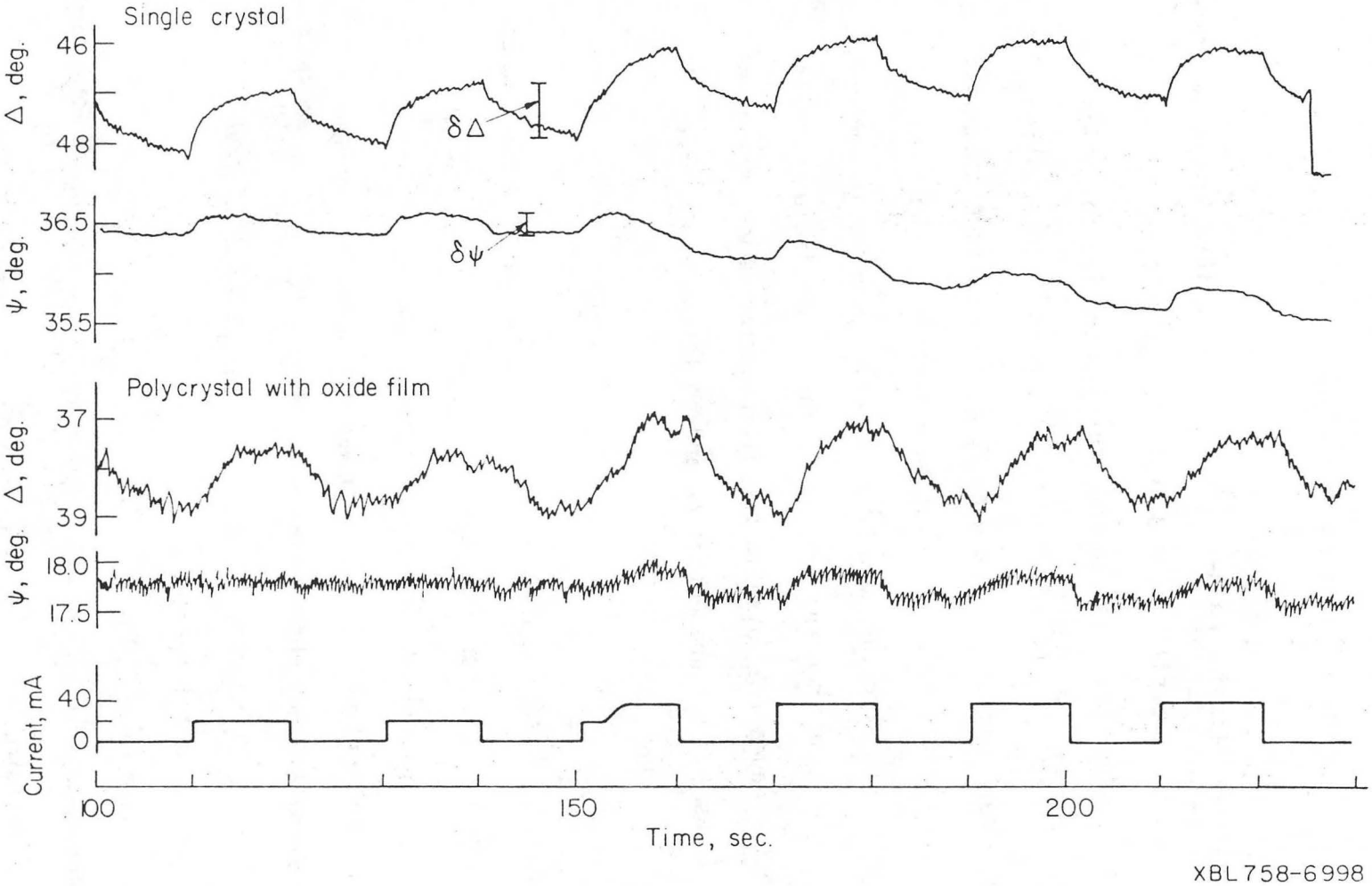



Fig. 34. Experimental observation of cathodic convective diffusion boundary layer (Re = 500) by interruption technique. Cu deposition from 0.1 M $CuSO_4$. Single crystal (111) face. Polycrystalline Cu with oxide film. Electrode $3.3^4 cm^2$.

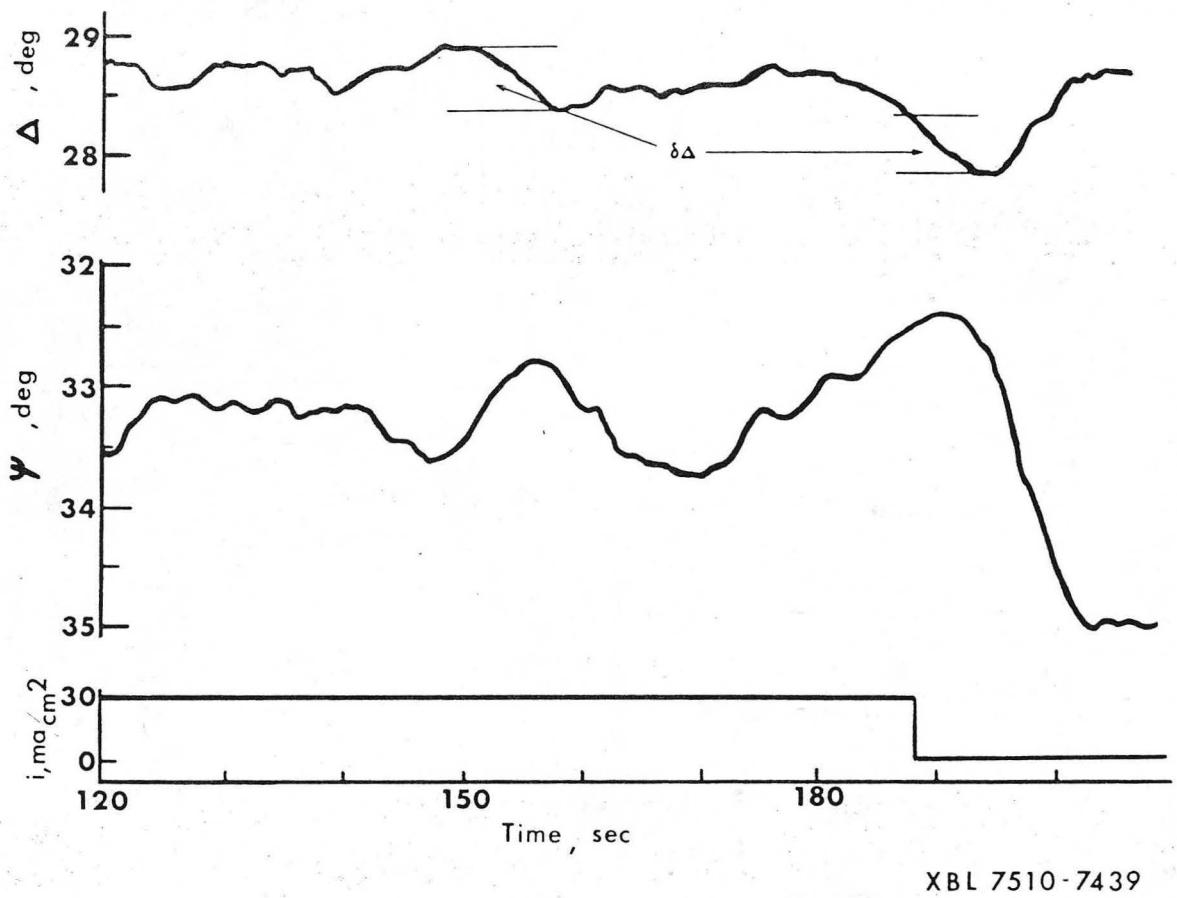



Fig. 35. Experimental observation of natural convection formed by anodic dissolution of Cu in 0.2 M $CuSO_4$. Single crystal electrode of dimensions 2.7×1.2 cm.



0 0 0 4 3 0 5 0 1 0

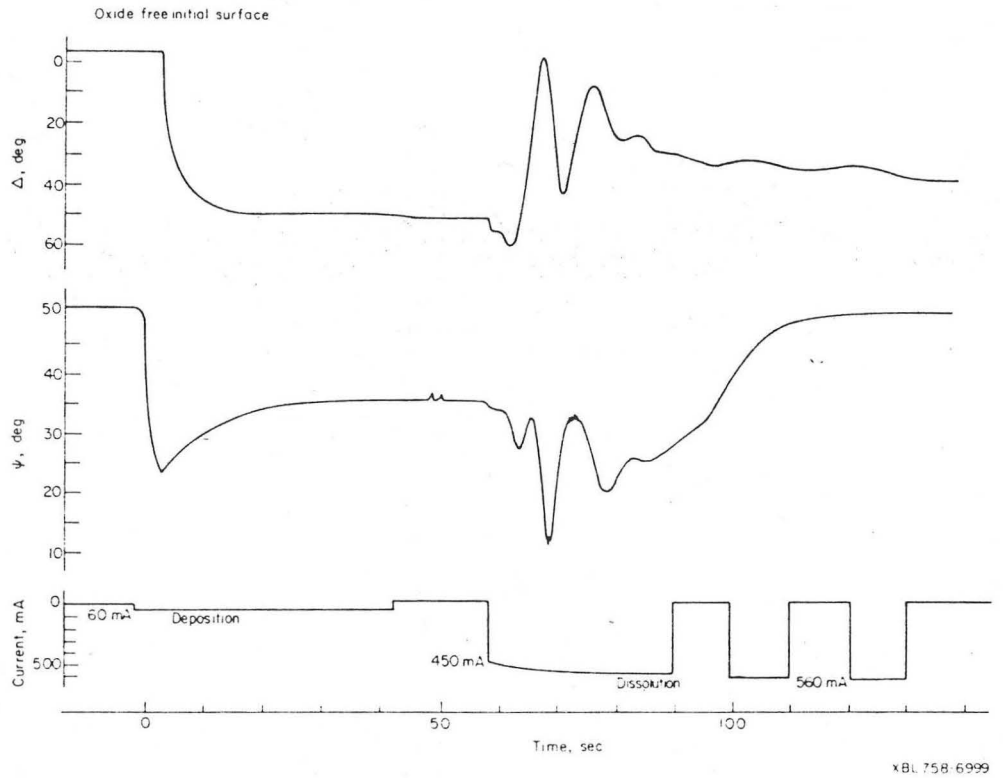



Fig. 36. Dissolution of Cu in 0.1 M $CuSO_4$ accompanied by $Cu_2O$ film formation, after deposition period forming oxide free initial surface. Convective diffusion (Re = 600). Single crystal electrode of dimensions 2.7×1.2 cm. $\phi$ = 75°.

0 0 0 0 4 3 0 5 0 1 1



## D. Method of Analysis

The equations describing mass transfer presented in Section II indicate that for the experimental conditions investigated, the thick-film limit for the mass-transport boundary layer applies. The calculations presented in Section IV have shown that $\delta\Delta$ and $\delta\psi$ depend upon the optical constants of the substrate. Calculations which model surface roughness and oxide films as homogeneous layers show that, in general, the values of $\delta\Delta$ and $\delta\psi$ are different from values calculated using an effective substrate formed by determining optical constants from the values of $\Delta$ and $\psi$ given by the film/actual-substrate system. $\delta\Delta$ decreases and $\delta\psi$ increases for $Cu_2O$ films and roughening Cu, with $\delta\psi$ being more sensitive than $\delta\Delta$. These trends for $\delta\Delta$ and $\delta\psi$ were observed for forced convection. The effective substrate approach is applicable for small roughness conditions. Comparison of the interfacial concentrations determined from $\delta\Delta$ and $\delta\psi$ give an indication of whether or not effective substrates may be used. When $\delta\Delta$ and $\delta\psi$ give interfacial concentrations in agreement, optical constants for an effective substrate are determined from the experimental values of $\Delta$ and $\psi$ in the absence of the boundary layer. Figure 37 relates $\Delta$ and $\psi$ to the effective substrate optical constants $n - ik$.

Calculations have shown $\delta\Delta$ to vary approximately linearly with $\delta n_i$ for $\Delta C (= C_b - C_1) < 0.3$ M $CuSO_4$, as indicated in Fig. 38. Figures 39 and 40 give values of $\delta\Delta$ and $\delta\psi$ for various effective substrate values and $\Delta C = \pm 0.1$ M $CuSO_4$. The method for determining interfacial concentrations used here is to first determine the effective

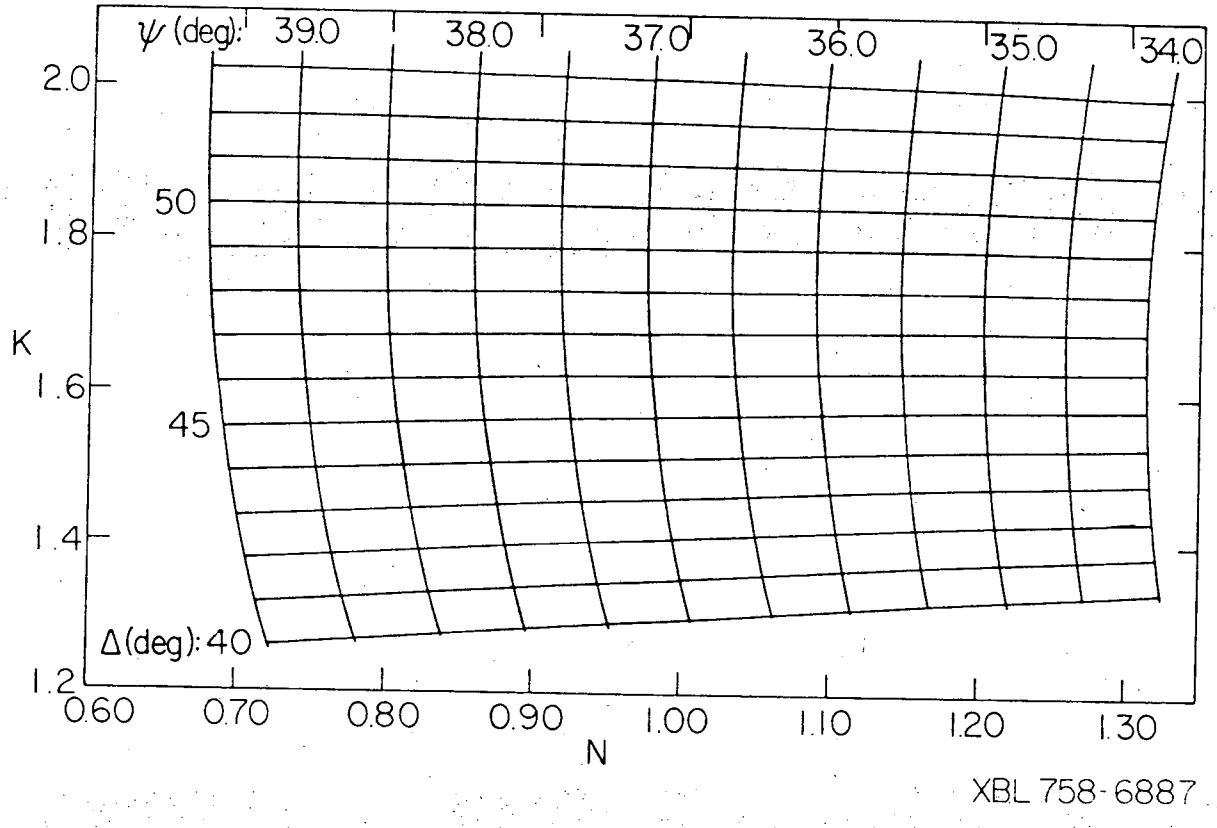



Fig. 37. Calculated relationship between Δ, ψ and substrate refractive index n - ik. Incident medium refractive index n = 1.3374. Angle of incidence $\phi$ = 75°.

0 0 0 0 4 3 0 5 0 1 2



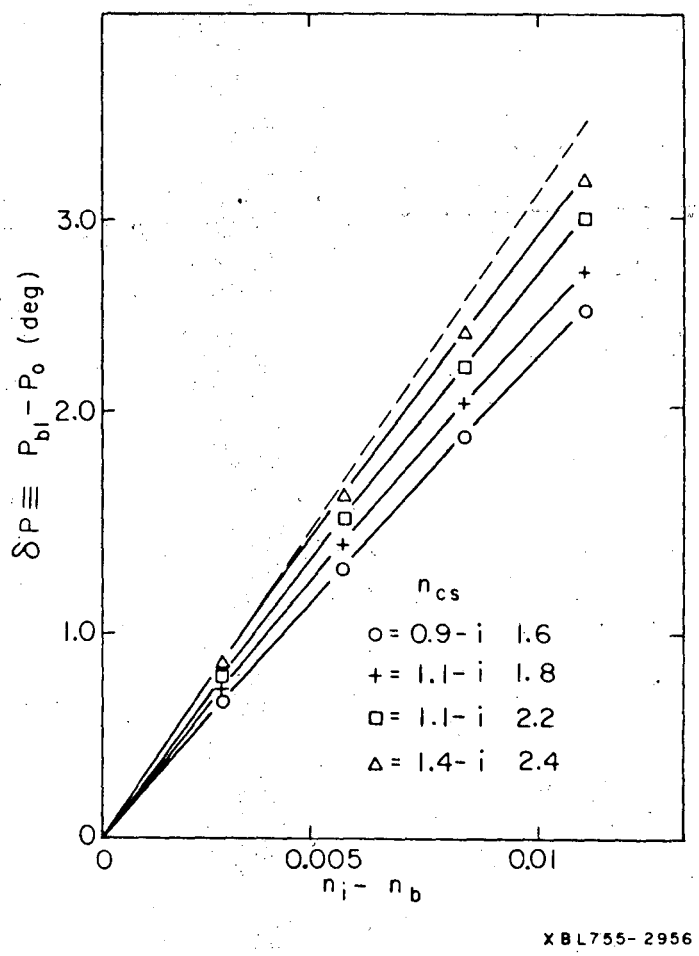



Fig. 38. Dependence of change in polarizer azimuth with refractive index difference $n_i - n_{bg}$ for various substrate optical constants $n_{cs}$. For zone A3, $\Delta = 90-2P$. $\phi = 75°$.

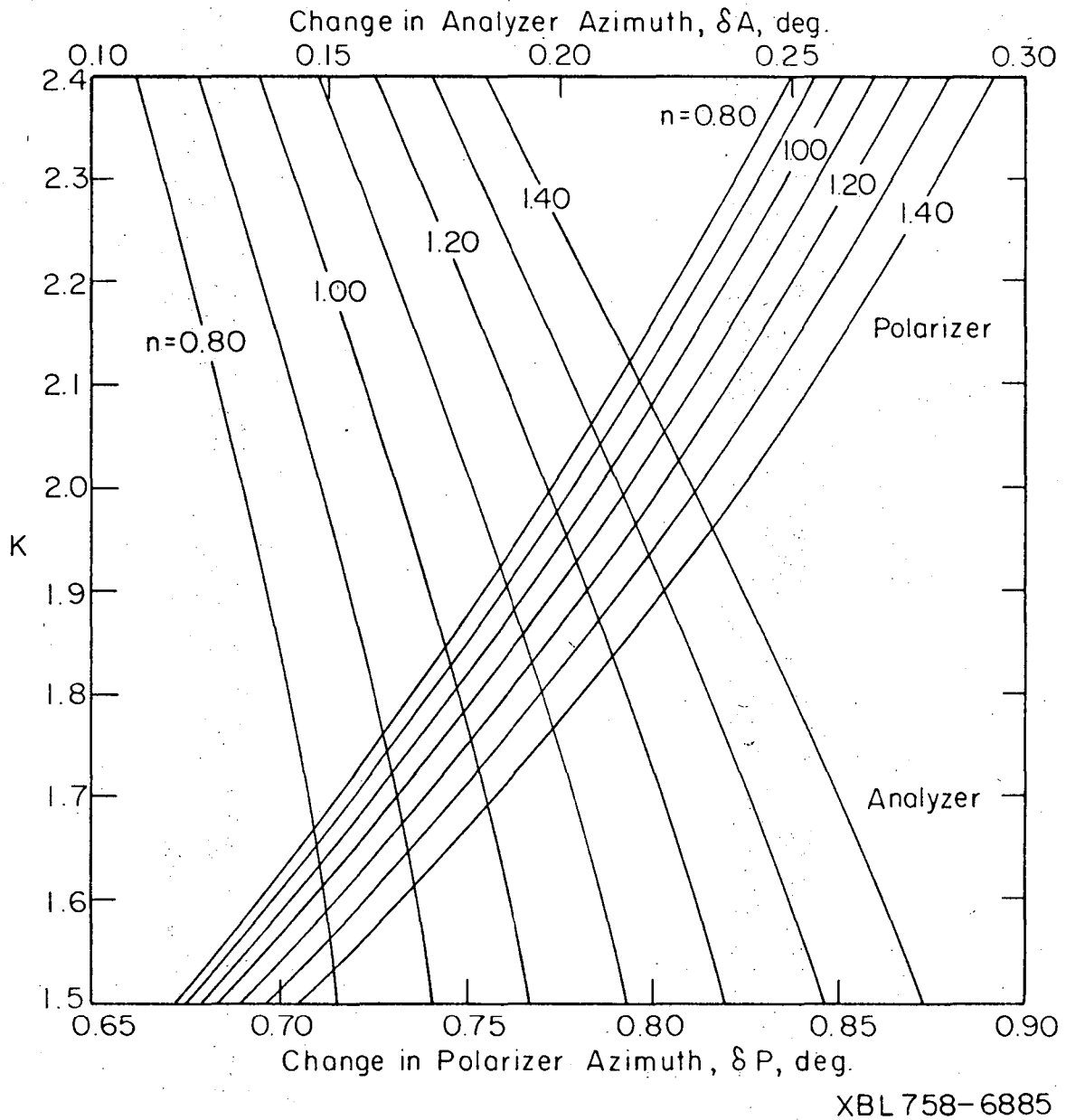



Fig. 39. Dependence of change in polarizer and analyzer azimuths with effective Cu substrate optical constants $n_{cs} = n - ik$. Cathodic deposition ($\Delta C$ = 0.1 M) from 0.1 M $CuSO_4$, $\phi = 75°$. $\psi = A-90$, $\Delta = 90-2P$.

0 0 0 0 4 3 0 5 0 1 3



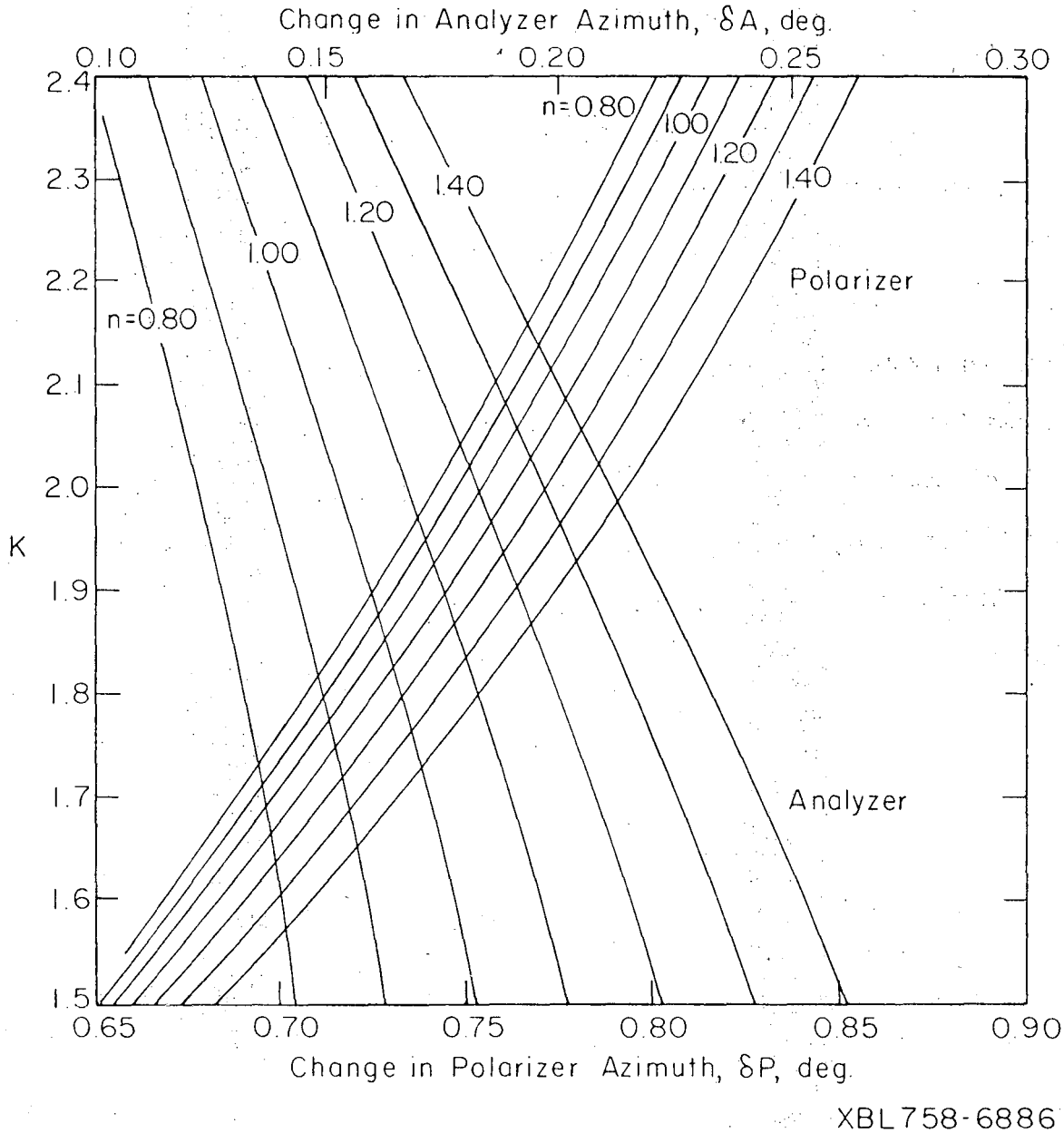



Fig. 40. Dependence of change in polarizer and analyzer azimuth with effective Cu substrate optical constants $n_{cs} = n - ik$. Anodic dissolution ($\Delta C$ = 0.1 M) in 0.1 M $CuSO_4$, $\phi$ = 75°. $\psi$ = A-90, $\Delta$ = 90-2P for zone $\Lambda$3.

substrate refractive index from measurements and the use of Fig. 37. Linear interpolation (or extrapolation for $\Delta C > 0.1$ M $CuSO_4$) of the experimental values of $\delta\Delta$ and $\delta\psi$ from the values given in Fig. 39 and 40 gives the interfacial concentration.

Complications

For large concentration differences occurring across the boundary layer, linear interpolation is no longer adequate. Equations (20) and (21) must be modified to include the non-linear dependence of refractive index upon concentration. It might also be desirable to use a more accurate description of the concentration profile. The actual implementation of these refinements into the multiple-film calculations are quite easy, however. For the program INFILM in Appendix C, this is accomplished by adding the corresponding algebraic equation into the subroutine PROFYL (with the appropriate routing logic statements).

0 0 0 0 4 3 0 5 0 1 4



# VI. RESULTS AND DISCUSSION

## A. Convection-Free Diffusion

Figure 41 presents interfacial concentrations as a function of $t^{1/2}$ for electrode current densities of 5, 10 and 20 $mA/cm^2$. There is a systematic deviation from the Sand Eq. (7). The direction is consistent with an analysis by McLarnon[10] which solves Eqs. (3) through (6) with allowance for variable D and $t_+$. Other sources of deviation, which would result in the same trend, are convection due to the fact the electrode does not cover the whole cell, and the use of an effective substrate in the analysis scheme. It is believed that these three sources of deviation have been presented in the order corresponding to their relative importance.

## B. Forced Convection

Table IV presents forced-convection results which verify the independence of ellipsometer parameters upon film thickness and their sensitivity to interfacial concentration. The largest deviation is observed for the dissolution results. The deposition experiments were performed on surfaces with small roughness, while the dissolution experiments were done with surfaces having oxide films. Most of the deviation for the condition $\Delta C = 0.714$ is probably due to the use of an effective substrate. Another possibility is the decrease in current efficiency due to the oxide film formation.

Figure 42 presents the change in concentration across the boundary layer as functions of Re and current density for potentiostatic deposition from 0.1 M $CuSO_4$. The major source of experimental error is the electrolyte flow rate. The dashed line in the laminar regime is from Eqs. (12) and (13). The deviation at low Re is probably due to natural

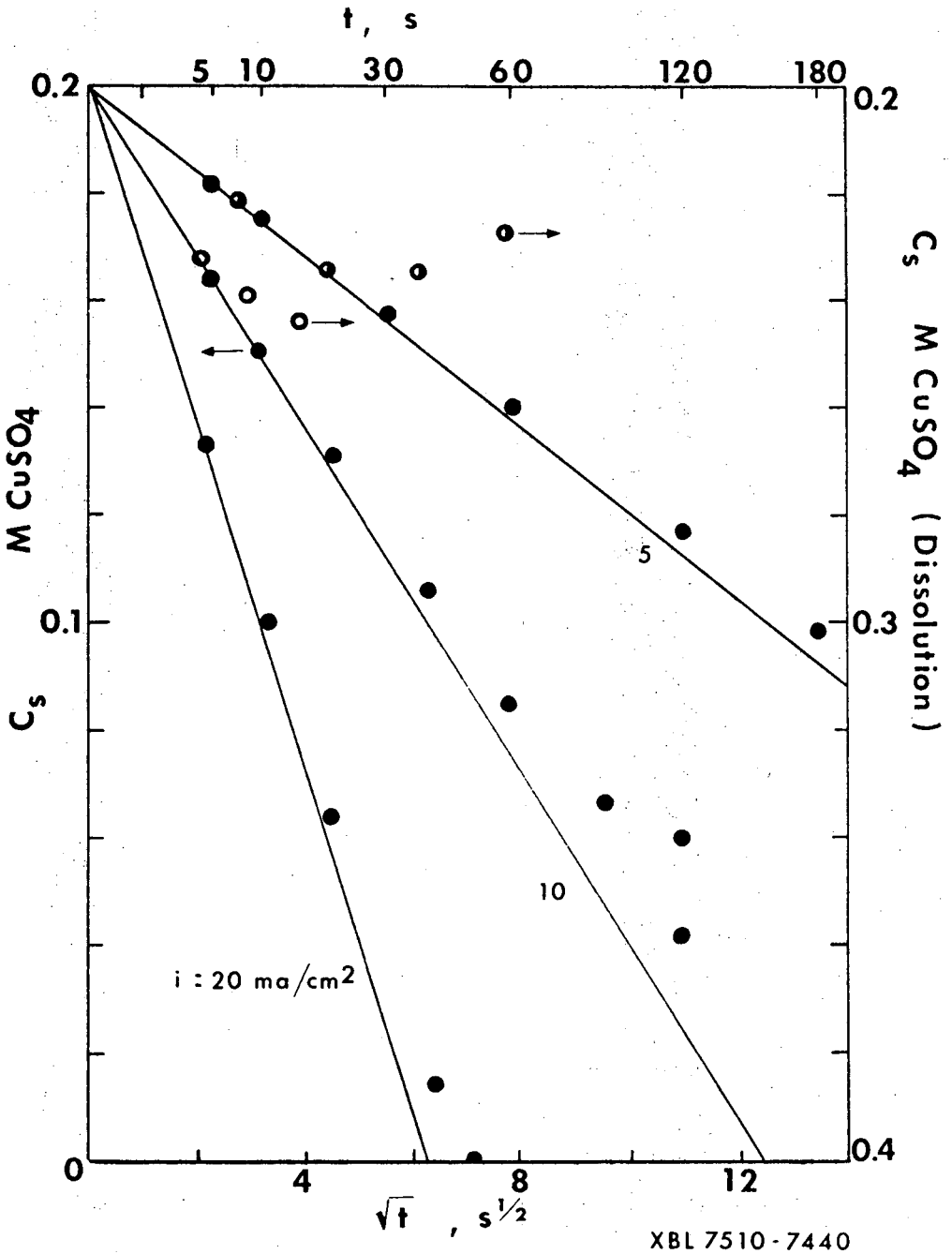


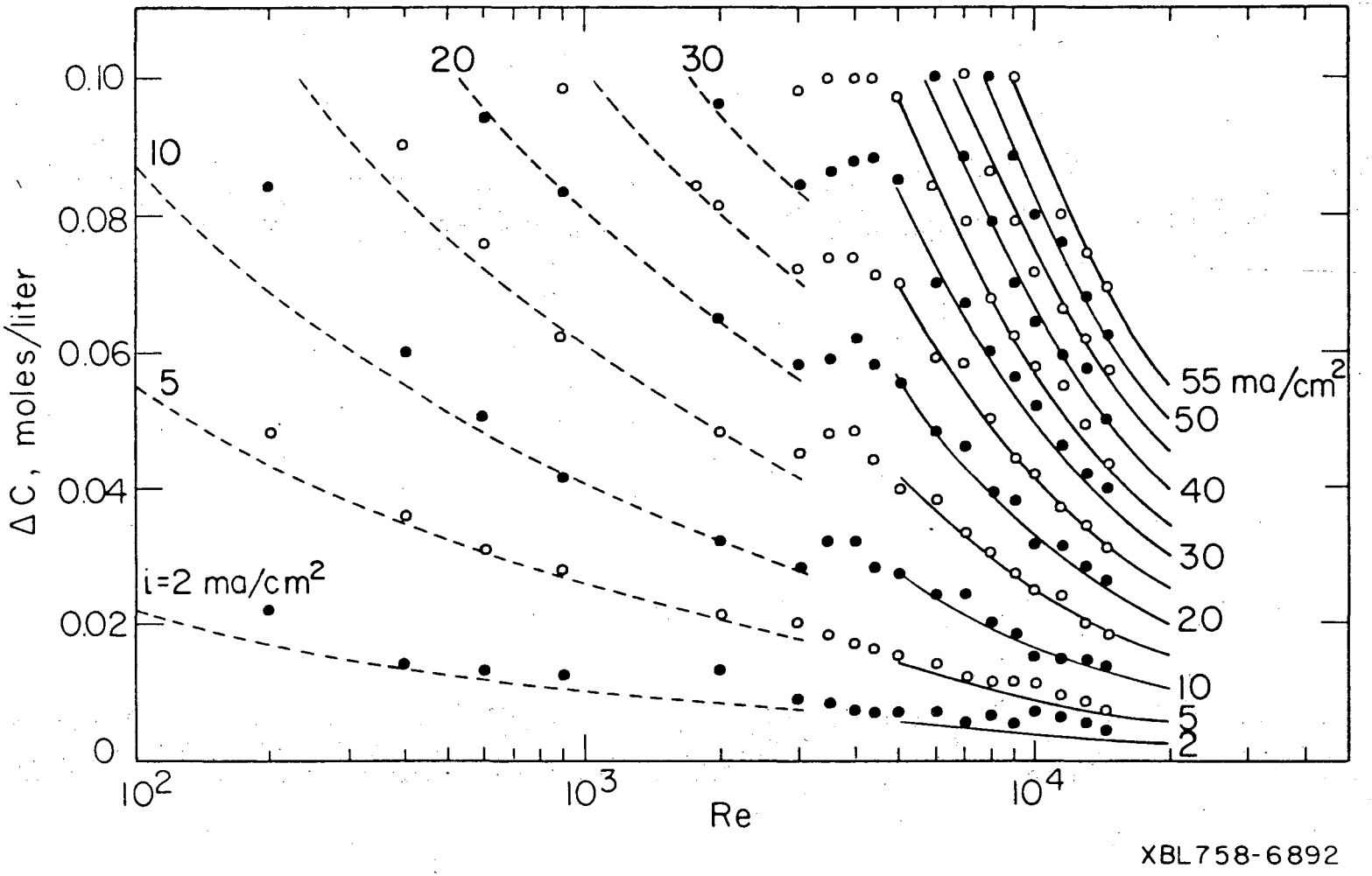

Fig. 41. Experimental dependence of the interfacial $CuSO_4$ concentration $C_s$ with $t^{1/2}$. ◐, convection-free deposition from 0.2 M $CuSO_4$. ○, ◑ convection-free dissolution in 0.2 M $CuSO_4$. Electrode current density indicated next to solid curves given by Sand Eq. (7). $D = 5\times10^{-6}$ $cm^2/s$, $t_+ = 0.385$.

Table IV. Experimental test of computed changes in ellipsometer parameters $\Delta$ and $\psi$ due to the presence of mass-transport boundary layers with different thickness and concentration difference. Electrochemical deposition and dissolution of copper in aqueous copper sulfate, $\phi = 75°$, $\lambda = 546.1$ nm, convective diffusion.

| | Boundary Layer | | Changes in $\Delta$ | | Changes in $\psi$ | |
|---|---|---|---|---|---|---|
| Nature | Thickness $\mu$ | Conc. Difference M $CuSO_4$ | Calculated deg | Experimental deg | Calculated deg | Experimental deg |
| Deposition | 50 | -0.016 | -0.23 | -0.30 | +0.04 | +0.16 |
| | 50 | -0.096 | -1.39 | -1.40 | +0.18 | +0.18 |
| | 87 | -0.083 | -1.25 | -1.38 | +0.11 | +0.14 |
| | 26 | -0.080 | -1.16 | -1.16 | +0.13 | +0.20 |
| | 76 | -0.094 | -1.36 | -1.36 | +0.17 | +0.25 |
| Dissolution | 80 | 0.108 | +1.54 | +1.67 | -0.23 | -0.30 |
| | 80 | 0.206 | +2.93 | +3.02 | -0.30 | -0.52 |
| | 80 | 0.714 | +8.92 | +8.50 | -0.99 | -1.42 |



0 0 0 4 3 0 5 0 1 5




XBL758-6892

Fig. 42. Experimental dependence of concentration difference on electrode current density and Re for cathodic deposition of Cu from 0.1 M $CuSO_4$. Convective diffusion. - - - given by Eq. (12), ——— given by Eq. (30), for $\nu = 1.065\times10^{-2}$ $cm^2/s$, $D = 5\times10^{-6}$ $cm^2/s$, and $t_+ = 0.385$.

0 0 0 0 4 3 0 5 0 1 6



convection being superimposed on forced convection. The effect would be to provide a more uniform current density in relation to the $X^{1/3}$ dependence given in Eq. (12). Increased transport in the center of the electrode, where the measurements are made, would increase $\Delta C$.

The solid curves in the turbulent regime are a least-squares correlation of the data found here to be

$$Nu = 0.042\ Re^{0.743}\ Sc^{1/3}$$

The correlation used a constant value of $D = 5\times10^{-6}$ cm/s. By considering only values of $\Delta C \geqslant 0.070$,

$$Nu = 0.035\ Re^{0.763}\ Sc^{1/3}$$

Insufficient data were obtained to determine the Re dependence close to limiting current. However, the results do not seem to be inconsistent with Hickman's[7] results if the dependence of D with c is taken into account.

## C. Natural Convection

These results are meant to be qualitative. The value of $\delta_c$ in Eq. (18) was first assumed to be in the regime of the thick-film limit. As no information may be obtained by ellipsometry for $\delta_c$, the concentration driving force was correlated by using the length of the electrode (2.7 cm) as the characteristic length in the Grashaf number. Table V presents this result. The average value of the coefficient was K = 5.42. The approximate value of $\delta_c$ was determined by using Eqs. (17) and (18). The value of $\delta$ = 2.7 cm was decreased such that K decreases from 5.42 to the value 0.265 given in Eq. (17). This gives $\delta_c$ = 50 μ, which is in the thick-film limit. Effective substrate values

Table V. Experimental correlation of the concentration driving force occurring in natural convection. Cu dissolution in $CuSO_4$.

| Current Density $ma/cm^2$ | $\Delta C$ M $CuSO_4$ | $(GrSc)^{1/4}$* | Nu | $K = NuGr^{-1/4}Sc^{-1/4}$ |
|---|---|---|---|---|
| 5 | 0.016 | 177 | 989 | 5.59 |
| 10 | 0.028 | 204 | 1130 | 5.54 |
| 15 | 0.041 | 223 | 1160 | 5.22 |
| 20 | 0.050 | 236 | 1270 | 5.36 |
| 30 | 0.069 | 255 | 1380 | 5.39 |
| 40 | 0.087 | 270 | 1460 | 5.39 |

*The Grashof Number has used the length of the electrode for a characteristic length instead of $\delta_c$, the boundary layer thickness.

0 0 0 0 4 3 0 5 0 1 7



were used in the analysis, although an oxide layer was present. This procedure would result in $\Delta c$ values smaller than the actual values, and $\delta c$ would subsequently be slightly greater then 50 $\mu$ (within a factor of 2).

## D. Growth of $Cu_2O$ Film

Figure 43 is a plot of $\psi$ vs $\Delta$ for the growth of a $Cu_2O$ layer accompanying the anodic dissolusion process given in Fig. 35. The refractive index of the copper substrate following deposition is 1.14-1.88i. In the initial portion of the dissolution process, the substrate is roughened considerably, giving a substrate refractive index of 1.9-2.0i. A homogeneous oxide film of refractive index 2.45-0.60i fits the experimental curve up to point P1. The thickness of the oxide layer has been indicated along the curve. The discontinuity in the curve at P1 corresponds closely to the point where transport theory (Eq. (12)) indicates the interfacial concentration reaches the solubility limit of $CuSO_4$ in water. Point P2 is a second discontinuity. The experimental data have not been interpreted beyond P1 because experimental observations in addition to the 2-parameter ellipsometer measurements are necessary to uniquely classify the surface.

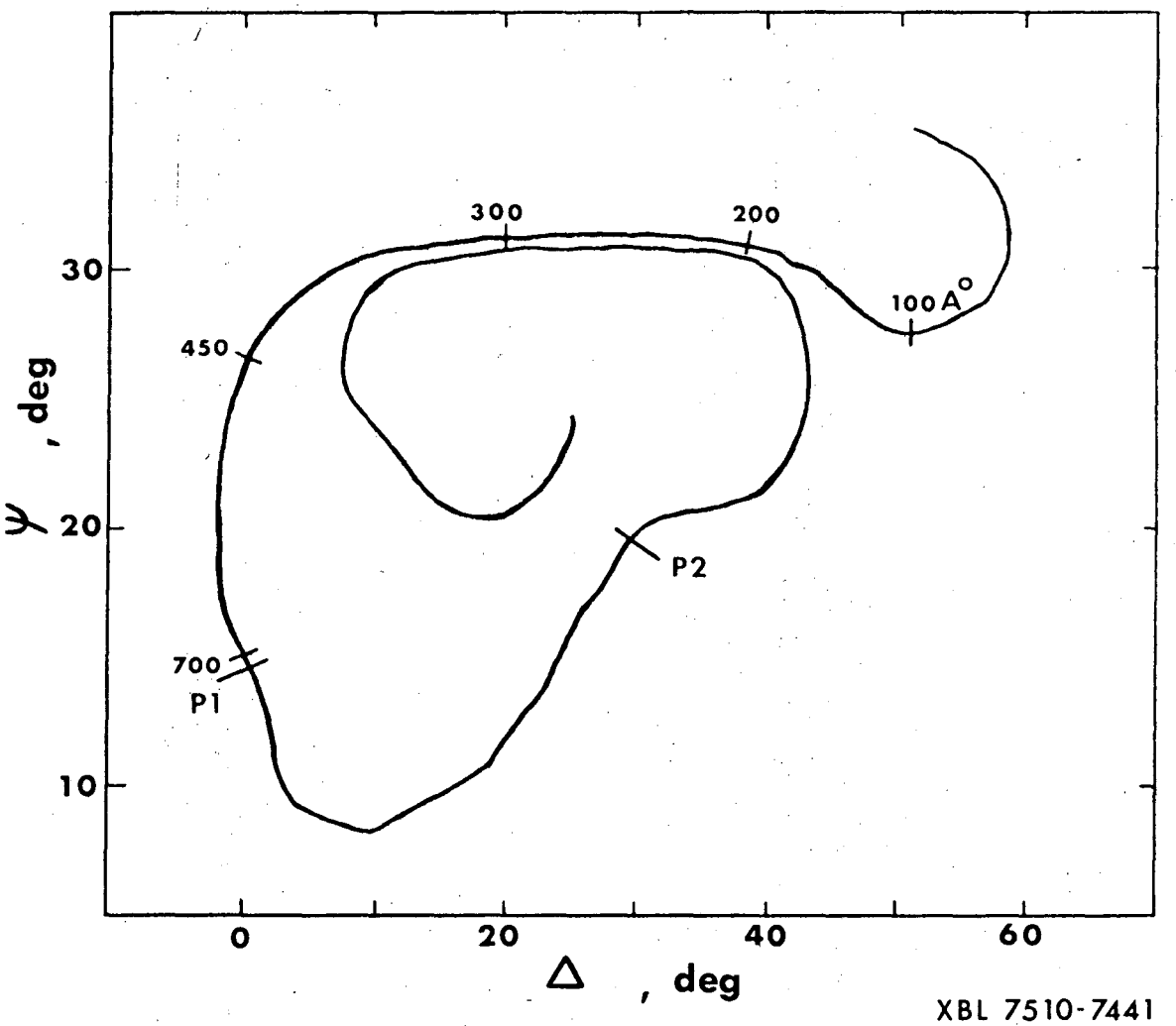



Fig. 43. Variation of $\Delta$ and $\psi$ for Cu dissolution in 0.1 M $CuSO_4$ accompanied by oxide film growth. Convective diffusion with Re = 600 corresponding to an average linear flow velocity $\bar{u}$ = 8.7 cm/s. Film thickness indicated along curves. Electrode area 3.2 $cm^2$. Current density varies from 140 to 175 $ma/cm^2$.

0 0 0 0 4 3 0 5 0 1 8



## VII. CONCLUSIONS

For most transport conditions in liquids, the effect of mass-transport boundary layers is sensitive to the refractive index (concentration, temperature) at the interface but not to the thickness of the layer. The magnitude of the effect greatly depends on the angle of incidence and the optical constants of the solid phase. The effect can reach amounts that can significantly alter the interpretation of measurements. The ellipsometric determination of interfacial concentration complements the observation of boundary layers by interferometry, where this quantity may be difficult to derive precisely from the observations.[32,33]

## ACKNOWLEDGEMENTS

I would like to express my gratitude to Dr. Rolf Muller for his guidance and his patronage, and to Walter Giba for applying his mechanical skills with an active interest and concern. Lee Johnson gave me valuable metallurgical assistance, while Gloria Pelatowski's excellent work is responsible for many of the figures.

This work was done under the auspices of the U. S. Energy Research and Development Administration.

0 0 5 0 4 3 0 5 0 1 9



# APPENDIX A. PHYSICAL PROPERTIES OF $CuSO_4$

## Refractive Index, n'

The physical refractive index n' (Appendix B, p. 90) of $CuSO_4$ at 546.1 nm wavelength was determined with a Bausch and Lomb refractometer. The measurement is made by rotating a prism (#749) of known refractive index n = 1.5256 until total reflection at the solution-prism interface is obtained. A sample of 1.0 M $CuSO_4$ was prepared from $CuSO_4 \cdot 5H_2O$ and diluted to 0.1, 0.2, 0.5, 0.65 and 0.8 M samples. The least squares fit for $0 < C < 0.2$ M as a function of temperature is

$$n = n_{H_2O}(T) + (0.0290 \pm 0.0002)\ C \quad . \tag{1}$$

The slope agrees with results presented by McLarnon.[10] At 20°C, $n_{H_2O} = 1.33447$, compared with a literature value of 1.33445.[13] The data are presented in Fig. A1.

## Absorption Coefficient, k'

The imaginary part of the refractive index k' is related to the absorption of light by (Appendix B)

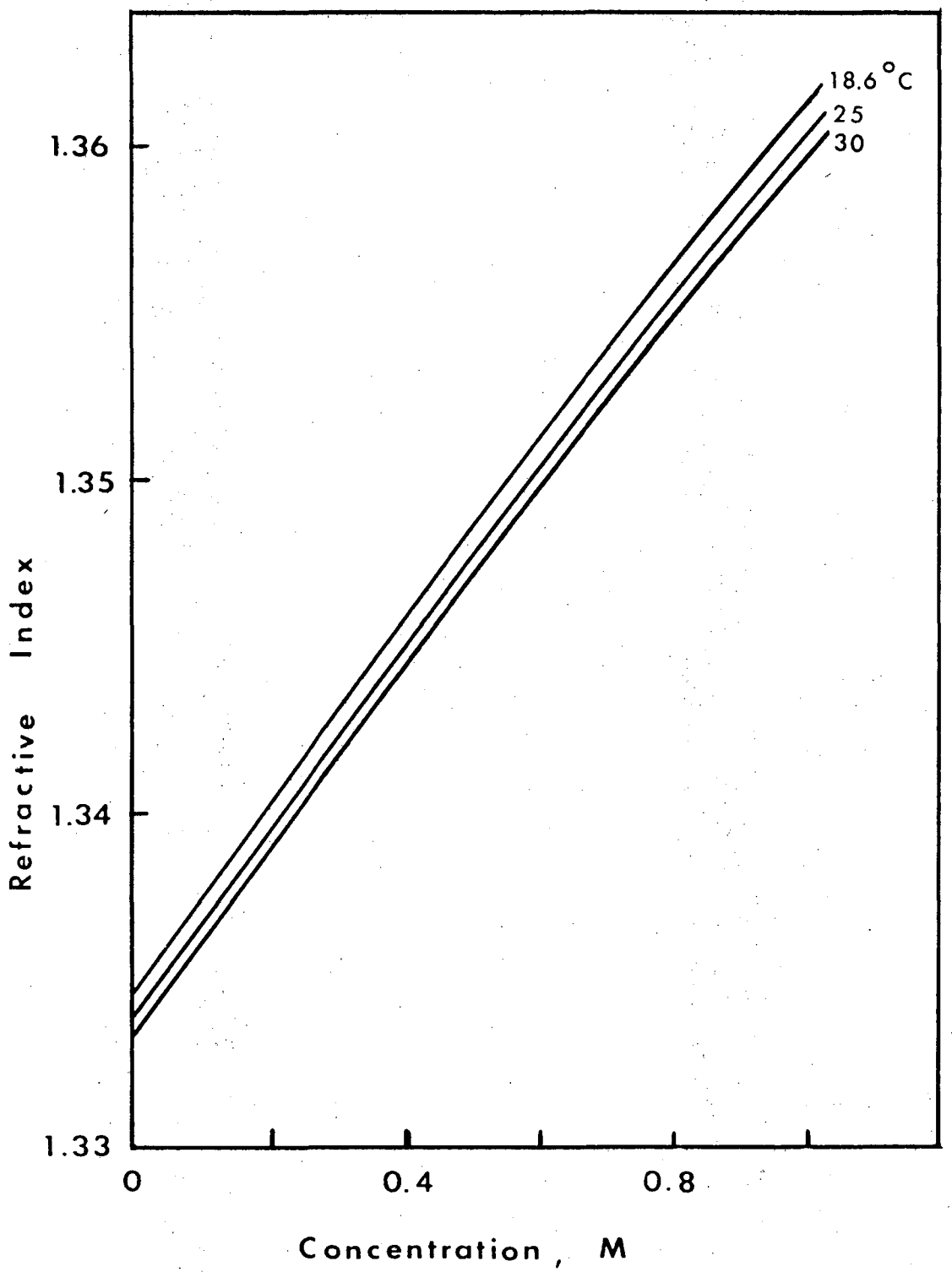
$$k' = \frac{\lambda_o \alpha}{2\pi} \tag{2}$$

$\alpha$ is determined from intensity measurements by

$$\log_{10}(I/I_o) = \alpha_{10}\ z(\text{cm}) \tag{3}$$

From Refs. 14 to 20, $\bar{\alpha}_{10} = 0.177C$. Converting to the natural logarithm,

$$\alpha = 0.408C\ \text{cm}^{-1} \tag{4}$$




XBL 759-7339

Fig. A1. Dependence of refractive index on $CuSO_4$ concentration. Temperature dependence indicated next to curves. Refractive index measured by author.

0 0 0 0 4 3 0 5 0 2 0



Use of Eq. (2) gives

$$k' = 1.77\times10^{-6}C$$

Diffusion Coefficient, D

The dependence of the diffusion coefficient upon concentration is presented in Fig. A2. The data are found in Ref. 21 and taken from Refs. 22 and 23.

Transference Number, $t_+$

The dependence of the transference $t_+$ upon concentration is presented in Fig. A3. The data found in Ref. 21 were taken from Ref. 24.

Viscosity $\mu$ and Density $\rho$

The dependence of viscosity $\mu$ and density $\rho$ upon concentration is presented in Fig. A4. The data were taken from Refs. 25 and 26.

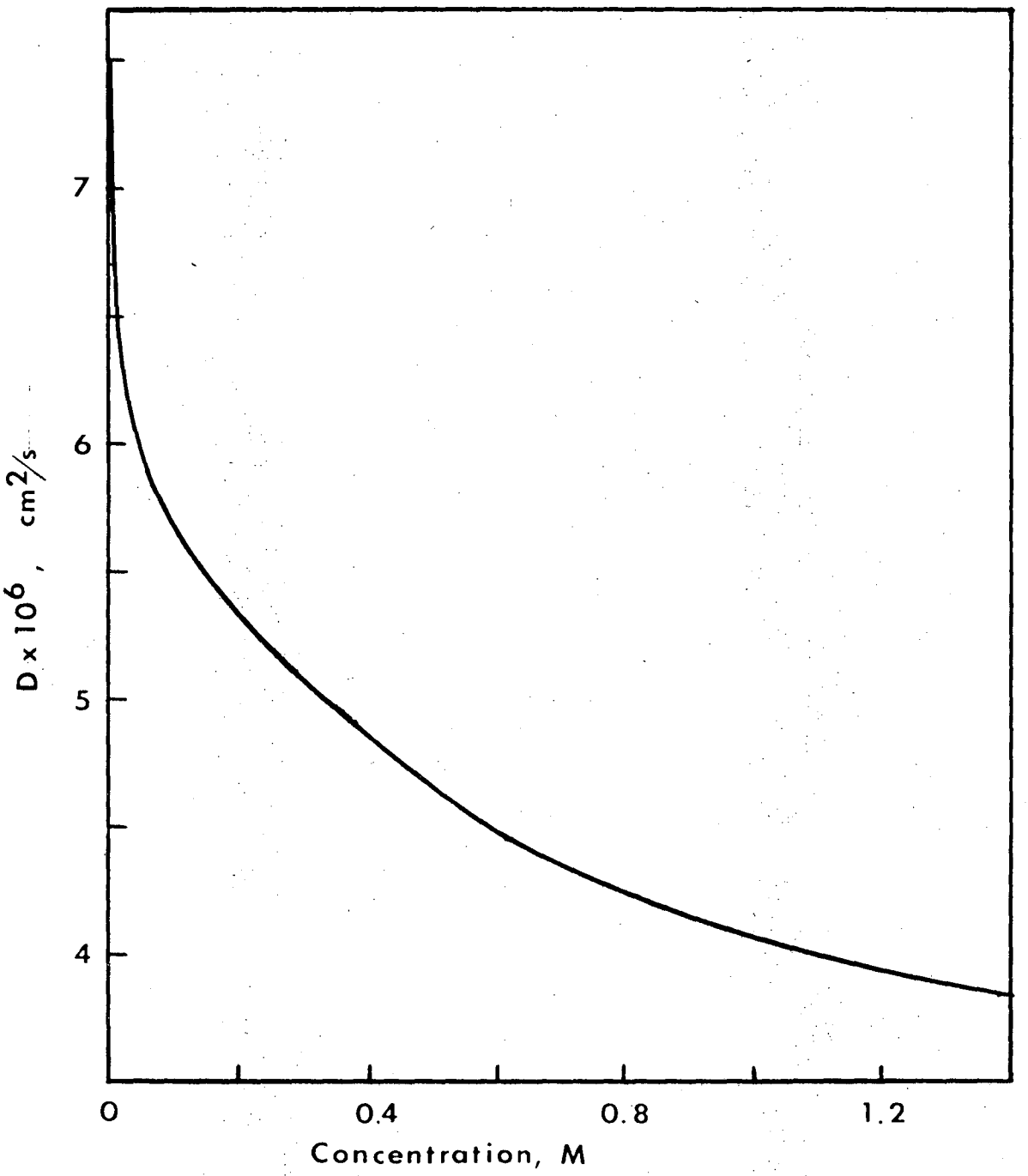
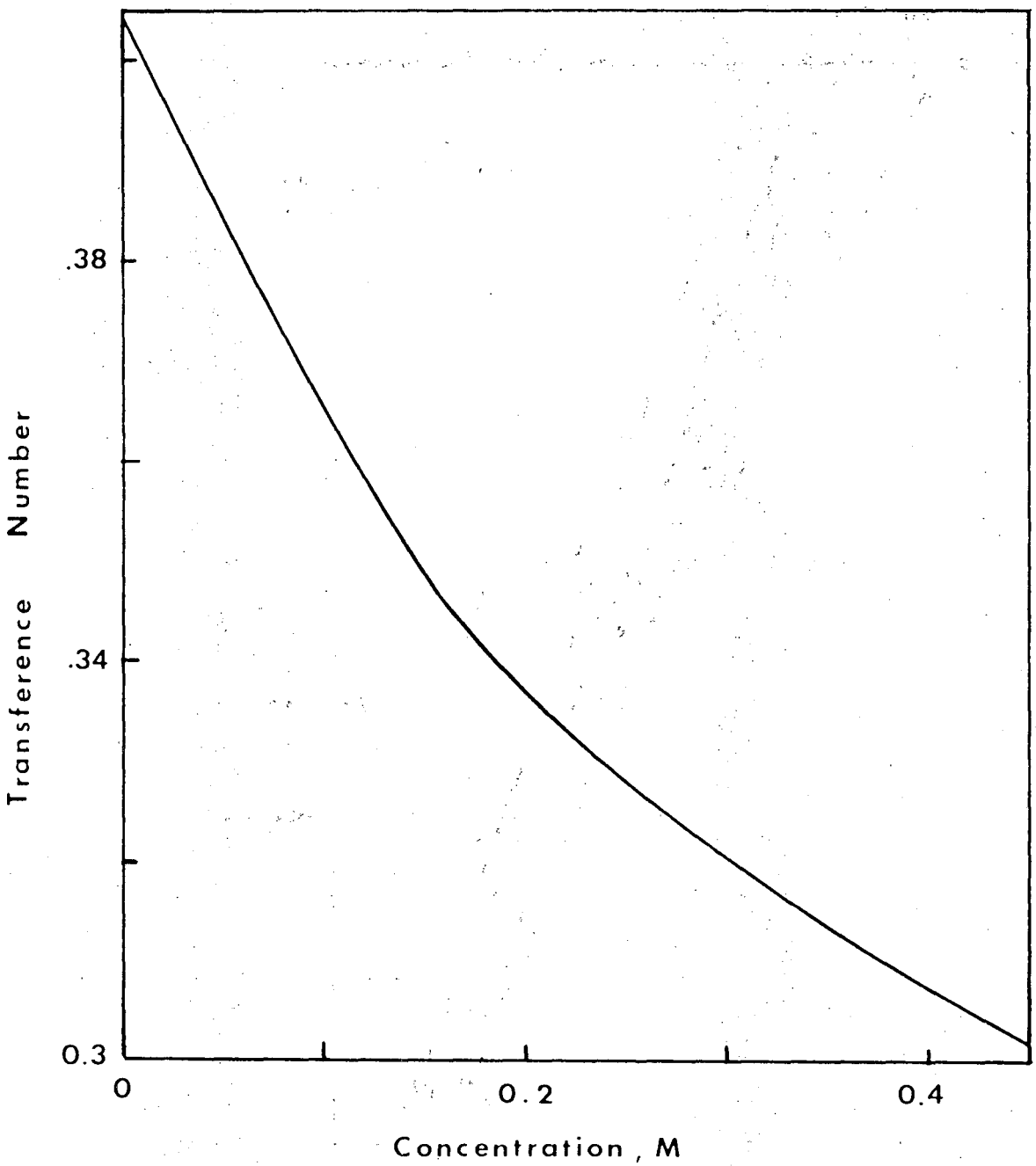



Fig. A2. Dependence of diffusion coefficient D on $CuSO_4$ concentration. Data taken from Refs. 22 and 23.

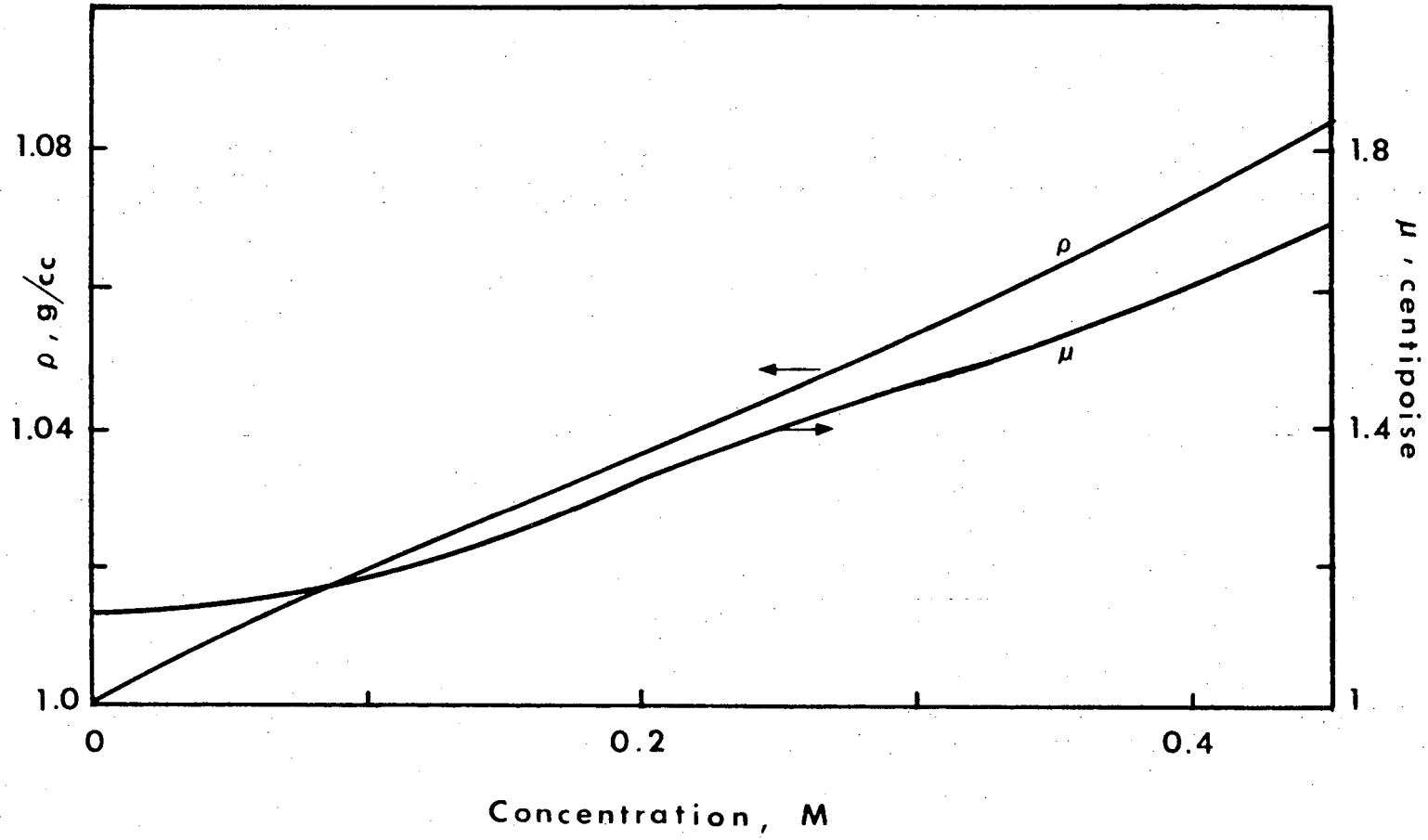
0 0 0 0 4 3 0 5 0 2 1






XBL 759-7337

Fig. A3. Dependence of transference number $t_+$ on $CuSO_4$ concentration. Data taken from Ref. 24.




XBL 759-7336

Fig. A4. Dependence of density ρ and viscosity μ on $CuSO_4$ concentration. Data taken from Refs. 25 and 26.

0 0 0 0 4 3 0 5 0 2 2



# APPENDIX B. FRESNEL AND DRUDE EQUATIONS AND THE ELLIPSOMETER PARAMETERS $\psi$ AND $\Delta$

This section presents the derivation of the reflection coefficients for both reflection at a bare surface and reflection from a film-covered surface. The ellipsometer parameters $\psi$ and $\Delta$ are also introduced.

## The Electromagnetic Theory of Reflection

The classical description of the reflection of light from a boundary between two media is based upon the macroscopic Maxwell Equations. The assumptions involved are that the surface is planar, both media are continuous, linear, and isotropic, and each field is represented as a monochromatic, sinusoidal disturbance.

This derivation gives the Fresnel equations, which represent the ratios of reflected to incident electric field intensities for two orthogonal states of polarization. With the exception of Section 2, which is original, this work is a modification of the notation used in a derivation presented by Muller and Mowat.[27,28]

### 1. The Maxwell Equations

Light is assumed to obey the macroscopic Maxwell Equations (1) through (4):

$$\text{div } \vec{D} = 4\pi\rho_{free} \tag{1}$$

$$\text{curl } \vec{E} = -\frac{1}{c}\frac{\partial \vec{B}}{\partial t} \tag{2}$$

$$\text{div } \vec{B} = 0 \tag{3}$$

$$\text{curl } \vec{H} = \frac{1}{c}\frac{\partial \vec{D}}{\partial t} + \frac{4\pi}{c}\vec{J}_{free} \tag{4}$$

in addition,

$$\vec{D} \equiv \vec{E} + 4\pi\vec{P} \tag{5}$$

$$\vec{B} = \vec{H} + 4\pi\vec{M} \quad . \tag{6}$$

$\vec{E}$ is the electric field intensity, $\vec{P}$ is the electric polarization, $\vec{B}$ is the magnetic induction, $\vec{M}$ is the magnetization, $\vec{J}_{free}$ is the free current, $\vec{H}$ is the magnetic field intensity, $\vec{D}$ is the displacement current, and $\rho_{free}$ the free charge density.

The following assumptions are also made:

(1) The media considered are all linear and isotropic, that is

$$\vec{P}_s = X_e\vec{E}_s \ , \ \vec{M}_s = X_m\vec{H}_s \ , \ \vec{J}_s = \sigma\vec{E}_s \tag{7a-c}$$

and the magnetic and electric susceptibilities $X_e$ and $X_m$ as well as the conductivity $\sigma$ are constant throughout space. The subscript s refers to the spatially dependent parts of their corresponding vectors.

(2) The equation of continuity holds:

$$\frac{\partial\rho_{free}}{\partial t} = - \text{ div } \vec{J}_{free} \quad . \tag{8}$$

(3) Each field quantity is represented by a monochromatic, sinusoidal disturbance. For example,

$$\vec{E} = e^{-\alpha z}|E| \cos(\omega t - \vec{k}\cdot\vec{r}) \quad . \tag{9}$$

The term $e^{-\alpha z}$ represents the amplitude attenuation in the direction normal to the reflecting surface, $|E|$ is the "undampened" amplitude, $\omega$ is the frequency, $\vec{k}$ is a vector in the direction of propagation, and $\vec{r}$ is the position vector.

0 0 0 0 4 3 0 5 0 2 3



2. Wave Propagation

As shown in Ref. 29, the proper application of the Fourier cosine representation of a function demands that

$$2e^{-\alpha z}|E|\cos(\omega t - \vec{k}\cdot\vec{r}) = \vec{E}_o e^{i(\omega t-\vec{k}\cdot\vec{r})} + E_o^* e^{-i(\omega t-\vec{k}\cdot\vec{r})}\ e^{-\alpha z} \qquad (10)$$

where $\vec{E}_o$ is a constant, complex vector.

However, as will be shown for Eq. (1), the fact that the Maxwell Equations are self-adjoint, will allow a simpler representation:

Substitute the first term on the right in Eq. (10) into Eq. (1) to yield

$$e^{-\alpha z}[-ik\sin\phi_r - ik\cos\phi_r - \alpha]$$
$$[\cos(\omega t - \vec{k}\cdot\vec{r}) + i\sin(\omega t - \vec{k}\cdot\vec{r})]\ E_o = 4\pi\rho_{free} \qquad (1a)$$

where k is the magnitude of $\vec{k}$ referred to Fig. 1b.

Substituting the second term on the right in Eq. (10) into Eq. (1) gives:

$$e^{-\alpha z}[+ik\sin\phi_r + ik\cos\phi_r - \alpha]$$
$$[\cos(\omega t - \vec{k}\cdot\vec{r}) - i\sin(\omega t - \vec{k}\cdot\vec{r})]\ E_o^* = 4\pi\rho_{free} \qquad (1b)$$

The complex conjugate of Eq. (1b) is identical to Eq. (1a). As $\vec{E}_o^*$ obeys the same relationship as does $\vec{E}_o$, we need only solve for $\vec{E}_o$. This is also true for Eqs. (2) through (4).

Therefore,

$$\vec{E} = \vec{E}_o e^{-\alpha z} e^{i(\omega t-\vec{k}\cdot\vec{r})} = \vec{E}_s e^{+i\omega t} \qquad (11a)$$

Proceeding with similar assumptions gives:

$$\vec{P} = \vec{P}_s e^{i\omega t} \qquad \vec{J}_{free} = \vec{J}_s e^{i\omega t}$$

$$\vec{B} = \vec{B}_s e^{i\omega t} \qquad \vec{M} = \vec{M}_s e^{i\omega t} \qquad \text{(11b-g)}$$

$$\vec{D} = \vec{D}_s e^{i\omega t} \qquad \vec{H} = \vec{H}_s e^{i\omega t}$$

The fact that the Maxwell relationships are self-adjoint is implicit in Eqs. (11a-g).

Substituting for $\vec{J}_{free}$ into Eq. (8) and integrating with respect to time gives

$$\rho_{free} = \frac{i}{\omega} \operatorname{div}(\sigma \vec{E}_s)\, e^{i\omega t} \quad . \qquad (12)$$

Eliminate the time dependence from Eqs. (1) through (4). Substitute Eqs. (7a-c) into Eqs. (11a-g), then into Eqs. (5) and (6), divide out the common term $e^{i\omega t}$ to leave

$$\vec{D}_s = (1 + 4\pi X_e)\, \vec{E}_s \qquad (5a)$$

$$\vec{B}_s = (1 + 4\pi X_m)\, \vec{H}_s \quad . \qquad (6a)$$

Equivalently,

$$\vec{D}_s = \varepsilon \vec{E}_s \;,\; \vec{B}_s = \mu \vec{H}_s \quad . \qquad (5b,6b)$$

Substitute Eqs. (5b) and (12) into Eq. (1) to give

$$\operatorname{div}\left(\varepsilon - \frac{4\pi\sigma}{\omega} i\right) \vec{E}_s = 0 \quad . \qquad (1a)$$

0 0 0 0 4 3 0 5 0 2 4



Since

$$\frac{\partial \vec{B}}{\partial t} = i\omega \vec{B}_s e^{i\omega t} = i\omega\mu \vec{H}_s e^{i\omega t} \quad , \tag{13}$$

equation (2) can be written as

$$\text{curl } \vec{E}_s = - i\omega\mu/c \; \vec{H}_s \quad . \tag{2a}$$

Equation (3), using Eq. (6b), becomes

$$\text{div } \mu\vec{H}_s = 0 \quad . \tag{3a}$$

Using Eqs. (5b), (11f), and (7c), Eq. (4) becomes

$$\text{curl } \vec{H}_s = i\omega/c\left(\varepsilon - i\,\frac{4\pi\sigma}{\omega}\right) \vec{E}_s \quad . \tag{4a}$$

Taking the curl of Eq. (2a) and substitute Eq. (4a),

$$\text{curl curl } \vec{E}_s = \omega^2\mu/c^2\left(\varepsilon - i\,\frac{4\pi\sigma}{\omega}\right) \vec{E}_s \quad . \tag{14}$$

The L.H.S. of Eq. (14) equals:

$$\text{curl curl } \vec{E}_s = \text{grad div } \vec{E}_s - \nabla^2\vec{E}_s \quad .$$

As $\varepsilon$ and $\sigma$ are isotropic,

$$\nabla^2 E_s + \frac{\omega^2}{c^2}\mu\left(\varepsilon - i\,\frac{4\pi\sigma}{\omega}\right) \vec{E}_s = 0 \quad . \tag{15}$$

3. The Complex Refractive Index

By defining

$$n_c^2 \equiv \mu\left(\varepsilon - i\,\frac{4\pi\sigma}{\omega}\right) \quad , \tag{16}$$

Eq. (15) becomes

$$\nabla^2 \vec{E}_s + \frac{\omega^2}{c^2} n_c^2 \vec{E}_s = 0 \quad . \tag{15a}$$

The quantity $n_c$ is the complex index of refraction and is further defined by

$$n_c \equiv n - i\kappa \quad . \tag{16a}$$

$\kappa$ replaces the conventional use of k for the purpose of clarity. As shown in Refs. 29, 30 and 31, Eq. (15a) is satisfied by Eq. (11a) if the magnitude of $\vec{k}$,

$$k = \omega/v \tag{17}$$

where v is the velocity of the propagation of light in the medium.

The ratio of the vacuum phase velocity c to the phase velocity v is the physical index of refraction n'.

$$c/v \equiv n' \quad . \tag{18}$$

Thus

$$k = \omega/v = \frac{\omega}{c} n' = k_o n' \tag{17a}$$

where $k_o$ refers to the vacuum propagation vector.

Expanding $\vec{k}\cdot\vec{r}$ (vis Fig. B1) and inserting into Eq. (11a) gives

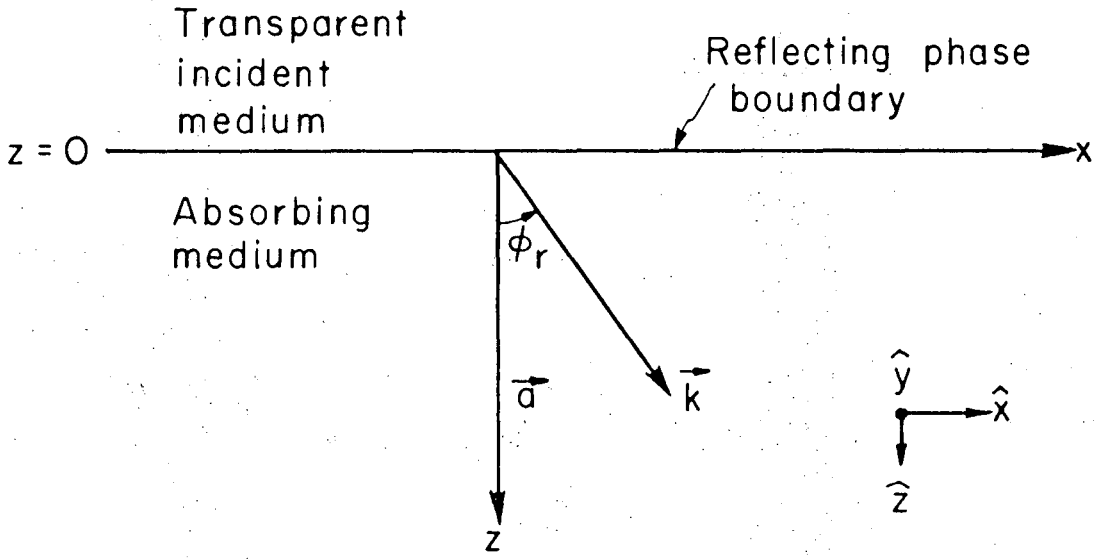
$$\vec{E}_s = \vec{E}_o \exp\left[-i\left(\frac{\omega n'}{c}\left[x\sin\phi_r + z\cos\phi_r\right] - i\alpha z\right)\right] \quad . \tag{19}$$

Define

$$\kappa' : \kappa' \equiv \frac{n'\alpha}{k} = \frac{\alpha c}{\omega} \geqslant 0 \tag{20}$$

0 0 0 0 4 3 0 5 0 2 5






MUB 12898

Fig. B1. When light propagates in an absorbing medium, the propagation vector $\vec{k}$ forms an angle $\phi_r$ with the normal to the surface of the medium while the attenuation vector $\vec{a}$ lies along the normal. Planes of equal phase are normal to $\vec{k}$ while planes of equal amplitude are normal to $\vec{a}$. The angle $\phi_r$ is the real angle of refraction in the medium, while the plane z = 0 is its surface. The figure is taken from Ref. 27.

and

$$n_c' : n_c' \equiv n' - i\kappa' \quad . \tag{16c}$$

From Eq. (20),

$$\alpha = \frac{2\pi\kappa'}{\lambda_o} \quad . \tag{20a}$$

Equation (19) now becomes

$$\vec{E}_s = \vec{E}_o \exp\left[-\frac{i\omega n'}{c} x\left(\sin\phi_r + z\left(\cos\phi_r - i\frac{\kappa'}{n'}\right)\right)\right] . \tag{20b}$$

It is very useful to be able to relate the four quantities n, $\kappa$, and n', $\kappa'$. The proper expressions are found to be[27,30]

$$n^2 - \kappa^2 = n'^2 - \kappa'^2 \tag{21}$$

and

$$n\kappa = n'\kappa'\cos\phi_r \quad . \tag{22}$$

Equations (21) and (22) connect n' and $\kappa'$, physically measurable quantities which are used in the descriptive Eq. (20b), with $n_c = n - i\kappa$, which will be found to occur in the equations which describe reflection from an interphase.

4. The Boundary Conditions for Reflection

With the definition Eq. (16) for $n_c^2$, Eqs. (1a) and (4a) become

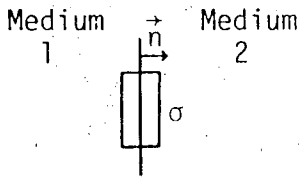
$$\text{div } n_c^2 \vec{E}_s = 0 \tag{16}$$

$$\text{curl } \vec{H}_s = -ik_o n_c^2 \vec{E} \quad . \tag{4b}$$

0 0 0 0 4 3 0 5 0 2 6



The boundary conditions, which are a conservation of energy across the reflecting surface, are now derived. Let two homogeneous media be separated by a plane boundary, with n the unit normal vector in either direction. Construct a surface σ as shown, and let the thickness of the volume t enclosed by σ be small compared with the width, and also small enough to assume small changes in the various fields.




The application of Gauss's Theorem

$$\int_t \text{div } \vec{F} dt = \int_\sigma n \cdot \vec{F} d\sigma$$

to Eqs. (1b) and (3a) gives, as $t \to 0$,

$$n_{c1}^2 \vec{E}_1 \cdot \vec{n} = n_{c2}^2 \vec{E}_2 \cdot \vec{n} \tag{35a}$$

$$\vec{H}_1 \cdot \vec{n} = \vec{H}_2 \cdot \vec{n} \quad . \tag{35b}$$

Stokes theorem,

$$\int_t \text{curl } \vec{F} = \int_\sigma \vec{n} x \vec{F} d\sigma$$

when applied to Eq. (4b) and Eq. (2a), gives the result that

$$\vec{E}_1 x \vec{n} = \vec{E}_2 x \vec{n} \tag{35c}$$

$$\vec{H}_1 x \vec{n} = \vec{H}_2 x \vec{n} \quad . \tag{35d}$$

This occurs because as t strinks to zero, the right-hand sides of Eqs. (4b) and (2a) approach zero.

The boundary conditions require the normal components of $n_c^2\vec{E}$ and $\vec{H}$ and the tangential components of $\vec{E}$ and $\vec{H}$ to be continuous across the surface.

Consider a plane wave suffering reflection and refraction. Figure B2 shows the coordinate system and the sign convention to be used. The subscript p refers to the polarization of $\vec{E}$ parallel to the plane of incidence, while s refers to the polarization normal to the plane of incidence. $\vec{E}$, $\vec{E}''$, and $\vec{E}'$ refer to the incident, reflected, and refracted waves. The xz plane is the plane of incidence while z = 0 corresponds to the boundary between the two absorbing media. The corresponding $\vec{H}$ vectors are directed such that the vector $\vec{E}\times\vec{H}$ in a right-handed coordinate system lies along $\vec{k}$.

For the incident vector $\vec{E}$, when $\vec{E}_o$ is expressed as

$$\vec{E}_o = \varepsilon_1 E_p \hat{x} + E_s \hat{y} + \varepsilon_3 E_p \hat{z} \quad , \tag{23}$$

values for $\varepsilon_1$ and $\varepsilon_3$ which provide unique solutions to Eqs. (1) through (4) are[27]

$$\varepsilon_1 = \cos\phi - i\kappa_o'/n_o' \tag{24}$$

$$\varepsilon_3 = -\sin\phi \quad . \tag{25}$$

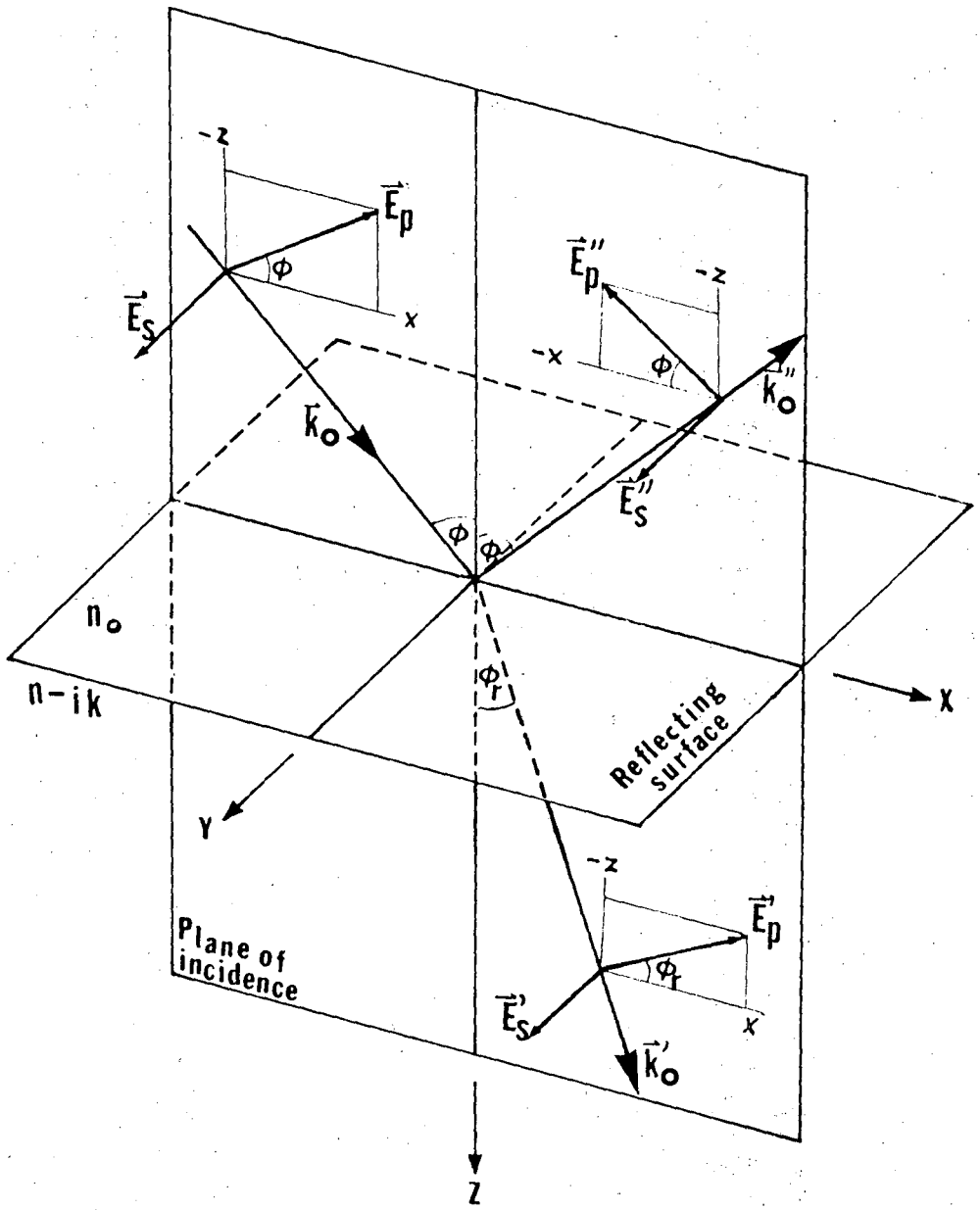
When $\vec{H}_s$ is represented as[27]

$$\vec{H}_s = \vec{H}_o \exp\left[-\frac{i\omega n'}{c}\left(x\sin\phi + z(\cos\phi - i\kappa_o'/n_o')\right)\right] \quad , \tag{26}$$

$$\vec{H}_o = n_o'\left[-E_s(\cos\phi - i\kappa_o'/n_o')\,\hat{x} + E_p\left(1 - \frac{\kappa_o'^2}{n_o'^2} - 2i\,\frac{\kappa_o'}{n_o'}\cos\phi\right)\hat{y} + E_s\sin\phi\hat{z}\right] . \tag{27}$$

0 0 0 0 4 3 0 5 0 2 7






XBL 7110-7420

Fig. B2. Coordinate system and sign convections for the electric field (positive direction of $E_p$ and $E_s$ in incident, reflected and refracted waves is indicated by arrows). The propagation vectors are presented by $k_o$, $k'_o$ and $k''_o$. Subscript p stands for polarization parallel to the plane of incidence and subscript s stands for polarization normal to the plane of incidence. The complex index of refraction of the adsorbing medium is designated n - ik. Figure taken from Ref. 28.

The expressions for $\vec{E}'$ and $\vec{E}''$ are found by priming Eqs. (23) through (27), with $\hat{x} \rightarrow -\hat{x}$ and $\hat{z} \rightarrow -\hat{z}$ for $\vec{E}''$.

To present the final representations of the electric waves, Snell's Law

$$n_o' \sin\phi = n' \sin\phi_r \tag{28}$$

is used.

$$\vec{E} = \left(E_p\left(\cos\phi - i\,\frac{\kappa_o'}{n_o'}\right)\hat{x} + E_s\hat{y} - E_p\sin\phi\hat{z}\right) \exp\left[\frac{2\pi i}{\lambda_o}\left(ct - n_o'\left(x\sin\phi + z\left(\cos\phi - i\,\frac{\kappa_o'}{n_o'}\right)\right)\right)\right] \tag{29}$$

$$\vec{E}'' = \left(-E_p''\left(\cos\phi - i\,\frac{\kappa_o'}{n_o'}\right)\hat{x} + E_s''\hat{y} - E_p''\sin\phi\hat{z}\right) \exp\left[\frac{2\pi i}{\lambda_o}\left(ct - n_o'\left(x\sin\phi - z\left(\cos\phi - i\,\frac{\kappa_o'}{n_o'}\right)\right)\right)\right] \tag{30}$$

$$\vec{E}' = \left(E_p\left(\cos\phi_r - i\,\frac{\kappa_1'}{n_1'}\right)\hat{x} + E_s'\hat{y} - E_p'\sin\phi_r\hat{z}\right) \exp\left[\frac{2\pi i}{\lambda_o}\left(ct - n_o'x\sin\phi - n_1'z\left(\cos\phi_r - i\,\frac{\kappa_1'}{n_1'}\right)\right)\right] \tag{31}$$

The relation $\omega/c = \frac{2\pi}{\lambda_o}$ has been used.

Expressing only the pre-exponential terms for $\vec{H}$, $\vec{H}'$ and $\vec{H}''$:

$$\vec{H} = n_o'\left[-E_s\left(\cos\phi - i\,\frac{\kappa_o'}{n_o'}\right)\hat{x} + E_p\left(1 - \frac{\kappa_o'^2}{n_o'^2} - \frac{2i\kappa_o'}{n_o'}\cos\phi\right)\hat{y} + E_s\sin\phi\hat{z}\right] \tag{32}$$

0 0 0 0 4 3 0 5 0 2 8



$$\vec{H}'' = n_o' \left[ E_s'' \left( \cos\phi - i \frac{\kappa_o'}{n_o'} \right) \hat{x} + E_p'' \left( 1 - \frac{\kappa_o'^2}{n_o'^2} - \frac{2i\kappa_o'}{n_o'} \cos\phi \right) \hat{y} - E_s'' \sin\phi \hat{z} \right] \tag{33}$$

$$\vec{H}' = n_1' \left[ -E_s \left( \cos\phi_r - i \frac{\kappa_1'}{n_1'} \right) \hat{x} + E_p' \left( 1 - \frac{\kappa_1'^2}{n_1'^2} - \frac{2i\kappa_1'}{n_1'} \cos\phi_r \right) \hat{y} + E_s' \sin\phi_r \hat{z} \right] \tag{34}$$

The boundary conditions at $z = 0$, if it is assumed that no surface charges or currents exist, are that[30] the components of $\vec{B}$ and $n_c^2\vec{E}$ normal to the surface and that the components of $\vec{E}$ and $\vec{H}$ parallel to the surface be continuous:

$$n_{co}^2(\vec{E} + \vec{E}'')\cdot z = n_{c1}^2 \vec{E}'\cdot\hat{z} \tag{35}$$

$$(\vec{H} + \vec{H}'')\cdot\hat{z} = \vec{H}'\cdot\hat{z} \tag{36}$$

$$(\vec{E} + \vec{E}'') \times\hat{z} = \vec{E}'\times\hat{z} \tag{37}$$

$$(\vec{H} + \vec{H}'') \times\hat{z} - H'\times\hat{z} \quad . \tag{38}$$

Expressions are now derived relating $E_p$, $E_p'$, $E_p''$, $E_s$, $E_s'$, and $E_s''$, using Eqs. (35) through (38). Substitute Eqs. (29), (30), and (31) into Eq. (35) and evaluate at $z = 0$.

$$n_{co}^2(-E_p - E_p'')\sin\phi = n_{c1}^2(-E_p' \sin\phi_r)$$

or

$$\frac{n_{co}^2}{n_o'}(E_p + E_p'') = \frac{n_{c1}^2}{n_1'} E_p' \quad . \tag{39}$$

Substitute Eqs. (29) through (31) into Eq. (37) and evaluate at $z = 0$.

$$\left[-E_p\left(\cos\phi - i\,\frac{\kappa_o'}{n_o'}\right) + E_p''\left(\cos\phi - i\,\frac{\kappa_o'}{n_o'}\right)\right]\hat{y} + \tag{40}$$

$$+ (E_s'' + E_s)\,\hat{x} = -E_p'\left(\cos\phi_r - i\,\frac{\kappa_1'}{n_1'}\right)\hat{y} + E_s'\hat{x} \quad .$$

To simplify notation, let

$$\kappa_o'/n_o' \equiv k_o' \quad \text{and} \quad \kappa_1'/n_1' \equiv k_1' \quad . \tag{41}$$

Equating coefficients of $\hat{y}$ and $\hat{x}$ in Eq. (40) gives

$$(E_p + E_p'')(\cos\phi - ik_o') = E_p'(\cos\phi_r - ik_1') \tag{42}$$

and

$$E_s'' + E_s = E_s' \quad . \tag{43}$$

By substituting Eqs. (32) and (33) into Eq. (38), evaluating at $z = 0$, and equating coefficients,

$$n_o'(E_s - E_s'')(\cos\phi - ik_o') = n_1'E_s'(\cos\phi_r - ik_1') \tag{44}$$

and

$$n_o'(E_p + E_p'')\left(1 - k_o'^2 - 2ik_o'\cos\phi\right) = n_1'E_p'\left(1 - k_1'^2 - 2ik_1'\cos\phi_r\right) \quad . \tag{45}$$

It can be shown that Eq. (45) reduces to Eq. (39). To summarize, the boundary conditions (Eqs. (35) through (38)) give the following four relations:

$$n_{co}^2/n_o'(E_p + E_p'') = n_{c1}^2/n_1'E_p' \tag{39}$$

$$(E_p - E_p'')(\cos\phi - ik_o') = E_p'(\cos\phi_r - ik_1') \tag{42}$$

0 0 0 0 4 3 0 5 0 2 9



$$E_s'' + E_s = E_s' \tag{43}$$

$$n_o'(\cos\phi - ik_o')(E_s - E_s'') = n_1'E_s'(\cos\phi_r - ik_1') \quad . \tag{44}$$

5. Reflection Coefficients

The reflection coefficients are defined as

$$r_\nu \equiv \frac{E_{\nu\text{reflected}}}{E_{\nu\text{incident}}} \tag{46}$$

where $\nu$ is either s or p.

For the present notation,

$$r_\nu = E_\nu''/E_\nu \quad . \tag{47}$$

By the use of Eqs. (43) and (44), straightforward manipulations yield

$$r_s = \frac{n_o'(\cos\phi - ik_o') - n_1'(\cos\phi_r - ik_1')}{n_o'(\cos\phi - ik_o') + n_1'(\cos\phi_r - ik_1')} \quad . \tag{49}$$

The use of Eqs. (39) and (42) results in:

$$r_p = \frac{n_{c1}^2 n_o'(\cos\phi - ik_o') - n_{co}^2 n_1'(\cos\phi_r - ik_1')}{n_{c1}^2 n_o'(\cos\phi - ik_o') - n_{co}^2 n_1'(\cos\phi_r - ik_1')} \tag{50}$$

6. The Complex Angle of Refraction

For absorbing incident and refracting media, Eqs. (49) and (50) may be simplified if Snell's Law is modified to include complex angles:

$$n_{co}\sin\phi_{co} = n_o'\sin\phi = n_1'\sin\phi_r = n_{c1}\sin\phi_{c1} \quad . \tag{51}$$

This equation is consistent with the further definition[27]

$$n_{c1}\cos\phi_{c1} \equiv n_1'(\cos\phi_r - i\kappa_1'/n_1') \tag{52}$$

## 7. The Fresnel Equations

Equations (49) and (50) may now be written

$$r_s = \frac{n_{co}\cos\phi_{co} - n_{cl}\cos\phi_{cl}}{n_{co}\cos\phi_{co} + n_{cl}\cos\phi_{cl}} \tag{53}$$

$$r_p = \frac{n_{cl}\cos\phi_{co} - n_{co}\cos\phi_{cl}}{n_{cl}\cos\phi_{co} + n_{co}\cos\phi_{cl}}$$

Alternate expressions are now derived. For $r_s$, substitute for $n_{cl}$ from Eq. (51).

$$r_s = \frac{n_{co}\cos\phi_{co} - n_{co}\sin\phi_{co}\cos\phi_{cl}/\sin\phi_{cl}}{n_{co}\cos\phi_{co} + n_{co}\sin\phi_{co}\cos\phi_{cl}/\sin\phi_{cl}} \tag{55}$$

$$= \frac{\sin\phi_{cl}\cos\phi_{co} - \sin\phi_{co}\cos\phi_{cl}}{\sin\phi_{cl}\cos\phi_{co} + \sin\phi_{co}\cos\phi_{cl}}$$

$$= -\frac{\sin(\phi_{co} - \phi_{cl})}{\sin(\phi_{co} + \phi_{cl})}$$

For $r_p$, again use Eq. (51)

$$r_p = \frac{n_{co}^3(\cos\phi_{co}\sin^2\phi_{co}/\sin^2\phi_{cl} - \sin\phi_{co}\cos\phi_{cl}/\sin\phi_{cl})}{n_{co}^3(\cos\phi_{co}\sin^2\phi_{co}/\sin^2\phi_{cl} + \sin\phi_{co}\cos\phi_{cl}/\sin\phi_{cl})} \tag{56a}$$

$$= \frac{(\cos\phi_{co}\sin^2\phi_{co} - \sin\phi_{co}\cos\phi_{cl}\sin\phi_{cl})}{(\cos\phi_{co}\sin^2\phi_{co} + \sin\phi_{co}\cos\phi_{cl}\sin\phi_{cl})}$$

$$= \frac{\cos\phi_{co}\sin\phi_{co} - \cos\phi_{cl}\sin\phi_{cl}}{\cos\phi_{co}\sin\phi_{co} + \cos\phi_{cl}\sin\phi_{cl}}$$

0 0 0 0 4 3 0 5 0 3 6



Equation (56a) is trigonometrically equivalent[27] to

$$r_p = \frac{\tan(\phi_{co} - \phi_{cl})}{\tan(\phi_{co} + \phi_{cl})} \quad . \tag{56}$$

To summarize, let the subscript m refer to the $m^{th}$ medium involved,

$$n_{cm} \equiv \sqrt{\mu(\varepsilon_m - i4\pi\sigma_m/\omega)} \equiv n_m - i\kappa_m \tag{16}$$

$$n'_{cm} \equiv n'_m - i\kappa'_m \tag{16c}$$

$$n'_m \equiv c/v_m \tag{18}$$

$$\kappa' \equiv n'\alpha/k = \alpha c/w$$

where

$$\alpha \text{ is the absorption coefficient} \tag{20}$$

$$n_m^2 - \kappa_m^2 = n_m'^2 - \kappa_m'^2 \tag{21}$$

$$n_m\kappa_m = n'_m\kappa'_m\cos\phi_m \tag{22}$$

$$n_o\sin\phi = n_1\sin\phi_r \quad . \tag{28}$$

The reflection coefficients are

$$r_s = \frac{n_{co}\cos\phi_{co} - n_{cl}\cos\phi_{cl}}{n_{co}\cos\phi_{co} + n_{cl}\cos\phi_{cl}} = E''_s/E_s \tag{53}$$

$$r_p = \frac{n_{cl}\cos\phi_{co} - n_{co}\cos\phi_{cl}}{n_{cl}\cos\phi_{co} + n_{co}\cos\phi_{cl}} = E''_p/E_p \tag{54}$$

where

$$n'_m \sin\phi_m \equiv n_{cm} \sin\phi_{cm} \tag{51}$$

and

$$n_{cm} \cos\phi_{cm} \equiv n'_m (\cos\phi_m - ik'_m) \tag{52}$$

where

$$k'_m \equiv \kappa'_m / n'_m \quad . \tag{53}$$

The Fresnel coefficients $r_p$ and $r_s$ may also be written as

$$r_s = - \frac{\sin(\phi_{co} - \phi_{cl})}{\sin(\phi_{co} + \phi_{cl})} \tag{55}$$

and

$$r_p = \frac{\tan(\phi_{co} - \phi_{cl})}{\tan(\phi_{co} + \phi_{cl})} \tag{56}$$

The Reflection Coefficients for a Film-Covered Surface. The Drude Equations

Figure B3 shows the notations used to represent the electric field vectors for a film-covered surface. The boundary conditions (Eqs. (35) through (38)) become

$$n_{co}^2 (\vec{E} + \vec{E}'') \hat{z} = n_c^2 (\vec{E}' + \vec{E}''') \cdot \hat{z} \tag{57}$$

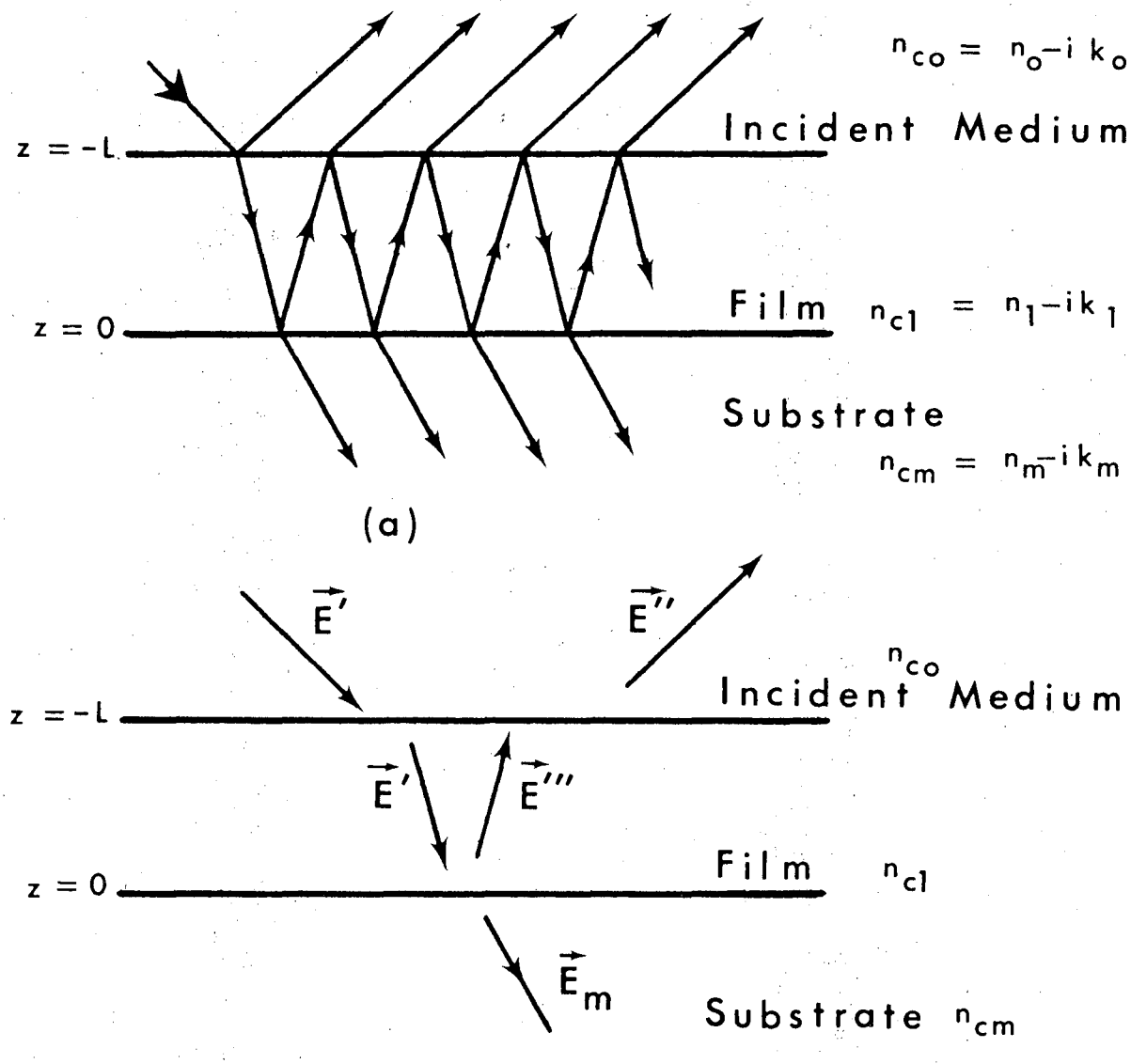
$$(\vec{H} + \vec{H}'') \cdot \hat{z} = (\vec{H}' + \vec{H}''') \cdot \hat{z} \tag{58}$$

$$(\vec{E} + \vec{E}'') \times \hat{z} = (\vec{E}' + \vec{E}''') \times \hat{z} \tag{59}$$

$$(\vec{H} + \vec{H}'') \times \hat{z} = (\vec{H}' + \vec{H}''') \times \hat{z} \tag{60}$$

0 0 0 0 4 3 0 5 0 3 1






XBL 759-7341

Fig. B3. Reflection from idealized film-covered surface.
(a) Representation by multiple-beam reflections.
(b) Representation in terms of equivalent waves.

At the first interface, Z = -L. Substituting Eqs. (29) through (31) into Eq. (57), and noting E"' is analogous to E', and using Eq. (51),

$$\frac{n_{co}^2}{n_o'}\left[E_p e^{i\tau_o} + E_p'' e^{-i\tau_o}\right] = \frac{n_{cl}^2}{n_o'}\left[E_p' e^{i\tau} + E_p''' e^{-i\tau}\right] \tag{61}$$

where

$$\tau_o = 2\pi L n_{co}\cos\phi_{co}/\lambda_o$$

$$\tau = 2\pi L n_{cl}\cos\phi_{cl}/\lambda_o$$

Substituting Eqs. (29) through (31) into Eq. (58), and equating coefficients of $\hat{x}$ and $\hat{y}$, gives

$$\frac{n_{co}\cos\phi_{co}}{n_o'}\left[E_p e^{i\tau_o} - E_p'' e^{-i\tau_o}\right] = \frac{n_{cl}\cos\phi_{cl}}{n_o'}\left[E_p' e^{i\tau} - E_p''' e^{-i\tau}\right] \tag{62}$$

$$E_s e^{i\tau_o} + E_s'' e^{-i\tau_o} = E_s' e^{i\tau} + E_s''' e^{-i\tau} \tag{63}$$

The substitution of Eqs. (32) through (34) into Eq. (60) gives

$$n_{co}\cos\phi_{co}\left[E_s e^{i\tau_o} - E_s'' e^{-i\tau_o}\right] = n_{cl}\cos\phi_{cl}\left[E_s' e^{i\tau} - E_s''' e^{-i\tau}\right] \tag{64}$$

At the substrate interface, Z = 0. The results similar to Eqs. (61) through (64) are

$$n_{cl}^2/n_l'(E_p' + E_p''') = n_{cm}^2/n_m' E_{pm} \tag{65}$$

$$n_{cl}\cos\phi_{cl}/n_l'(E_p' - E_p''') = n_{cm}\cos\phi_{cm}/n_m' E_{pm} \tag{66}$$

$$E_s' + E_s''' = E_{sm} \tag{67}$$

$$n_{cl}\cos\phi_{cl}(E_s' - E_s''') = n_{cm}\cos\phi_{cm} E_{sm} \tag{68}$$

0 0 0 0 4 3 0 5 0 3 2



Divide Eq. (66) by Eq. (65) to give, after simplifications,

$$n_{cm}\cos\phi_{cl}\left[\frac{1 - E_p'''/E_p'}{1 + E_p'''/E_p'}\right] = n_{cl}\cos\phi_{cm} \tag{69}$$

Define

$$\left.\begin{aligned} E_p'''/E_p' &= r_{2p} \\ E_s'''/E_s' &= r_{2s} \end{aligned}\right\} \tag{70}$$

Equation (69) now becomes

$$\left[\frac{1 - r_{2p}}{1 - r_{2p}}\right] = \frac{n_{cl}\cos\phi_{cm}}{n_{cm}\cos\phi_{cl}} \tag{71}$$

Use of Eqs. (67) and (68) leads similarly to

$$\frac{1 - r_{2s}}{1 + r_{2s}} = \frac{n_{cm}\cos\phi_{cm}}{n_{cl}\cos\phi_{cl}} \tag{72}$$

The Fresnel coefficients, analogous to Eqs. (53) and (54) are

$$r_{2s} = \frac{n_{cl}\cos\phi_{cl} - n_{cm}\cos\phi_{cm}}{n_{cl}\cos\phi_{cl} + n_{cm}\cos\phi_{cm}} \; ; \; r_{2p} = \frac{n_{cm}\cos\phi_{cl} - n_{cl}\cos\phi_{cm}}{n_{cm}\cos\phi_{cl} + n_{cl}\cos\phi_{cl}} \tag{73),(74}$$

For the first interface, similar to Eq. (69), Eq. (71),

$$\frac{1 + r_{1p}}{1 - r_{1p}} = \frac{n_{cl}\cos\phi_{co}}{n_{co}\cos\phi_{cl}} \tag{75}$$

$$\frac{1 + r_{1s}}{1 - r_{1s}} = \frac{n_{co}\cos\phi_{co}}{n_{cl}\cos\phi_{cl}} \tag{76}$$

We wish to obtain for the final result

$$r_\nu = E''_\nu/E_\nu \,, \quad \nu = s \text{ or } p \tag{77}$$

Divide Eq. (61) by Eq. (62), rearrange, and substitute Eq. (75) to give

$$\frac{E_p + E''_p e^{-2i\tau_o}}{E_p - E''_p e^{-2i\tau_o}} = \left[\frac{1 + r_{1p}}{1 - r_{1p}}\right] \frac{E'_p + E'''_p e^{-2i\tau}}{E'_p - E'''_p e^{-2i\tau}} \tag{78}$$

A similar expression with $p \to s$ is obtained for the s component by using Eqs. (63), (64) and (76). Letting $\nu$ = s or p, Eq. (78) is

$$\frac{E_\nu + E''_\nu e^{-2i\tau_o}}{E_\nu - E''_\nu e^{-2i\tau_o}} = \left[\frac{1 + r_{1\nu}}{1 - r_{1\nu}}\right] \frac{E' + E'''e^{-2i\tau}}{E' - E'''e^{-2i\tau}} \tag{79}$$

From Eq. (79),

$$\frac{e^{2i\tau_o} + E''_\nu/E_\nu}{e^{2i\tau_o} - E''_\nu/E_\nu} = \left[\frac{1 + r_{1\nu}}{1 - r_{1\nu}}\right] \frac{1 + E'''_\nu/E_\nu e^{-2i\tau}}{1 - E'''_\nu/E_\nu e^{-2i\tau}} \tag{80}$$

Using Eqs. (77) and (70),

$$\frac{e^{2i\tau_o} + r_\nu}{e^{2i\tau_o} - r_\nu} = \left[\frac{1 + r_{1\nu}}{1 - r_{1\nu}}\right] \frac{1 + r_{2\nu} e^{-2i\tau}}{1 - r_{2\nu} e^{-2i\tau}} \tag{81}$$

For convenience, let

$$\xi = \frac{e^{2i\tau_o} + r_\nu}{e^{2i\tau_o} - r_\nu}$$

0 0 0 0 4 3 0 5 0 3 3



then $r_\nu$,

$$r_\nu = e^{2i\tau_o} \frac{\xi - 1}{\xi + 1} \tag{82}$$

As $\xi$ is the left-hand side of Eq. (81),

$$\frac{\xi - 1}{\xi + 1} = \frac{(1 + r_{1\nu})\left(1 + r_{2\nu}e^{-2i\tau}\right) - (1 - r_{1\nu})\left(1 - r_{2\nu}e^{-2i\tau}\right)}{(1 + r_{1\nu})\left(1 + r_{2\nu}e^{-2i\tau}\right) + (1 - r_{1\nu})\left(1 - r_{2\nu}e^{-2i\tau}\right)} = \frac{r_{1\nu} + r_{2\nu}e^{-2i\tau}}{1 + r_{1\nu}r_{2\nu}e^{-2i\tau}} \tag{83}$$

As only the ratio of $r_p/r_s$ is involved in ellipsometric measurements, the term $\exp(2i\tau_o)$ in Eq. (82) is dropped. Equation (83) is the Drude equations.

$$r_\nu = \frac{r_{1\nu} + r_{2\nu}e^{-2i\tau}}{1 + r_{1\nu}r_{2\nu}e^{-2i\tau}} \tag{84}$$

where $\nu$ = s or p.

The Ellipsometer Parameters $\psi$ and $\Delta$

When polarized light is reflected from the boundary which separates two media, the components of the electric field parallel and normal to the plane of incidence suffer unequal amplitude attenuation, and a phase difference $\Delta$ occurs between them. Let

$$\tan\psi_i \equiv |E_p|/|E_s| \tag{85}$$

and

$$\tan\psi_r \equiv |E''_p|/|E''_s| \tag{86}$$

The amplitude ratio is changed by the factor

$$\tan\psi \equiv \frac{\tan\psi_r}{\tan\psi_i} \tag{87}$$

The ratios $E''_s/E_s$ and $E''_p/E_p$ are related to the angles of incidence and refraction by the Fresnel Eqs. (53) through (56). The reflection coefficients may be represented as an amplitude ratio and a phase change:

$$r_\nu = \frac{E''_\nu}{E_\nu} = \frac{|E''_\nu|\ e^{i\varepsilon''_\nu}}{|E_\nu|\ e^{i\varepsilon_\nu}} = \frac{|E''_\nu|}{|E_\nu|}\ e^{i(\varepsilon''_\nu - \varepsilon_\nu)} \tag{88}$$

where $\nu$ = s or p, and the epsilons are the phases of the various components with respect to an arbitrary time change. Define the absolute phase change by

$$\delta_\nu = \varepsilon''_\nu - \varepsilon_\nu \tag{89}$$

The ratio of the reflection coefficients is

$$\rho = r_p/r_s = \frac{\tan\psi_r}{\tan\psi_i}\ \exp(i(\delta_p - \delta_s)) \tag{90}$$

Define also

$$\Delta \equiv \delta_p - \delta_s \tag{91}$$

Then

$$\rho = \tan\psi e^{i\Delta} \tag{92}$$

0 0 0 0 4 3 0 5 0 3 4



# APPENDIX C. COMPUTER PROGRAMS

## INFILM

The program INFILM calculates $\Delta$ and $\psi$ for a system of up to 3 films, with each film either being homogeneous, or having an inhomogeneity in the direction normal to the interface described by a linear, parabolic, or exponential profile. For each film, the number of homogeneous layers in the multiple-film model is increased, within specified limits, by increments of 10 until convergence of $\Delta$ and $\psi$ within 0.003° is obtained. The maximum number of layers per film is 999.

The computational procedure begins with the film next to the substrate and works upward, as indicated in Fig. 3.

The program allows the conversion from the primed quantities n' and k' to the unprimed complex refractive index n = ik (Appendix B). The appropriate relationships are

$$n^2 - k^2 = n'^2 - k'^2 \tag{1}$$

$$nk = n'k'\cos\phi_r \tag{2}$$

In n and k are assumed to be independent of $\phi_r$, then n' and k' depend on $\phi_r$. The known quantities are n' (measured at a given angle, say at total reflection with a prism of known refractive index) and k (if measured at normal incidence and, therefore, equal to k').

The variable KCONV controls the conversion.

For KCONV = 1, n and k are read in and no conversion is made.

For KCONV = 2, n' and k are read in and the angles in the system of films are used for the conversion.

For KCONV = 3, n' and k are read in along with the refractive index of the prism used to measure n' at total reflection.

The substrate is assumed to be given as n - ik.

The thickness of each film is free to vary. The refractive index of the substrate and the angle of incidence may be varied if desired. The refractive index of the lower boundary for each film may also be varied.

KFORM(I) is the variable controlling the inhomogeneity of film I:

KFORM(I) = 0, homogeneous film

KFORM(I) = 1, linear profile

$$n = n_i + \frac{(n_b - n_i)}{\delta} \; y \tag{3}$$

KFORM(I) = 2, exponential profile

$$n = n_i \exp\left(\left[\ln \frac{n_b}{n_1}\right] y/\delta\right) \tag{4}$$

KFORM(I) = 3, increasing parabola

$$n = n_i + (n_b - n_i)\,[1 - (1 - y/\delta)^2] \tag{5}$$

KFORM(I) = 4, decreasing parabola

$$n = n_i + (n_b - n_i)(1 - y/\delta)^2 \tag{6}$$

KFORM(I) = 5, inverted increasing parabola

$$n = n_i - (n_b - n_i)[1 - (1 - y/\delta)^2] \tag{7}$$

0 0 0 0 4 3 0 3 0 3 5



KFORM(I) = 6, inverted decreasing parabola

$$n = n_i - (n_b - n_i)(1 - y/\delta)^2] \tag{8}$$

$n_b$ = refractive index at the top boundary of the film

$n_i$ = refractive index at the bottom boundary of the film

n is in general complex. The actual value of n(y) is obtained by integrating the function between the limits a and b of the layer. As an example, for the linear profile,

$$n = \frac{1}{b - a}\left[n_i(b - a) + \frac{n_b - n_i}{\delta}\left(\frac{b^2 - a^2}{2}\right)\right] \tag{9}$$

Input Variables

| | |
|---|---|
| TITLE | Alphanumeric label |
| RANGE | Alphanumeric label |
| WL | Wavelength of light, Å |
| PHID | Angle of incidence, $\phi$ deg |
| TNO | Real part of refractive index (r.i.) of the incident medium |
| TNKO | Imaginary part of incident medium r.i. |
| KCONV(1) | Controls conversion of r.i. of incident medium |
| RPRISM(1) | Refractive index of prism measuring r.i. of incident medium at total reflection |
| NPHI | Number of increments for $\phi$ |
| DELPHI | Increment for $\phi$, deg |
| TNS | Real part of substrate r.i. |
| TNKS | Imaginary part of substrate r.i. |
| NFILMS | Number of films, from 1 to 3, integer |
| NBASER | Number of increments for TNS, integer |

| | |
|---|---|
| NBASEI | Number of increments for TNKS, integer |
| DBASER | Increment for TNS |
| DBASEI | Increment for TNKS |
| TNU(I) | Real part of the r.i. of film I at the upper boundary. For a homogeneous film, equals r.i. of the medium above the boundary |
| TNKU(I) | Imaginary part of the r.i. of film I at the upper boundary. For a homogeneous film, equals r.i. of medium above the boundary |
| TNL(I) | Real part of r.i. of film I at lower boundary |
| TNKL(I) | Imaginary part of r.i. of film I at lower boundary |
| THICK(I) | Thickness of film I, Å |
| NTHICK(I) | Number of increments for THICK(I) |
| DTHICK(I) | Increment for THICK(I), Å |
| KCONV(I) | Controls conversion of r.i. for film I |
| KLAYU(I) | Upper limit for number of layers approximating the inhomogeneity of film I |
| KLAYL(I) | Initial number of layers for film I |
| RPRISM(I) | See PRSISM(1) above |
| KFORM(I) | Chooses function describing the inhomogeneity of film I |
| NTNL(I) | Number of increments for TNL(I) |
| NTNKL(I) | Number of increments for TNKL(I) |
| DTNL(I) | Increment for TNL(I) |
| DTNKL(I) | Increment for TNKL(I) |

Input Format for Data Cards

| Card No. | Column: 0-9 | 10-19 | 20-29 | 30-39 | 40-49 | 50-59 | 60-69 | 70-79 |
|---|---|---|---|---|---|---|---|---|
| 1 | Title (0-80) | | | | | | | |
| 2 | Range (0-80) | | | | | | | |
| 3 | WL | PHID | TNO | KCONV(1) | RPRISM(1) | RPRISM(1) | NPHI | DELPHI |
| 4 | TNS | TNKS | NFILMS | NBASER | NBASEI | DBASER | DBASEI | |
| 5 I = 1, NFILMS | TNU(I) | TNKU(I) | TNL(I) | TNKL(I) | THICK(I) | NTHICK(I) | DTHICK(I) | KCONV(I) |
| 6 | KLAYU(I) | KLAYL(I) | RPRISM(I) | KFORM(I) | NTNL(I) | NTNKL(I) | DTNL(I) | DTNKL(I) |

This is one data set. Any number of sets may follow, with 3 blank cards after the last set.

A fixed-point integer (I - N) is right justified in its appropriate column.

Film 1 (I = 1) is the top film.

For a homogeneous film, TNU(I) - iTNKU(I) is the refractive index of the film above film I, or the incident medium for I = 1.



0 0 0 4 3 0 5 0 3 6

```
      PROGRAM INFILM(INPUT,OUTPUT)
C
C
C        INFILM CALCULATES DELTA AND PSI FOR A SYSTEM
         OF UP TO 3 FILMS.  THE FILMS CAN BE HOMOGENEOUS OR
C        HAVE AN INHOMOGENEITY DESCRIBED BY LINEAR,
C        PARABOLIC, OR EXPONENTIAL PROFILES.
C
C
      COMPLEX X0,XBASE,XUP,XLOW,XLF,R1S,R1P,R2S,R2P,RS,RP,RHO
      COMPLEX D,A,B,C,R,D1,X1,CC,XLOW1,XUP1,XBASE1,XLU
      COMPLEX RSH,RPH
      DIMENSION RSH(10),RPH(10)
      DIMENSION THICK(3),TNU(3),TNKU(3),TNL(3),TNKL(3),NTHICK(3)
      DIMENSION DTHICK(3),NTNL(3),NTNKL(3),DTNL(3),DTNKL(8),TITLE(8)
      DIMENSION RANGE(8),KCONV(4),KFORM(3),XUP(3),XLOW(3),XLOW1(3)
      DIMENSION KLAYU(3),KLAYL(3)
      COMMON/REFRACT/RPRISM(6)
      COMMON /XINC/TN,SC,WL,ALPHA
C
C        THE COMPLEX COSINE
C
      CC(E,F,X1)=CSQRT(1.-E*E*F*F/X1/X1)
C
C       THE DRUDE EQNS FOR THE REFLECTION COEFFICIENT
C
      R(A,B,C)=(A+B*CEXP(-C))/(1.+A*B*CEXP(-C))
    7 CONTINUE
      READ 1,TITLE,RANGE
    1 FORMAT(8A10/8A10)
      IF(TITLE.EQ.12H            ) GO TO 5000
      READ 2,WL,PHI1,TN0,TNK0,KCONV(1),RPRISM(1),NPHI,DELPHI
    2 FORMAT(F9.0,3F10.0,I10,F10.0,I10,F10.0)
      READ 3,TNS,TNKS,NFILM,NBASER,NBASEI,DBASER,DBASEI
    3 FORMAT(F9.0,F10.0,3I10,2F10.0)
      DO 6 I=1,NFILM
      J=I+1
      READ 4,TNU(I),TNKU(I),TNL(I),TNKL(I),THICK(I),NTHICK(I),DTHICK(I)
     C ,KCONV(J)
    4 FORMAT(F9.0,4F10.0,I10,F10.0,I10)
      READ 5,KLAYU(I),KLAYL(I),RPRISM(J),KFORM(I),NTNL(I),NTNKL(I),
     C DTNL(I),DTNKL(I)
    5 FORMAT(I9,I10,F10.0,3I10,2F10.0)
   19 FORMAT(1H1,3X,8A10/3X,8A10)
   20 FORMAT(1H0,2X,*WAVELENGTH = *,F7.1,*ANGSTROMS ,* * PHI = *,F5.1,
     C*DEGREES , */2X*REFRACTIVE INDEX OF INC. MEDIUM = *,F7.4,3H I ,
     CE12.4)
   18 FORMAT(1H0,2X,*1   NBASE                NLOWER(NFILM)        NUPPER(
     CNFILM)        T(ANGSTROMS)   KFORM*)
   17 FORMAT(1H0,2X*2*20X*NLOWER(NFILM-1)     NUPPER(NFILM-1)     T(ANGS
     CTROMS)   KFORM*)
   16 FORMAT(1H0,2X*3*20X*NLOWER(NFILM-2)     NUPPER(NFILM-2)     T(ANGS
     CTROMS)   KFORM*)
   21 FORMAT(1H02X*1*3X,F7.4,2X,F7.4,4XF7.4,2X,F7.4,4X,F7.4,2X,F7.4,4X
     CF9.1,6X,I3)
   22 FORMAT(1H 2X,*2*,23X,F7.4,2X,F7.4,4X,F7.4,2X,F7.4,4X,F9.1,6X,I3)
   23 FORMAT(1H 2X,*3*,23X,F7.4,2X,F7.4,4X,F7.4,2X,F7.4,4X,F9.1,6X,I3)
   15 FORMAT(1H0,7X,*PSI         DELTA       AC          PC*)
   24 FORMAT(1H ,5X,4(F8.3,3X))
    6 CONTINUE
      ALPHA=.01745329252
      TN=TN0
```

0 0 0 0 4 3 0 5 0 3 7



```
C
C     VARIES THE ANGLE OF INCIDENCE
C
      DO 1100 NPH=1,NPHI
      PHI=PHI1*ALPHA
      XBASE=CMPLX(TNS,-TNKS)
C
C       CALCULATES THE COMPLEX REFRACTIVE INDEX
C
      CALL RINDEX(1,KCONV(1),TN0,TNK0,PHI,X0)
      DO 10 I=1,NFILM
      J=I+1
      CALL RINDEX(I,KCONV(J),TNU(I),TNKU(I),PHI,XUP(I))
      CALL RINDEX(I,KCONV(J),TNL(I),TNKL(I),PHI,XLOW(I))
   10 CONTINUE
      SC=SIN(PHI)
      D1=(0.,1.)*4.*3.1415927/WL
      J=NFILM-1
      K=NFILM-2
      PRINT 19,TITLE,RANGE
      PRINT 20,WL,PHI1,X0
      PRINT 18
      IF(NFILM.GT.1) PRINT 17
      IF(NFILM.GT.2) PRINT 16
      PRINT 15
      XBASE1=XBASE
C
C       VARIES THE REAL PART OF THE SUBSTRATE REFRACTIVE INDEX
C
      DO 1000 J1=1,NBASER
      XBASE1=CMPLX(REAL(XBASE1),AIMAG(XBASE))
      XLOW1(NFILM)=XLOW(NFILM)
C
C       VARIES THE IMAGINGARY PART OF THE SUBSTRATE REFRACTIVE INDEX
C
      DO 990 J2=1,NBASEI
      N1=NTNL(NFILM)
C
C     VARIES THE REAL PART OF FILM 1 REFRACTIVE INDEX
C
      DO 980 J3=1,N1
      XLOW1(NFILM)=CMPLX(REAL(XLOW1(NFILM)),AIMAG(XLOW(NFILM)))
      N2=NTNKL(NFILM)
C
C     VARIES THE IMAGINARY PART OF FILM 1 REFRACTIVE INDEX
C
      DO 970 J4=1,N2
      XLF=XLOW1(NFILM)
      CALL COEFF(XLF,XBASE1,R2S,R2P)
      CALL COEFF(XLOW1(NFILM),XLF,R1S,R1P)
      D=.00001*XLF*CC(SC,TN,XLF)*D1
      RS=R(R1S,R2S,D)
      RP=R(R1P,R2P,D)
      T=THICK(NFILM)
      N3=NTHICK(NFILM)
      RSH(1)=RS
      RPH(1)=RP
C
C     VARIES THE THICKNESS OF THE TOP FILM
C
      DO 960 J5=1,N3
      RS=RSH(1)
```

```
      RP=RPH(1)
C
C     CALCULATES THE CHANGE IN REFLECTION COEFFICIENTS DUE TO FILM 1
C
      CALL FILM(KFORM(NFILM),T,XUP(NFILM),XLOW1(NFILM),KLAYU(NFILM),
     C KLAYL(NFILM),RS,RP)
      IF(NFILM.LT.2) GO TO 30
      RSH(2)=RS
      RPH(2)=RP
      XLOW1(J)=XLOW(J)
      N4=NTNL(J)
C
C      VARIES THE REAL PART OF FILM 2 REFRACTIVE INDEX
C
      DO 950 J6=1,N4
      XLOW1(J)=CMPLX(REAL(XLOW1(J)),AIMAG(XLOW(J)))
      N5=NTNKL(J)
C
C     VARIES THE IMAGINARY PART OF FILM 2 REFRACTIVE INDEX
C
      DO 940 J7=1,N5
      RS=RSH(2)
      RP=RPH(2)
      XLF=(XLOW1(J)+XUP(NFILM))/2.
      CALL COEFF(XLOW1(J),XLF,R1S,R1P)
      D=0.001*XLF*CC(SC,TN,XLF)*D1
      RS=R(R1S,RS,D)
      RP=R(R1P,RP,D)
      T1=THICK(J)
      N6=NTHICK(J)
      RSH(3)=RS
      RPH(3)=RP
C
C     VARIES THE THICKNESS OF FILM 2
C
      DO 930 J8=1,N6
      RS=RSH(3)
      RP=RPH(3)
C
C     CALCULATES THE CHANGE IN REFLECTION COEFFICIENTS DUE TO FILM 2
C
      CALL FILM(KFORM(J),T1,XUP(J),XLOW1(J),KLAYU(J),KLAYL(J),RS,RP)
      IF(NFILM.LT.3) GO TO 30
      RSH(4)=RS
      RPH(4)=RP
      XLOW1(K)=XLOW(K)
      N7=NTNL(K)
C
C     VARIES THE REAL PART OF FILM 3 REFRACTIVE INDEX
C
      DO 920 J9=1,N7
      XLOW1(K)=CMPLX(REAL(XLOW1(K)),AIMAG(XLOW(K)))
      N8=NTNKL(K)
C
C     VARIES THE IMAGINARY PART OF FILM 3 REFRACTIVE INDEX

      DO 910 J10=1,N8
      RS=RSH(4)
      RP=RPH(4)
      XLF=(XLOW1(K)+XUP(J))/2.
            CALL COEFF(XLOW1(K),XLF,R1S,R1P)
      D=0.001*XLF*CC(SC,TN,XLF)*D1
```

0 0 0 0 4 3 0 5 0 3 8



```
      RS=R(R1S,RS,D)
      RP=R(R1P,RP,D)
      T2=THICK(K)
      N9=NTHICK(K)
      RSH(5)=RS
      RPH(5)=RP
C
C     VARIES THE THICKNESS OF FILM 3
C
      DO 900 J11=1,N9
      RS=RSH(5)
      RP=RPH(5)
C
C     CALCULATES THE CHANGE IN REFLECTION COEFFICIENTS DUE TO FILM 3
C
      CALL FILM(KFORM(K),T2,XUP(K),XLOW1(K),KLAYU(K),KLAYL(K),RS,RP)
   30 CONTINUE
      XLF=(XUP(K)+X0)/2.
      CALL COEFF(X0,XLF,R1S,R1P)
      D=.1*XLF*CC(SC,TN,XLF)*01
      RS=R(R1S,RS,D)
      RP=R(R1P,RP,D)
      D=01*X0*CC(SC,TN,X0)
      CALL COEFF(X0,X0,R1S,R1P)
      RS=R(R1S,RS,D)
      RP=R(R1P,RP,D)
      RHO=RP/RS
      PSIC=ATAN(CABS(RHO))/ALPHA
      DELC=ATAN2(AIMAG(RHO),REAL(RHO))/ALPHA
      AC=PSIC+90.
      PC=(90.-DELC)/2.
      IF(DELC.LT.0.) DELC=DELC+360.
      PRINT 21,XBASE1,XLOW1(NFILM),XUP(NFILM),T,KFORM(NFILM)
      IF(NFILM.GT.1) PRINT 22,XLOW1(J),XUP(J),T1,KFORM(J)
      IF(NFILM.GT.2) PRINT 23,XLOW1(K),XUP(K),T2,KFORM(K)
      PRINT 24,PSIC,DELC,AC,PC
  890 CONTINUE
      IF(NFILM.LT.3) GO TO 925
      T2=T2+DTHICK(K)
  900 CONTINUE
      XLOW1(K)=CMPLX(REAL(XLOW1(K)),AIMAG(XLOW1(K))-DTNKL(K))
  910 CONTINUE
      XLOW1(K)=CMPLX(REAL(XLOW1(K))+DTNL(K),AIMAG(XLOW1(K)))
  920 CONTINUE
  925 CONTINUE
      IF(NFILM.LT.2) GO TO 955
      T1=T1+DTHICK(J)
  930  CONTINUE
      XLOW1(J)=CMPLX(REAL(XLOW1(J)),AIMAG(XLOW1(J))-DTNKL(J))
  940 CONTINUE
      XLOW1(J)=CMPLX(REAL(XLOW1(J))+DTNL(J),AIMAG(XLOW1(J)))
  950 CONTINUE
  955 CONTINUE
      T=T+DTHICK(NFILM)
  960 CONTINUE
      XLOW1(NFILM)=CMPLX(REAL(XLOW1(NFILM)),AIMAG(XLOW1(NFILM))-DTNKL(NF
     CILM))
  970 CONTINUE
      XLOW1(NFILM)=CMPLX(REAL(XLOW1(NFILM))+DTNL(NFILM),AIMAG(XLOW1(NFIL
     CM)))
  980 CONTINUE
      XBASE1=CMPLX(REAL(XBASE1),AIMAG(XBASE1)-DBASEI)
```

```
  990 CONTINUE
      XBASE1=CMPLX(REAL(XBASE1)+DBASER,AIMAG(XBASE1))
 1000 CONTINUE
      PHI1=PHI1+DELPHI
 1100 CONTINUE
      GO TO 7
 5000 CONTINUE
      END
      SUBROUTINE FILM(J,T,XU,XL,KU,KL,RS,RP)
C
C     FILM CALCULATES THE CHANGE IN REFLECTION COEFFICIENTS DUE TO A FILM
C     OF VARIABLE REFRACTIVE INDEX
C
      COMPLEX XU,XL,RS,RP,X,X1,A,B,C,D,D1,R,R1S,R1P,RHO
      COMPLEX AFILM,BFILM
      COMPLEX Z1,Z2
      DIMENSION X(1000)
      COMMON/XINC/TN,SC,WL,ALPHA
      COMMON/SEND/AFILM,BFILM,T1,FIT
      CC(E,F,X1)=CSQRT(1.-E*E*F*F/X1/X1)
      R(A,B,C)=(A+B*CEXP(-D))/(1.+A*B*CEXP(-C))
      AFILM=XL
      BFILM=XU
      T1=T
      FIT=FLOAT(J)
      D1=(0.,1.)*4.*3.1415927/WL
      IF(J.GT.0) GO TO 50
      CALL COEFF(XU,XL,R1S,R1P)
           D=T*XL*CC(SC,TN,XL)
      RS=R(R1S,RS,D)
      RP=R(R1P,RP,D)
      GO TO 100
   50 CONTINUE
      Z1=RS
      Z2=RP
      K=KL
   60 CONTINUE
      RP=Z2
      RS=Z1
      TT=T/FLOAT(K)
      U=1.
      DO 70 M=1,K
      Z=U*TT
      Y=Z-TT
C
C     FINDS THE REFRACTIVE INDEX AS A FUNCTION OF DISTANCE
C
      X(M)=PROFYL(Y,Z)
      U=U+1.
   70 CONTINUE
      L=K+1
      X(L)=XU
      DO 80 M=1,K
      I=M+1
      CALL COEFF(X(I),X(M),R1S,R1P)
      D=D1*TT*X(M)*CC(SC,TN,X(M))
        RS=R(R1S,RS,D)
      RP=R(R1P,RP,D)
   80 CONTINUE
      RHO=RP/RS
      PSIC=ATAN(CABS(RHO))/ALPHA
      DELC=ATAN2(AIMAG(RHO),REAL(RHO))/ALPHA
```

0 0 0 0 4 3 0 5 0 3 9



```
      IF(K.EQ.KL) GO TO 90
C
C     TESTS FOR CONVERGENCE WITH RESPECT TO NUMBER OF FILM LAYERS
C
   85 IF(ABS(H1-PSIC).GT..007) GO TO 90
      IF(ABS(H2-DELC).GT..007) GO TO 90
      GO TO 100
   90 H1=PSIC
      H2=DELC
      IF(K.GE.KU) GO TO 95
      K=K+10
      GO TO 60
   95 PRINT 1,XU
    1 FORMAT(1H ,* NO CONVERGENCE FOR LAYER WITH XU = *,F9.4,2X,F9.4)
  100 RETURN
      END
      SUBROUTINE RINDEX(I,NUM,A,B,PHI,RIND)
C
C     RINDEX GIVES THE COMPLEX REFRACTIVE INDEX
C
      COMPLEX RIND
      COMMON/REFRACT/RPRISM(6)
      IF(NUM.EQ.1) GO TO 5
      IF(NUM.EQ.2) GO TO 10
      IF(NUM.EQ.3) GO TO 15
C
C     STRAIGHT COMBINATION OF REAL AND IMAGINARY PARTS
C
    5 D=A
      E=B
      GO TO 100
C
C     USES FILM ANGLE FOR CONVERSION
C
   10 C=COS(PHI)
      CALL F3(A,B,C,D,E)
      GO TO 100
C
C     USES REFRACTOMETER ANGLE FOR CONVERSION
C
   15 IF(RPRISM(I).GE.A) S=A/RPRISM(I)
      IF(RPRISM(I).LT.A) S=RPRISM(I)/A
      C=SQRT(1.-S*S)
      CALL F3(A,B,C,D,E)
  100 RIND=CMPLX(D,-E)
      RETURN
      END
C
C      COEFF CALCULATES THE FRESNEL REFLECTION COEFFICIENTS
C
      SUBROUTINE COEFF(A,B,RS,RP)
      COMMON/XINC/TN,SC,WL,ALPHA
      COMPLEX C1,C2,A,B,RS,RP
      C1=CSQRT(1.-TN*TN*SC*SC/A/A)
      C2=CSQRT(1.-TN*TN*SC*SC/B/B)
      RS=(A*C1-B*C2)/(A*C1+B*C2)
      RP=-(A*C2-B*C1)/(A*C2+B*C1)
      RETURN
      END
      FUNCTION PROFYL(X,Y)
C      PROFYL CALCULATES THE REFRACTIVE INDEX
C      BETWEEN THE LIMITS Y(UPPER) AND X(LOWER)
```

```
C       USING THE (INTEGRAL N(Y) DY )/(Y-X).
        COMMON/SEND/AFILM,BFILM,TT,FIT
        COMPLEX PROFYL,AFILM,BFILM,A,B,C
        IF(FIT.EQ.1.) GO TO 10
        IF(FIT.EQ.2.) GO TO 20
        IF(FIT.EQ.3.) GO TO 30
        IF(FIT.EQ.4.) GO TO 40
        IF(FIT.EQ.5.) GO TO 50
        IF(FIT.EQ.6.) GO TO 60
C        LINEAR PROFILE
   10   B=(BFILM-AFILM)/TT
        PROFYL=AFILM+B*(Y*Y-X*X)/2./(Y-X)
        GO TO 100
C        EXPONENTIAL PROFILE
   20   IF(AIMAG(AFILM)) 21,25,21
   21   IF(AIMAG(BFILM))27,22,27
   27   C1=.01*AIMAG(AFILM)
        C2=REAL(BFILM)
        BFILM=CMPLX(C2,C1)
   22   B=BFILM/AFILM
        C=CLOG(B)/TT
        PROFYL=AFILM/C/(Y-X)*(CEXP(C*Y)-CEXP(C*X))
        GO TO 100
   25   IF(AIMAG(BFILM))26,22,26
   26   C1=.01*AIMAG(BFILM)
        C2=REAL(AFILM)
        AFILM=CMPLX(C2,C1)
        GO TO 22
C        INCREASING PARABOLA
   30   B=BFILM-AFILM
        C=(Y*Y-X*X)/TT-(Y*Y*Y-X*X*X)/3./TT/TT
        C=C/(Y-X)
        PROFYL=AFILM+B*C
        GO TO 100
C        DECREASING PARABOLA
   40   B=BFILM-AFILM
        C=Y-X-(Y*Y-X*X)/TT+(Y*Y*Y-X*X*X)/3./TT/TT
        C=C/(Y-X)
        PROFYL=AFILM+B*C
        GO TO 100
   50   B=BFILM-AFILM
        C=(Y*Y-X*X)/TT-(Y*Y*Y-X*X*X)/3./TT/TT
        C=C/(Y-X)
        PROFYL=AFILM-B*C
        GO TO 100
   60   B=BFILM-AFILM
        C=Y-X-(Y*Y-X*X)/TT+(Y*Y*Y-X*X*X)/3./TT/TT
        C=C/(Y-X)
        PROFYL=AFILM-B*C
        GO TO 100
  100   RETURN
        END
        SUBROUTINE F3(TN,TNK,AN,X,Y)
C        X AND Y ARE THE REAL AND IMAGINARY
C        PARTS OF THE UNPRIMED REFRACTIVE INDEX
        CORRESPONDING TO THE PRIMED TN AND
C        UNPRIMED TNK AT THE ANGLE ARCCOS(AN)
        IF(TNK)1,5,1
     1  A=TN*TN+TNK*TNK
        B=TN/TNK*AN
        X=SQRT(A/(1.+1./B**2))
        Y=TNK

        GO TO 7
   5    X=TN
        Y=TNK
   7    CONTINUE
        RETURN
        END
```

0 0 0 0 4 3 0 5 0 4 0



DEPOSITION FROM 0.1M CUSO4 AT LIMITING CURRENT
POTENTIOSTATIC GROWTH OF BOUNDARY LAYER, LINEAR PROFILE

WAVELENGTH = 5461.0ANGSTROMS , PHI = 75.0DEGREES ,
REFRACTIVE INDEX OF INC. MEDIUM = 1.3374 ! -0.

| 1 | NBASE | | NLOWER(NFILM) | | NUPPER(NFILM) | | T(ANGSTROMS |
|---|---|---|---|---|---|---|---|
| | PSI | DELTA | AC | PC | | | |
| 1 | .9400 | -2.3300 | 1.3345 | -0.0000 | 1.3374 | -0.0000 | 1000.0 |
| | 37.386 | 58.374 | 127.386 | 15.813 | | | |
| 1 | .9400 | -2.3300 | 1.3345 | -0.0000 | 1.3374 | -0.0000 | 2000.0 |
| | 37.366 | 58.092 | 127.366 | 15.954 | | | |
| 1 | .9400 | -2.3300 | 1.3345 | -0.0000 | 1.3374 | -0.0000 | 3000.0 |
| | 37.393 | 57.589 | 127.393 | 16.205 | | | |
| 1 | .9400 | -2.3300 | 1.3345 | -0.0000 | 1.3374 | -0.0000 | 4000.0 |
| | 37.450 | 57.048 | 127.450 | 16.476 | | | |
| 1 | .9400 | -2.3300 | 1.3345 | -0.0000 | 1.3374 | -0.0000 | 5000.0 |
| | 37.515 | 56.638 | 127.515 | 16.681 | | | |
| 1 | .9400 | -2.3300 | 1.3345 | -0.0000 | 1.3374 | -0.0000 | 6000.0 |
| | 37.564 | 56.450 | 127.564 | 16.775 | | | |
| 1 | .9400 | -2.3300 | 1.3345 | -0.0000 | 1.3374 | -0.0000 | 7000.0 |
| | 37.585 | 56.481 | 127.585 | 16.760 | | | |
| 1 | .9400 | -2.3300 | 1.3345 | -0.0000 | 1.3374 | -0.0000 | 8000.0 |
| | 37.581 | 56.646 | 127.581 | 16.677 | | | |
| 1 | .9400 | -2.3300 | 1.3345 | -0.0000 | 1.3374 | -0.0000 | 9000.0 |
| | 37.561 | 56.827 | 127.561 | 16.587 | | | |
| 1 | .9400 | -2.3300 | 1.3345 | -0.0000 | 1.3374 | -0.0000 | 10000.0 |
| | 37.541 | 56.922 | 127.541 | 16.539 | | | |
| 1 | .9400 | -2.3300 | 1.3345 | -0.0000 | 1.3374 | -0.0000 | 11000.0 |
| | 37.533 | 56.894 | 127.533 | 16.553 | | | |
| 1 | .9400 | -2.3300 | 1.3345 | -0.0000 | 1.3374 | -0.0000 | 12000.0 |
| | 37.540 | 56.775 | 127.540 | 16.613 | | | |
| 1 | .9400 | -2.3300 | 1.3345 | -0.0000 | 1.3374 | -0.0000 | 13000.0 |
| | 37.558 | 56.640 | 127.558 | 16.680 | | | |
| 1 | .9400 | -2.3300 | 1.3345 | -0.0000 | 1.3374 | -0.0000 | 14000.0 |
| | 37.575 | 56.559 | 127.575 | 16.721 | | | |
| 1 | .9400 | -2.3300 | 1.3345 | -0.0000 | 1.3374 | -0.0000 | 15000.0 |
| | 37.585 | 56.566 | 127.585 | 16.717 | | | |
| 1 | .9400 | -2.3300 | 1.3345 | -0.0000 | 1.3374 | -0.0000 | 16000.0 |
| | 37.583 | 56.643 | 127.583 | 16.679 | | | |
| 1 | .9400 | -2.3300 | 1.3345 | -0.0000 | 1.3374 | -0.0000 | 17000.0 |
| | 37.572 | 56.738 | 127.572 | 16.631 | | | |
| 1 | .9400 | -2.3300 | 1.3345 | -0.0000 | 1.3374 | -0.0000 | 18000.0 |

DEFLCT

The program DEFLCT calculates $\Delta$ and $\psi$ for a substrate covered by a mass-transport boundary layer at the thick film limit. The light-deflection model is used. The angle of incidence $\phi$ and the substrate refractive index may be varied if desired.

Input Variables

| | |
|---|---|
| TITLE | Alphanumeric label |
| RANGE | Alphanumeric label |
| TNO | Refractive index of incident medium (real) |
| WL | Wavelength of light, Å |
| TNS | Real part of substrate refractive index |
| TNKS | Imaginary part of substrate refractive index |
| PHI1 | Angle of incidence $\phi$, deg |
| DPHI | Increment in PHI1 |
| NPHI | Number of increments for PHI1 |
| TNI | Real part of interfacial refractive index |
| TNKI | Imaginary part of interfacial refractive index |
| DTNS | Increment in TNS |
| DTNKS | Increment in TNKS |
| NS | Number of increments for TNS |
| NKS | Number of increments of TNKS |

Input Format for Data Cards

| Card No. | Column: | 0-9 | 10-19 | 20-29 | 30-39 | 40-49 | 50-59 | 60-69 |
|---|---|---|---|---|---|---|---|---|
| 1 | | TITLE (0-80) | | | | | | |
| 2 | | RANGE (0-80) | | | | | | |
| 3 | | TNO | WL | TNS | TNKS | PHI1 | DPHI | NPHI |
| 4 | | TNI | TNKI | DTNS | DTNKS | NS | NKS | |

This is one data set. Any number of sets may follow, with 3 blank cards after the last set.
Fixed-point variables are right-justified in their appropriate column.



0 0 0 4 3 0 5 0 4 1

```
      PROGRAM DEFLCT(INPUT,OUTPUT)
C
C
C        DEFLCT CALCULATES DEL AND PSI FOR THE LIGHT DEFLECTION
         MODEL FOR THE BOUNDARY LAYER)  THICK FILM LIMIT
C
C
      REAL PHI1,PHI,CP,SP,LNK,LN,L,TN,TNK,T,PSIC,DELC,DT,TM
      COMPLEX TN1,T2,S2,TN3,LN3, LN2    ,S1,T1,SC,CC,D
      COMPLEX TN2,CPHI2,CPHI3,R1S,R1P,R2S,R2P,RS,RP,RHO
      REAL DTNK1,TNKM,T1M,TN1M,TNK1M,WL,AC,PC
      REAL TNKS,TNM,TNO,TNS
      REAL TNK1I,TN1I,T1I,TNI,TNKI,TI,DTNK,DTN,D1T,DTN1
      DIMENSION DELT(20,200),PSIT(20,200),DEL2(200),PSI2(200)
      DIMENSION THICK(1000)
      DIMENSION DELTAV(200)
      DIMENSION DFLM(2)
      DIMENSION TITLE (8), RANGE (8)
    1 READ 2, TITLE,RANGE
    2 FORMAT (8A10/8A10)
      IF(TITLE.EQ.5H      ) GO TO 3000
    3 PRINT 4, TITLE,RANGE
    4 FORMAT (1H1, 8A10//8A10)
      READ 17,TNO,WL,TNS,TNKS,PHI1,DPHI,NPHI
   17 FORMAT(F9.0,5F10.0,I10)
    6 READ 9,TNI,TNKI,DTNS,DTNKS,NS,NKS
    9 FORMAT(F9.0,3F10.0,2I10)
      PRINT 13,PHI1,TNO,WL,TNS,TNKS
   13 FORMAT(1H0///6HPHI = ,F5.2,10X,4HN = ,F7.4, 10X, 13HWAVELENGTH = ,
     C F5.0, 11H  ANGSTROMS//33H REFRACTIVE INDEX OF SUBSTRATE = , F7.4,
     C 2X, 4H-  I, F7.4)
      TNN=TNO
      DO 700 LLL=1,NPHI
      PRINT 37,PHI1
   37 FORMAT(1H0,*  PHI = *,F9.4)
      PRINT 42
   42 FORMAT(1H0,//*       TNS                TNI                        DEL
     C      PSI      DDEL     DPSI*)
      Z1=TNS
      DO 770 MN=1,NS
      Z2=TNKS
      DO 750 NM=1,NKS
      PHI=PHI1*.01745329252
      SP=SIN(PHI)
      CP=COS(PHI)
      DO 660 MM=1,2
C
C       FOR MM=1, CALCULATES DEL AND PSI FOR NO B.L.
C      FOR MM=2, CALCULATES DEL AND PSI WITH B.L.
C
      IF(MM.EQ.1) TNO=TNN
      IF(MM.EQ.1) TN2=CMPLX(TNO,-0.)
      IF(MM.EQ.2) TN2=CMPLX(TNI,-TNKI)
      TN3=CMPLX(Z1,-Z2)
      TNO=REAL(TN2)
      CPHI2=CSQRT(1.-TNO*TNO*SP*SP/TN2/TN2)
      CPHI3=CSQRT(1.-TNO*TNO*SP*SP/TN3/TN3)
      R2S=(TN2*CPHI2-TN3*CPHI3)/(TN2*CPHI2+TN3*CPHI3)
      R2P=-(TN2*CPHI3-TN3*CPHI2)/(TN2*CPHI3+TN3*CPHI2)
  555 CONTINUE
      RHO=R2P/R2S
      DEL=ATAN2(AIMAG(RHO),REAL(RHO))/.01745329252
```

0 0 0 0 4 3 0 5 0 4 2



```
      PSI=ATAN(CABS(RHO))/.01745329252
      IF(DEL.LT.0.) DEL=DEL+360.
      AC=PSI+90.
      PC=(90.-DEL)/2.
      IF(MM.EQ.1) HP=DEL
      IF(MM.EQ.1) HA=PSI
      IF(MM.EQ.2) DELT(MN,NM)=ABS(HP-DEL)
      IF(MM.EQ.2) PSIT(MN,NM)=ABS(HA-PSI)
      THICK(NM)=Z2
      SP=TNO*SP/TNI
  660 CONTINUE
      IF(DELT(MN,NM).GE.180.) DELT(MN,NM)=DELT(MN,NM)-180.
  550 CONTINUE
  600 CONTINUE
      PRINT 43,TN3,TN2,DEL,PSI,DELT(MN,NM),PSIT(MN,NM)
   43 FORMAT(1H ,2X,F7.4,2X,F7.4,4X,F7.4,2X,F7.4,3X,F8.3,3X,F8.3,
     CF8.3,F7.3)
      Z2=Z2+DTNKS
  750 CONTINUE
      Z1=Z1+DTNS
  770 CONTINUE
      PHI1=PHI1+DPHI
  700 CONTINUE
  710 CONTINUE
      GO TO 1
 3000 CONTINUE
      END
```

DEPOSITION FROM 0.1 M CUSO4

LIMITING CURRENT , THICK FILM LIMIT

PHI = 70.00 N = 1.3374 WAVELENGTH = 5461 ANGSTROMS

REFRACTIVE INDEX OF SUBSTRATE = .9000 - I 2.0000

PHI = 70.0000

| TNS | | TNI | | DEL | PSI | DDEL | DPSI |
|---|---|---|---|---|---|---|---|
| .9000 | -2.0000 | 1.3345 | -0.0000 | 68.561 | 36.340 | 1.058 | .058 |
| .9000 | -2.0500 | 1.3345 | -0.0000 | 69.582 | 36.394 | 1.065 | .055 |
| .9000 | -2.1000 | 1.3345 | -0.0000 | 70.592 | 36.452 | 1.071 | .052 |
| .9000 | -2.1500 | 1.3345 | -0.0000 | 71.592 | 36.512 | 1.076 | .049 |
| .9000 | -2.2000 | 1.3345 | -0.0000 | 72.581 | 36.575 | 1.081 | .046 |
| .9500 | -2.0000 | 1.3345 | -0.0000 | 68.677 | 35.850 | 1.065 | .060 |
| .9500 | -2.0500 | 1.3345 | -0.0000 | 69.704 | 35.909 | 1.071 | .057 |
| .9500 | -2.1000 | 1.3345 | -0.0000 | 70.721 | 35.971 | 1.077 | .054 |
| .9500 | -2.1500 | 1.3345 | -0.0000 | 71.726 | 36.037 | 1.083 | .051 |
| .9500 | -2.2000 | 1.3345 | -0.0000 | 72.721 | 36.105 | 1.088 | .048 |

PHI = 75.0000

| TNS | | TNI | | DEL | PSI | DDEL | DPSI |
|---|---|---|---|---|---|---|---|
| .9000 | -2.0000 | 1.3345 | -0.0000 | 51.074 | 37.799 | 1.556 | .149 |
| .9000 | -2.0500 | 1.3345 | -0.0000 | 51.923 | 37.807 | 1.574 | .146 |
| .9000 | -2.1000 | 1.3345 | -0.0000 | 52.759 | 37.819 | 1.592 | .142 |
| .9000 | -2.1500 | 1.3345 | -0.0000 | 53.611 | 37.833 | 1.609 | .139 |
| .9000 | -2.2000 | 1.3345 | -0.0000 | 54.449 | 37.849 | 1.625 | .136 |
| .9500 | -2.0000 | 1.3345 | -0.0000 | 51.090 | 37.386 | 1.562 | .157 |
| .9500 | -2.0500 | 1.3345 | -0.0000 | 51.945 | 37.396 | 1.581 | .154 |
| .9500 | -2.1000 | 1.3345 | -0.0000 | 52.797 | 37.409 | 1.598 | .150 |
| .9500 | -2.1500 | 1.3345 | -0.0000 | 53.645 | 37.425 | 1.615 | .147 |
| .9500 | -2.2000 | 1.3345 | -0.0000 | 54.488 | 37.444 | 1.632 | .143 |

0 0 0 0 4 3 0 5 0 4 3



REFERENCES

1. J. S. Newman, Electrochemical Systems (Prentice-Hall, Inc., Englewood Cliffs, NJ, 1973), pp. 305-318.
2. V. G. Levich, Physicochemical Hydrodynamics (Prentice-Hall, Inc., Englewood Cliffs, NJ, 1962), p. 3.
3. H. J. S. Sand, Phil. Mag. 1(6), 45 (1901).
4. T. K. Sherwood, Chem. Eng. Progress Symp. Series 55(25), 71 (1959).
5. R. Acosta, Transport Processing in High Rate Electrolysis (Ph. D. Thesis), LBL-2242, May 1974.
6. C. H. Chilton and A. P. Colburn, Ind. Eng. Chem. 26, 1183 (1934).
7. C. W. Tobias and R. G. Hickman, Z. Phys. Chem. 229, 145 (1965) (Leipzig).
8. R. H. Perry, Perry's Chemical Engineers' Handbook (McGraw-Hill, NY, 1963), pp. 10-10, 10-13.
9. F. R. McLarnon, Interferometry of Electrochemical Mass Transfer Boundary Layers (Ph. D. Thesis), LBL-3500, December 1974.
10. O. S. Heavens, Optical Properties of Thin Solid Films (Dover, NY, 1956), p. 63.
11. P. Drude, Ueber Oberflächenschickten, Ann. Der Physik und Chemis 36, 531/561, 865/897 (1889).
12. H. J. Mathieu, D. E. McClure and R. H. Muller, Rev. Sci. Instrum. 45, 789 (1974).
13. W. A. Roth and K. Scheel, eds., Landolt-Boernstein, Physikatisch-Chemische Tabellen (Springer Verlag, Berlin, 1923), p. 28512.

14. M. G. Mellon, J. Phys. Chem. 31, 161 (1927).

15. R. Mecke, Z. Phys. Chem. 111, 385 (1929).

16. E. Mueller, Ann. Phys. 12, 767 (1903).

17. F. Graunbaum, Ann. Phys. 12, 1008 (1903).

18. D. Brodsky, Acta Physiochim URSS 5, 919 (1936).

19. D. Bhagwat, J. Phys. Chem. 35, 2386 (1931).

20. P. Bovis, Ann. Physique 10, 232 (1928).

21. T. W. Chapman and J. S. Newman, A Compilation of Selected Thermodynamics and Transport Properties of Binary Electrolytes in Aqueous Solution, UCRL-17767, 41 (1968).

22. A. Emanuel and D. R. Olander, J. Chem. Engr. Data 8, 31 (1963).

23. W. G. Eversole, H. M. Kindsvater and J. D. Peterson, J. Phys. Chem. 46, 370 (1942).

24. J. J. Fritz and C. R. Fuget, J. Phys. Chem. 62, 303 (1958).

25. W. Herz, Z. Anorg. Chemie 89, 393 (1914).

26. J. N. Pearce and G. G. Pumplin, J. Amer. Chem. Soc. 59, 1221 (1937).

27. R. H. Muller, J. R. Mowat, Reflection of Polarized Light from Absorbing Media, UCRL-11813 (1966).

28. R. H. Muller, J. R. Mowat, Reflection of Polarized Light from Film-Covered Surfaces, UCRL-17128 (1967).

29. R. W. Ditchburn, Light (Blackie, London, 1963), Ch. 13-15, pp. 106-114.

30. J. Stone, Radiation and Optics (McGraw-Hill, NY, 1963), Ch. 15 and 16.

0 0 0 0 4 3 0 5 0 4 4



31. M. Born, E. Wolf, Principles of Optics (Pergamon Press, NY, 1964), pp. 14-24.

32. F. R. McLarnon, R. H. Muller and C. W. Tobias, Appl. Opt., in press.

33. F. R. McLarnon, R. H. Muller and C. W. Tobias, J. Opt. Soc. Am., in press.

34. H. J. Mathieu, Computer Programs for Ellipsometry II, LBL-2517 (1973).

35. H. J. Mathieu and R. H. Muller, Anodic Behavior of Copper in Aqueous Solutions Determined with a Self-Nulling Ellipsometer, LBL-2520 (1973).

LEGAL NOTICE

*This report was prepared as an account of work sponsored by the United States Government. Neither the United States nor the United States Energy Research and Development Administration, nor any of their employees, nor any of their contractors, subcontractors, or their employees, makes any warranty, express or implied, or assumes any legal liability or responsibility for the accuracy, completeness or usefulness of any information, apparatus, product or process disclosed, or represents that its use would not infringe privately owned rights.*

*TECHNICAL INFORMATION DIVISION*
*LAWRENCE BERKELEY LABORATORY*
*UNIVERSITY OF CALIFORNIA*
*BERKELEY, CALIFORNIA 94720*